Anti-Diabetic Activity from a Marine Lipid Analogue

Analysis of a Potential New Therapeutic Agent Targeting the Nuclear Receptors PPARα and -γ

MSc Thesis
by Henriette Arnesen

Department of Nutrition
Institute of Basic Medical Sciences
Faculty of Medicine
UNIVERSITY OF OSLO

November 2017

Anti-Diabetic Activity from a Marine Lipid Analogue

Analysis of a Potential New Therapeutic Agent Targeting the Nuclear Receptors PPARα and -γ

MSc Thesis by Henriette Arnesen

Supervisor: Thomas Sæther

Department of Nutrition
Institute of Basic Medical Sciences
Faculty of Medicine
UNIVERSITY OF OSLO

November 2017

2017

Anti-Diabetic Activity from a Marine Lipid Analogue

Henriette Arnesen

http://www.duo.uio.no/

Print: Reprosentralen, University of Oslo

Acknowledgements

The work presented in this master's thesis was carried out at Department of Nutrition, at the Institute of Basic Medical Sciences from January to November 2017.

First of all, I would like to thank my inspiring supervisor Thomas Sæther. Thank you for always taking time to guide and motivate me. Your optimism and enthusiasm have been invaluable for me going through with this work. I would also like to thank Christin Lucas, Qiong Fan, and the rest of the Nuclear Receptor and Molecular Toxicology research groups at Division of Molecular Nutrition. Thank you for readily sharing your knowledge with me and forming a great learning environment. I really appreciate all the support in the lab, valuable discussions, and advice you have given me this past year. Also, thanks for all the tasty cakes. You have all made me feel very included.

A special thanks to my amazing family and friends for always having my back and cheering me on. I am utterly grateful for everything you have done for me, and by no means would I have come to where I am today without you. I would also like to express my gratitude to Raisa for her endless patience, and for unconditionally encouraging and comforting me. You are extraordinary.

November 2017

Henriette Arnesen

Abstract

The steadily increasing prevalence of Diabetes Mellitus is expected to reach over 640 million individuals by 2040, predominantly attributed the type 2 (T2DM). As current approaches to treat T2DM fail to limit the growing prevalence, an urgent need for new strategies has arisen. To offer individuals suffering from T2DM an effective and holistic treatment, a combination of lifestyle interventions and medical therapy is often necessary. Pharmaceuticals currently in use for this purpose include agents targeting Peroxisome Proliferator-Activated Receptors (PPARs). Upon activation by ligand, these receptors activate metabolic and inflammatory pathways that are dysregulated in T2DM patients. However, previously developed drugs exhibit adverse side-effects, limiting their application in this patient group. Previous studies have pointed out agents targeting both PPARα and -γ isoforms as novel candidates for developing new and safer anti-diabetic pharmaceuticals. Increased energy metabolism, safe storage of lipids, and production of beneficial signal molecules through PPARα and -γ activation, respectively, is hypothesized to improve insulin sensitization, without the side-effects observed with each separate PPAR agonist.

In the present work a novel fatty acid mimetic, ADAM1, was evaluated as a potential new, anti-diabetic agent, targeting human nuclear receptors PPARα and -γ. ADAM1 is the first generation analogue of two oxo-fatty acid isolated from the microalgae *Chaetoceros karianus*. Chemical modifications were made to the parent compound to limit its cytotoxicity and increase its stability. Through *in vitro* cell studies we found that ADAM1 strongly activated human PPARα through its ligand-binding domain (EC_{50} = 23 μM), but showed little or no effect on human PPARγ. The cytotoxic effect of ADAM1 was relatively high, perhaps higher than the parent compound with approximately 20 % of the cells dying at EC_{50}. ADAM1 exhibited a modest ability to induce expression of genes involved in lipid metabolism in hepatocytes, as well as ability to drive differentiation of adipocytes. High doses of ADAM1 may evoke greater PPARγ-mediated responses, but due to its cytotoxic effects, such doses are not realistic for human administration. Although more data are needed, we conclude that the current ADAM1 activation profile, cytotoxicity and target gene repertoire are unsatisfactory with respect to being evaluated as a dual PPARα/γ agonist.

List of abbreviations

ACOX	Acyl-CoA Oxidase
ACSL	Acyl-CoA Synthetase Long-Chain
ADAM	Anti-Diabetic Activity from Marine lipids
AF	Activation Function
ALA	α-Linolenic Acid (All-cis-9,12,15-octadecatrienoic Acid)
AMPK	AMP-Activated Protein Kinase
ANGPTL	Angiopoietin-Like Protein
ARA	Arachidonic Acid (All-cis-5,8,11,14-eicosatetraenoic Acid)
BAT	Brown Adipose Tissue
β-ME	2-Mercaptoethanol
bp	Base Pairs
BSA	Bovine Serum Albumin
cDNA	Complementary Deoxyribonucleic Acid
C/EBP	CCAAT/Enhancer-Binding Protein
CD36	Cluster of Differentiation 36/Fatty Acid Translocase
CMV	Cytomegalovirus
CPT1	Carnitine Palmitoyltransferase
COX	Cyclooxygenase
CYP	Cytochrome P450
Ct	Cycle Threshold
CVD	Cardiovascular Disease
DBD	DNA-Binding Domain
d/ddH_2O	Distilled/Double Distilled H_2O
DMEM	Dulbecco's Modified Eagle's Medium
DMSO	Dimethyl Sulphoxide
EDTA	Ethylenediaminetetraacetic Acid
EtOH	Ethanol
FA	Fatty Acid
FABP	Fatty Acid Binding Protein
FBS	Fetal Bovine Serum
FFA	Free Fatty Acid
GLA	γ-Linolenic Acid (All-cis-6,9,12-octadecatrienoic Acid)
GLUT	Glucose Transporter
HEPE	Hydroxyeicosapentaenoic Acid
HETE	Hydroxyeicosatetraenoic Acid
HODE	Hydroxyoctadecadienoic Acid
IBMX	1-Methyl-3-Isobutylxanthine
INT	2-(4-iodophenyl)-3-(4-nitrophenyl)-5-phenyl-2*H*-tetrazolium
IR	Insulin Receptor
ITS	Insulin-Transferrin-Selenium
LA	Linoleic Acid (All-cis-9,12-octadecadienoic Acid)
LBD	Ligand-Binding Domain
LDH	Lactate Dehydrogenase
LEP	Leptin
LOX	Lipoxygenase
LUC	Luciferase
LXR	Liver X Receptor
L-Gln	L-Glutamine
MW	Molecular Weight

NaAc	Sodium Acetate
NaCl	Sodium Chloride
NR	Nuclear Receptor
NTC	No Template Control
ORO	Oil Red O
OxLDL	Oxidized Low-Density Lipoprotein
PA	Pirinixic Acid (WY-14643)
PCR	Polymerase Chain Reaction
PBS	Phosphate-Buffered Saline
PGA	Prostaglandin A
PMS	Phenazine Methosulfate
PLIN	Perilipin
PPAR	Peroxisome Proliferator-Activated Receptor
PP_i	Pyrophosphate
PPRE	Peroxisome Proliferator Response Element
P/S	Penicillin Streptomycin Solution
qPCR	Quantitative Polymerase Chain Reaction
rcf	Relative Centrifugal Force
RLT	RNeasy Lysis Buffer
RLUC	Renilla Luciferase
rpm	Revolutions per minute
RSD	Relative Standard Deviation
RSG	Rosiglitazone (BRL-49653)
RT	Reverse Transcriptase
RXR	Retinoid X Receptor
SCD	Stearoyl-CoA Desaturase
SGBS	Simpson-Golabi-Behmel Syndrome
SPPARM	Selective PPAR Modulator
SREBP	Sterol Regulatory Element-Binding Transcription Protein
SV40	Simian Virus 40
T2DM	Type 2 Diabetes Mellitus
TAE	Tris(hydroxymethyl)aminomethane-Acetic acid-EDTA Buffer
TAG	Triacylglycerol
TBP	TATA-Box Binding Protein
TCA	Tricarboxylic Acid Cycle (Krebs cycle)
TE	Tris(hydroxymethyl)aminomethane-EDTA Buffer
Tm	Melting temperature
TNF-α	Tumor Necrosis Factor α
TSS	Transcription Start Site
UAS	Upstream Activation Sequence
UCP	Uncoupling Protein
WAT	White Adipose Tissue
XTT	Sodium-2,3-bis(2-Methoxy-4-Nitro-5-Sulfophenyl)-5-[(Phenylamino)-Carbonyl]-2H-Tetrazolium (inner salt)
(7E)-9-OHE	(7E)-9-Oxohexadec-7-Enoic Acid
(10E)-9-OHE	(10E)-9-Oxohexadec-10-Enoic Acid
15d-PGJ_2	15-Deoxy-Delta-12,14-prostaglandin J2

Table of contents

Pages

1 Introduction ... 1

1.1 Metabolism ... 1

1.1.1 Glucose and lipid metabolism ... 1

1.1.2 Adipose tissue ... 5

1.2 Metabolic regulation ... 7

1.3 Nuclear receptors (NRs) ... 8

1.3.1 Peroxisome proliferator-activated receptors ... 10

1.3.2 PPARα ... 11

1.3.3 PPARγ ... 12

1.4 Diabetes Mellitus ... 14

1.4.1 Background and definitions ... 14

1.4.2 Metabolic consequences ... 15

1.4.3 Current therapeutic approaches ... 17

1.5 The rationale behind the present project ... 18

1.6 Aims of the present project ... 20

2 Methods ... 21

2.1 Mammalian cell culturing ... 21

2.1.1 COS1 ... 22

2.1.2 HuH7 ... 22

2.1.3 SGBS ... 23

2.1.4 Cell cultivation procedures ... 24

2.1.5 Cell counting ... 25

2.2 Adipocyte differentiation assay ... 26

2.2.1 Oil Red O staining ... 27

2.3 Activity Assays ... 29

2.3.1 Transfection ... 29

2.3.2 Dual-Luciferase reporter assay system ... 31

2.3.3 Processing of activity data ... 33

2.3.4 DNA cloning ... 33

2.4 Gene expression assays ... 38

2.4.1 Total RNA isolation ... 39

2.4.2 Complementary DNA (cDNA) synthesis ... 40

2.4.3 Quantitative Polymerase Chain Reaction (qPCR) ... 41

2.4.4 Processing of qPCR data ... 43

2.5 Cell viability assays ... 43

2.5.1 Lactate Dehydrogenase (LDH) Cytotoxicity Assay 44
2.5.2 XTT-Based Cell Viability Assay 45
2.5.3 Processing of cell viability data 47
2.6 Statistical analysis 47
3 Results 49
3.1 Physicochemical properties of ADAM1 49
3.2 Dose-response and cytotoxicity 49
3.3 Cloning of a GAL4-RXRα-LBD expression construct 53
3.4 Specificity 55
3.5 Activation of natural promoters 58
3.6 Endogenous target gene expression in hepatocytes 60
3.7 Endogenous target gene expression in adipocytes 63
3.8 Adipocyte differentiation 67
4 Discussion 69
4.1 Methodological considerations 70
4.1.1 *In vitro* cell lines as model systems in biomedical research 70
4.1.2 Ligand-dependent activation studies 71
4.1.3 RNA analysis 72
4.2 General discussion 76
4.2.1 Nuclear receptor agonist activity of ADAM1 76
4.2.2 ADAM1 and the regulation of PPAR target genes in hepatocytes 78
4.2.3 ADAM1 and the regulation of PPAR target genes in adipocytes 79
4.2.4 Effects of ADAM1 on adipocyte differentiation 81
4.2.5 Anti-diabetic effects of PPARα and -γ activation 83
4.2.6 Properties of new, anti-diabetic drugs targeting PPARs 84
5 Conclusions 87
5.1 Future perspectives 87
6 References 89
Appendices 97

List of tables

Pages

Table 1: Freezing media 25
Table 2: Amounts of the DNA plasmids included in the nuclear receptor activity assays. 30
Table 3: Cutting reaction of DNA template and DNA vector. 36
Table 4: Ligation and control reactions. 36
Table 5: PPARα/γ agonism and cytotoxicity of relevant compounds 50
Table 6: Target gene expression in HuH7 cells 62
Table 7: Target gene expression in SGBS cells 64

List of figures

Pages

Figure 1: Glucose and lipid metabolism 3
Figure 2: Chemical structure of α-linolenic acid (C18) with nomenclature of carbons 4
Figure 3: White adipocyte differentiation 7
Figure 4: Illustrations of the general NR structure 9
Figure 5: Simplified illustration of PPAR transactivation 11
Figure 6: Metabolic effects of PPARα and -γ activation. 14
Figure 7: Simplified scheme for the pathophysiology of Type 2 Diabetes Mellitus 16
Figure 8: Chemical structures of the two isolated oxo-fatty acids 19
Figure 9: Areas of chemical modifications 19
Figure 10: Flow-chart the adipocyte differentiation assay 27
Figure 11: Simplified illustration of the firefly and renilla luciferase reactions 31
Figure 12: PCR amplification program. 35
Figure 13: Reverse transcription protocol 41
Figure 14: qPCR protocol. 43
Figure 15: Principle of the LDH Cytotoxicity assay 44
Figure 16: Principle of the XTT-based Cell Viability assay 46
Figure 17: Microscopic photographs of COS1 cells 50
Figure 18: Dose-response curves. 51
Figure 19: Effect of ADAM1 treatment on COS1 cell viability. 52
Figure 20: Verification of PCR product on agarose gel 53
Figure 21: Verification of DNA plasmid clones on agarose gel 54
Figure 22: Human RXRα-specific transactivation by 9-cis Retinoic acid 55
Figure 23: Nuclear receptor-specific transactivation by ADAM1 56
Figure 24: Human PPARα transactivation by PA and ADAM1 57
Figure 25: Activation of natural PPARα and -γ regulated promoters by ADAM1 59
Figure 26: Relative expression of endogenous PPAR target genes in HuH7 cells 61
Figure 27: Relative expression of endogenous PPAR target genes in SGBS cells. 66
Figure 28: Neutral lipid accumulation in SGBS cells. 68
Figure 29: Microscopic photographs of SGBS cells 68

List of appendices

Appendix I	Materials, equipment and software
Appendix II	Buffer and reagents recipes
Appendix III	SGBS cell culturing media
Appendix IV	DNA plasmids
Appendix V	qPCR primer sequences
Appendix VI	Cloned pSG5-GAL4-hRXRα-LBD plasmid sequence chromatogram

1 Introduction

1.1 Metabolism

Metabolism is the sum of all biochemical processes occurring in living organisms in order to maintain life. The overall purposes of metabolic processes is to extract energy from the environment to fuel cellular processes, convert environmental factors to building blocks required for synthesis of essential cellular components, and eliminate wastes and toxins. The reactions of metabolic processes are mediated by enzymes in complex systems, organized in pathways. Metabolism can be divided into two categories, i.e. anabolism and catabolism. Anabolism includes the processes of synthesis and construction of cellular components, which usually consumes energy. In the other end of the scale, catabolism refers to the breakdown of large molecules to smaller molecules, which usually releases energy. The balance between anabolic and catabolic processes in different situations is often referred to as the metabolic homeostasis.

1.1.1 Glucose and lipid metabolism

The fate of dietary nutrients following absorption from the small intestine is determined by the overall energy status in the body. Close collaboration between cellular, endocrine and neurological signaling systems is necessary to sense, report and react to the body's energy status. In periods of energy deficit, mobilization and utilization of energy is favored, while storage of energy is favored in periods when energy substrates are abundant. This stored energy can later be utilized in periods of energy deficit (1).

In most cells, utilization of energy from dietary nutrients is achieved by converting the macromolecules to chemical energy in form of adenosine trisphosphate (ATP). Yet, some specialized cells can dissipate energy as heat rather than for ATP production, as described in **section 1.1.2**. As the main energy currency of humans, ATP is essential for a broad spectra of biochemical processes in the body. Most anabolic processes, cardiac and skeletal muscle contractions, cell replication and

differentiation, transmembrane transport of compounds, and signal molecules are dependent on ATP (1, 2). In terms of ATP-production, the main energy-containing molecules are carbohydrates and lipids. Proteins are not a major energy source and are usually not considered in an energy homeostatic perspective. Therefore, the following paragraphs will focus on the most important energy yielding nutrients, i.e. carbohydrates and lipids.

During intestinal postprandial absorption, almost all dietary carbohydrates are degraded to glucose which directly enters the circulation through the portal vein. Dietary lipids are absorbed through enterocytes in sequential processes involving lipases for degradation and bile acids for emulsification, and are ultimately packed in chylomicrons (1, 2). Chylomicrons are lipoprotein complexes of triacylglycerols (TAGs), cholesteryl esters, apoliporoteins and phospholipids that enters the lymph vessels. An exception is short- and medium chained FAs which are absorbed across enterocytes directly to the circulation with minimal processing, due to their short hydrophobic chains (2). Chylomicrons enter the circulation via the subclavian vein. TAGs in chylomicrons are degraded to free fatty acids (FFAs) and glycerol by lipoprotein lipase (LPL) in the capillaries. The FFAs then enters adjacent cells or are transported in the circulation bound to albumin to other cells for energy production or storage. The liver packs FFAs in lipoprotein particles for safe transport throughout the body (1).

The concentration of all compounds present in blood is tightly regulated, as aberrant concentrations can damage cells, vessels and other biological structures, and disrupt the body’s signal systems. Understandably, this also applies to lipids and glucose. The delayed entrance of chylomicrons to the circulation is a mechanism that prevents a rapid increase of postprandial lipid concentration. Blood glucose levels remain constant at concentrations of 4-7 mM despite prandial status, an equilibrium tightly regulated by insulin and glucagon (1, 3). Insulin and glucagon are peptide hormones produced by and secreted from α- and β-cells of the islet of Langerhans of the pancreas, respectively (1). Insulin is produced and secreted in response to elevated blood glucose concentrations, and through binding to its receptors (IRs), it initiates a wide array of signaling pathways affecting metabolism. Among important metabolic actions of insulin are reduced lipolysis, hepatic gluconeogenesis and glycogenolysis,

as well as increased rates of glucose uptake and protein synthesis (1-3). In contrast, glucagon is produced and secreted in response to decreased blood glucose levels, and acts to oppose insulin actions (2). Regulation of glucose and lipid metabolism is primarily controlled by the liver, skeletal muscles and adipose tissue, in a complex interplay of pathways as illustrated in **Figure 1**.

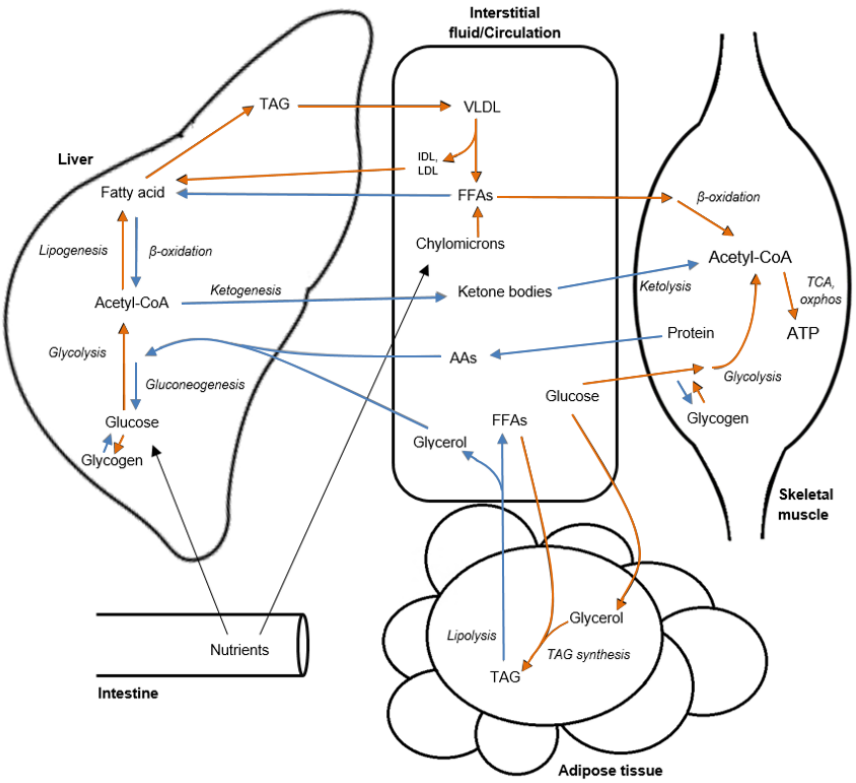

Figure 1: Glucose and lipid metabolism. Simplified illustration of the main pathways of human energy metabolism and how they are connected. The colored arrows indicate pathways mainly active during periods of energy excess (orange) and energy deficit (blue). AAs, amino acids; IDL, intermediate-density lipoprotein; LDL, low-density lipoprotein; oxphos, oxidative phosphorylation; TCA, tricarboxylic acid cycle.

All tissues are able to utilize glucose directly for ATP production through glycolysis, followed by the tricarboxylic acid (TCA) cycle and oxidative phosphorylation. Some tissues, such as brain and erythrocytes, are glucose-dependent and require a constant level of glucose to maintenance their biological processes. However, when glucose levels are severely low, acetyl-CoA derived from FA oxidation can enter ketogenesis in the liver, resulting in production of ketone bodies that can be utilized by brain. Most cell types containing mitochondria can utilize FFAs for ATP production, although liver and skeletal muscle are the main oxidative tissues (1). In humans, utilization of FFAs can occur through three different mechanisms, namely α-, β- and ω-oxidation (2).

The FA oxidation pathways are named after the direction of oxidation on the FA molecule, as illustrated in **Figure 2.** α-oxidation takes place exclusively in peroxisomes, ω-oxidation is carried out by enzymes located in endoplasmic reticulum, while both peroxisomes and mitochondria are able to β-oxidize FAs (2). Mitochondrial β-oxidation is the preferred mechanism of FA oxidation and involves cycles where two and two carbons are cleaved off, starting on the β-carbon (C3) (2, 4). Peroxisomal β-oxidation is mainly a shortening pathway for very-long-chained FAs (VLCAs), that are too long to enter the mitochondrial β-oxidation directly (2). Peroxisomal α-oxidation allows for cleavage of one carbon atom, the α-carbon. This is necessary for some branched-chained FAs, such as phytanic acid, which have a methyl group at its β-carbon, inhibiting it from being β-oxidized (2). The products of peroxisomal α-/β-oxidation can enter the mitochondrial β-oxidation pathway. ω-oxidation is executed by cytochrome P450 (CYP) monooxygenases, and this is normally a minor pathway that is up-regulated in cases of β-oxidation defects. The ω-oxidation pathway ultimately results in generation of dicarboxylic acids, which can be further metabolized through peroxisomal β-oxidation (4).

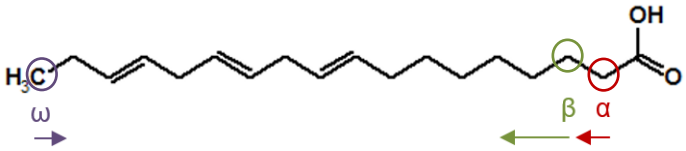

Figure 2: Chemical structure of α-linolenic acid (C18) with nomenclature of carbons. The directions of α-, β-, and ω-oxidation are illustrated with arrows.

In periods of low energy demands and abundance of substrates for energy production, the energy is stored. Glucose are directed to glycogenesis and stored as glycogen, while FFAs are esterified and stored in complex with glycerol as TAG, preferentially in adipocytes. Glycogen is a macromolecule serving as an energy reservoir for synthesis of ATP during muscle contractions in skeletal muscle, and as a source of glucose for the maintenance of blood glucose by the liver (2). Glycogen is always hydrated and associates with about three times its own weight of water. The high weight limits its use as an energy reservoir. Storage of TAGs in lipid droplets is a much more compact and effective way of preserving energy, as they contain more energy than carbohydrates, and do not include water (1). Carbohydrates exceeding the limit of carbohydrate storage as glycogen are converted to FAs for storage

through *de novo* lipogenesis. De novo lipogenesis occur in both liver and adipose tissue in response to high substrate availability (1).

In periods of energy deficit and high energy demand, mobilization of stored glucose from glycogen, and FFAs from TAG is required. Glucose can also be generated endogenously through gluconeogenesis in the liver, where glucose is produced from non-carbohydrate substrates. Stored TAG in lipid droplets is hydrolyzed to FFAs and glycerol by hormone sensitive lipase (HSL), a process known as lipolysis. Perilipins (PLINs) that coat lipid droplets are important in packing and organization of the lipid droplets in adipose tissue. PLINs also functions as shields from HSL and thereby from lipolysis. Upon insulin reduction, and/or catecholamine binding to receptors in response to energy deficit, PLINs are phosphorylated and inactivated simultaneously as HSL is activated, allowing for rapid lipolysis. The mobilized FFAs from TAG can directly enter adjacent cells, or be transported bound to albumin to enter cells elsewhere. The FFAs are activated to fatty acyl-CoA and oxidized to produce energy in the fasting state, or re-esterified to TAG for storage in the fed state. The remnants of chylomicrons and other lipoprotein particles are hydrolyzed in the liver and recycled after TAG has been removed (1, 2).

1.1.2 Adipose tissue

Adipose tissue is a heterogeneous mix of mature adipocytes, pre-adipocytes, immune cells and fibroblasts (5). Two main types of adipose tissue are identified, namely white (WAT) and brown adipose tissue (BAT), where WAT is the most abundant type in humans. These two types of adipose tissue differ with respect to function, morphology and physiology. BAT is named after the large number of mitochondria it contains, which also gives BAT its high oxidative capacity. Lipids in BAT are stored as multilocular droplets, while lipids in WAT are present as large unilocular droplets, typically filling most of the cell volume, leaving cell organelles pressed to the membrane (1). While WAT plays a crucial role in storing lipids safely in lipid droplets and thereby removing potentially harmful compounds from the circulation, BAT can uncouple the mitochondrial electron gradient and thereby oxidize substrates without production of ATP. This is accomplished by a special

family of proteins, i.e. uncoupling proteins (UCPs) (1). Consequently, oxidation of FAs in BAT leads to heat production. Certain white adipose tissue have been found to display some characteristics of BAT, e.g. expression of UCP1. This third type of adipocyte has been named beige adipocytes, and the development of such beige adipocytes is termed “browning” of WAT. This process is not yet completely understood, although physical exercise, prolonged exposure to cold, and β-adrenergic signals are among contributing factors reported (6, 7).

The main physiological function of adipose tissue is to serve as an energy reservoir, as well as providing mechanical cushioning and thermal insulation, but adipose tissue has several other metabolic and endocrine functions. Secretion of various adipokines is an important feature of adipose tissue. Adipokines, like cytokines, are signal molecules offer a communication channel between adipose tissue and other tissues (1, 8). These signal molecules are involved in inflammatory responses, blood coagulation, and certain adipokines also demonstrate endocrine-like, metabolism-modulating functions. Among the most studied adipokines are leptin and adiponectin. Leptin regulates energy intake and metabolic rate primarily by affecting the hypothalamic nuclei, resulting in an anorectic effect (1). Through binding to its receptors, adiponectin increase mitochondrial β-oxidation of FAs and cellular uptake of glucose via AMPK activation (9).

All adipocytes differentiate from mesenchymal stem cells, as illustrated for white adipocytes in **Figure 3**. This process is called adipogenesis and seems to peak during puberty, while it remains relatively steady throughout adulthood. In adults adipogenesis seems to take place to maintain the adipose tissue already generated, with an annual adipocyte turnover of 10 % (10). Adipogenesis is regulated by a series of transcription factors and signaling cascades. The terminal differentiation into mature adipocytes, expressing adipocyte specific genes, is stimulated by the activation of the transcription factors Peroxisome-Proliferator Activated Receptor (PPAR) γ, and in the CCAAT/Enhancer-binding protein (C/EBP) family (10).

The main type of adipose tissue in human adults is WAT. WAT is distributed throughout the body, but localization of the WAT seems to affect its metabolic functions. Visceral WAT surrounding internal organs is associated with inflammation and insulin resistance, which will be further described in **sections 1.4.1** and **1.4.2**

(10). Weight gain has been associated with initial increase in size of adipocytes (hypertrophy), with subsequent increase in adipocyte number (hyperplasia) in prolonged energy excess. However, the order of which these events occur are not yet clarified. Weight loss, on the other hand, is associated with reduced adipocyte size, but no effect on number has been observed (10). Small adipocytes seem to be more active in secreting adiponectin than larger, hypertrophied adipocytes. Hypertrophied adipocytes have been associated with increased generation of the pro-inflammatory cytokines such as Tumor Necrosis Factor α (TNF-α), Interleukin-6 (IL-6), and Monocyte Chemoattractant Protein-1 (MCP-1) (1, 11).

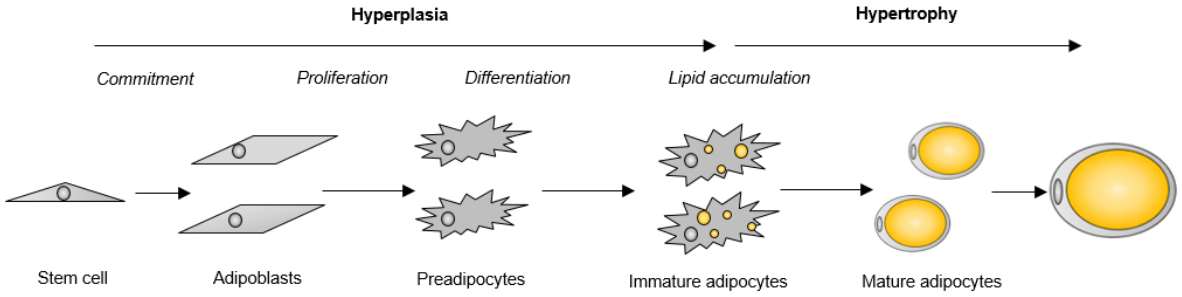

Figure 3: White adipocyte differentiation. Stem cells differentiate to white adipocytes upon commitment signals, leading to increased numbers of adipocytes (hyperplasia). White adipocytes continue to accumulate lipids and grow in size (hypertrophy) as excess energy requires storage.

1.2 Metabolic regulation

Different tissues have diverse metabolic needs according to their different roles in the body. Moreover, as previously implied, metabolism needs to change over time and adapt to the energy status and nutritional changes. This is a dynamic process regulated on different levels, which together ensures adequate metabolic homeostasis (1, 12). Short-term regulation of metabolism most often involves covalent modifications of enzymes, allosteric regulation, or translocation of enzymes and/or proteins within a cell. This type of metabolic regulation is mainly governed by hormones and other signal molecules acting through specific cellular receptors. Long-term regulation of metabolism involves hormonal regulation of gene expression through transcription, or regulation of protein synthesis through translational control. Additional levels of gene regulation through epigenetic histone modification and microRNAs also adds to the complex picture of metabolic regulation (1, 2, 12). Short-

term and long-term regulation of metabolism is frequently interconnected, and no definite line can be drawn between them (1, 2).

Controlling gene transcription seem to be the preferred mechanism for regulating protein levels, as no energy goes to waste generating useless gene products (2). Transcriptional regulation occurs over hours and days, in contrast to e.g. allosteric regulation which occurs in seconds to minutes. Transcription is the process where the cell copies a DNA sequence encoding a specific protein into a complementary messenger RNA (mRNA). This first step of gene expression is orchestrated by transcription factors and various co-factors. At the basal level we have general transcription factors which recognize core promoter elements, recruits RNA polymerase and initiates or prevent transcription. Specific transcription factors that bind various elements on DNA, so called recognition elements, often in response to different stimuli, ensures another layer of regulation. Along with co-factor complexes, acting as epigenetic modifiers and chromatin re-modellers, the transcriptional machinery provides exceptionally precise regulation of gene expression. The resulting mRNA molecules carry information needed for synthesis of specific proteins, through the process of translation (2).

1.3 Nuclear receptors (NRs)

Nuclear receptors (NRs) are ligand-activated transcription factors integrating various chemical signals, e.g. hormones and nutrients, to physiological responses through regulation of target genes. NRs are essential for regulation of metabolism, cell proliferation, cell differentiation and embryonic development, although the mechanisms of action differ among various NRs (13, 14).

The overall molecular structure is common for all NRs and illustrated in **Figure 4**. A NR consists of three major domains, specifically an N-terminal regulatory region (A/B), a central DNA binding domain (DBD) and a C-terminal ligand-binding domain (LBD) (13). The A/B region contains a transactivation domain termed activation function 1 (AF1) that vary between the various family members, but is often recognized by and interacting with co-factors and other transcription factors. The

DBD contain two zinc-finger motifs and are responsible for binding of the NRs to specific response elements on DNA. The LBD is a three-dimensional structure of 12 helices that, in addition to binding ligand, plays an important role in other NR functions, e.g. dimerization and ligand-dependent transactivation or -repression (13, 15). The latter is propagated through the second activation function, AF2, localized to the very C-terminus. The structure of DBD and LBD is well conserved between different NRs, but vary with respect to selective ligand recognition. For most NRs, the LBD is bound to corepressors in absence of ligand. Binding of ligand initiates a conformational change of LBD which disrupt binding of co-repressors and allow binding of co-activators. (13, 15).

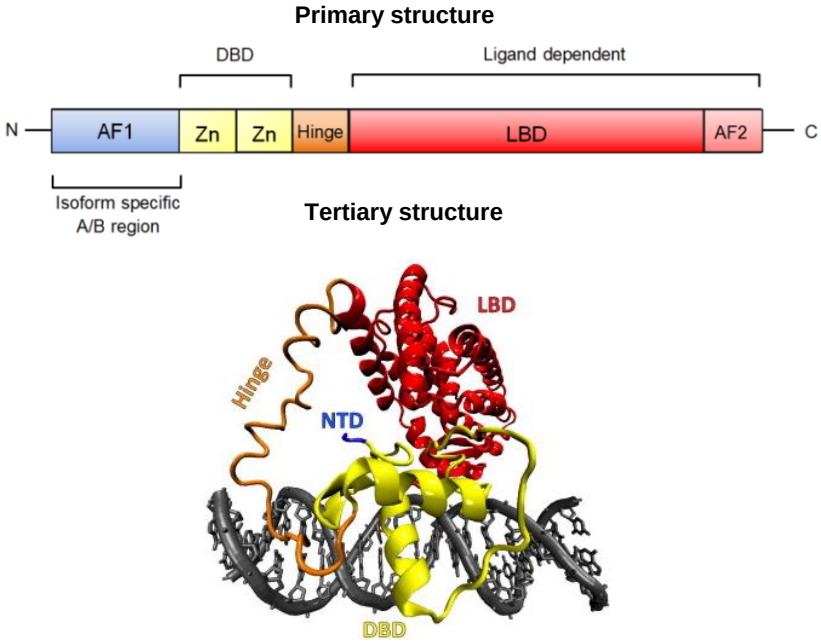

Figure 4: Illustrations of the general NR structure. AF1, activation function 1; AF2, activation function 2; DBD, DNA binding domain; LBD, ligand binding domain; NTB, N-terminal domain; Zn, Zinc fingers. Tertiary structure is reproduced from Aagaard et al. (14) with copyright permission.

Some NRs reside inside the cell nucleus awaiting ligand activation, while others translocate to the nucleus upon being activated by ligand. NRs form monomers, homodimers or heterodimers, and can regulate gene transcription by several mechanisms. Homo- or heterodimers complexed with co-activators and RNA polymerase bind response elements within regulatory regions of target genes (13). By such means, NR functions as transcriptional activators, i.e. transactivators, leading to upregulation of gene expression. NRs can also function as ligand-independent repressors and ligand-dependent transrepressors, leading to inhibition or down-regulation of gene expression. The mechanism of transrepression is not yet

fully understood, but it seems to involve NRs binding to non-conventional DNA response elements. Some NRs, e.g. Liver X Receptors (LXRs) and Reroxisome Proliferator-Activated Receptors (PPARs), also have the ability to bind to regulatory regions on target genes, co-repressors and/or other transcription factors in absence of ligand, and by such means repress transcription (15).

The NR transcriptional complexes can regulate transcription of target genes by binding to direct repeats, inverted repeats, or everted repeats on DNA (14, 16). Activating and repressing ligands, response element arrangements, and recruitment of co-factors represent different layers of control of NR activity. Dimerization, especially heterodimerization, adds another layer of control. As one or both of the dimerized NRs can bind ligand, the combined effect of availability and concentration of the ligands affects the total NR complex activity (13). Altogether, this results in a fine-tuned control of the organism's homeostasis.

1.3.1 Peroxisome proliferator-activated receptors

PPARs are NRs that regulate transcription in response to FAs and FA derivates, hence are they are considered as lipid sensors. The name Peroxisome proliferator-activated receptor (PPAR) is merely historical and relates to the discovery of the first PPAR, PPARα, and its induction of peroxisome proliferation in rodents. Later it has been determined that PPAR activation does not result in peroxisome proliferation in humans. PPARs bind Peroxisome proliferator-responsive elements (PPREs) on DNA. The PPRE consists of two direct repeats separated by one nucleotide (AGGTCA-N-AGGTCA) (17-19).

PPARs can be activated by endogenous ligands, such as fatty acids, intermediates or metabolites of fatty acids, like eicosanoids, exogenous ligands, such as dietary fatty acids, or synthetically engineered compounds (13). Upon activation by ligand, the PPARs heterodimerize with the retinoid X receptor (RXR). RXR function as heterodimerization partner for several NRs, including retinoid-acid receptors (RARs) and LXRs, in addition to PPARs (15). RXR exists in three isoforms, namely α, β and γ, which differs with respect to tissue distribution. Whether the isoforms exhibit different functions have not yet been clarified. The resulting PPAR:RXR heterodimer

binds to specific PPREs on DNA. Ligand binding causes a conformational change in the PPAR ligand-binding domain (LBD) that strengthens RXR binding, dissociate co-repressors, and recruits co-activators, ultimately resulting in initiation of gene transcription, as illustrated in **Figure 5** (13, 15). PPARs can also, as previously mentioned, repress target genes in absence of ligands, by binding PPREs in complex with RXR and co-repressors.

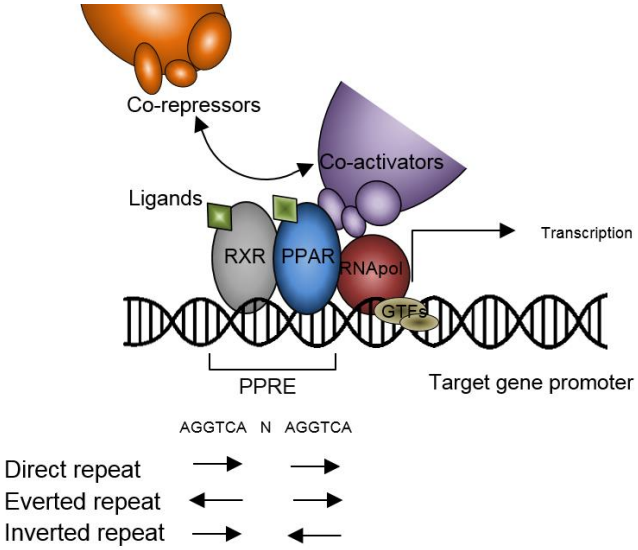

Figure 5: Simplified illustration of PPAR transactivation. PPRE, PPAR responsive element; GTFs, general transcription factors; RNAPol II, RNA polymerase.

The three PPAR isoforms identified in mammals, PPARα, β/δ, and γ, are encoded by *PPARA*, *PPARD* and *PPARG*, respectively. The PPAR isoforms differ with respect to tissue distribution, ligand preferences, and physiological roles. PPARα and PPARβ/δ mainly control energy expenditure, whereas PPARγ mainly control energy conservation. The PPARs control the expression of a broad network of genes involved in lipid metabolism, adipogenesis, inflammation, and overall maintenance of metabolic homeostasis (17). Therefore, disruption of PPAR signaling is often associated with metabolic and inflammatory disorders (5, 17, 20).

1.3.2 PPARα

PPARα is highly expressed in catabolically active tissues, such as liver, skeletal muscle and heart (21). PPARα activation by ligands results in lowered lipid levels in the circulation through increased expression of genes involved in FA oxidation and

hepatic uptake of TAG-rich particles. Studies using PPARα knockout mice have demonstrated that PPARα is indispensable for the regulation of genes encoding enzymes that are essential to meet the body's energy demands during fasting (22). PPARα also modulates genes involved in inflammatory pathways, with experimental studies suggesting that its activation attenuates several mediators of vascular damage, e.g. generation of ROS, and thrombosis (19). Among the PPARα regulated genes are *CPT1* and *CPT2*, encoding carnitine-palmitoyl transferases, and *ACOX*, encoding acyl-CoA oxidase, all involved in mitochondrial β-oxidation of FAs (23). Other PPARα regulated genes include *SCD1*, *FABP1*, and genes involved in HDL metabolism and synthesis of ketone bodies (19, 23). *SCD1* encodes stearoyl-CoA desaturase 1 involved in the conversion of saturated FAs to unsaturated FAs that can be incorporated in membrane phospholipids and TAG (24). *FABP1* encodes fatty acid binding protein in liver, essential for cellular uptake of FFAs (25). PPARα also regulates *UCP1* and other key components of thermogenesis in BAT (26).

PPARα have the highest affinity for unsaturated FAs of all the PPARs. Exogenous PPAR ligands provided by diet include arachidonic [ARA, 20:4(n-6)], linoleic [LA, 18:2(n-6)], and α- and γ-linolenic acids [ALA, 18:3(n-3), and GLA, 18:3(n-6), respectively] (27-29). Among the endogenous ligands for PPARα we find eicosanoids such as 8-Hydroxyeicosatetraenoic acid (HETE), leukotriene B4 (LTB_4) and prostaglandin A2 (PGA_2) (27). These eicosanoids are FA metabolites locally generated during inflammation through metabolism of arachidonic acid via cyclooxygenase (COX) and lipoxygenase (LOX) pathways, which indicates that PPARα may play a role in regulation of inflammatory responses (15). Oxidized LDL (oxLDL) has also been reported to activate PPARα (30). Synthetic PPARα ligands such as Pirinixic acid (PA, WY-14643) and various fibrates have been developed, originally as anti-hyperlipidaemic agents (27, 31).

1.3.3 PPARγ

PPARγ is highly expressed in white adipose tissue, the gastrointestinal tract and macrophages (20, 32). As of now, two isoforms of PPARγ have been identified in humans, i.e. PPARγ1 and PPARγ2, which differ with respect to tissue distribution.

While both isoforms are highly expressed in human adipocytes, PPARγ1 have been revealed as the dominant isoform in human skeletal myocytes (33).

PPARγ is essential for adipocyte differentiation, lipid accumulation in adipocytes, and activation of genes involved in lipid uptake and lipid metabolism. Among PPARγ-regulated genes we find *ADIPOQ*, *PLIN1* and *UCP1*, encoding adiponectin, perilipin 1 and UCP1 (20), whose physiological roles are presented in the previous sections. Other examples of PPARγ-responsive genes are *CEBPA* (34), *FABP4*, *LPL* and *CD36* (20). *FABP4*, often referred to as *aP2*, encodes FABP in adipocytes and macrophages, which is essential in cellular uptake of FFAs (25, 35). *LPL* encodes lipoprotein lipase, which is responsible for hydrolysis of TAGs in lipoprotein particles. *CD36* encodes cluster of differentiation 36, also known as fatty acid translocase, which is important in cellular uptake of long-chain FAs (1). *CEBPA* encodes CCAAT/Enhancer-binding protein α (C/EBPα), which is important in adipocyte differentiation and maturation. PPARγ activates C/EBPα, and vice versa in a cross-regulatory fashion controlling differentiation and maturation of adipocytes (36). PPARγ is hypothesized to stop cell proliferation and to terminate adipocyte differentiation when adipocytes are mature, an effect that may also apply to other cell types (32).

Among the exogenous PPARγ ligands that have been identified, we find several unsaturated FAs such as docosahexaenoic acid [DHA; 22:6(n-3)], ARA and ALA. Among the endogenous ligands for PPARγ are 9- and 13-Hydroxyoctadecadienoic Acids (HODEs), 15-HETE, oxLDL, 15-Deoxy-Delta-12,14-prostaglandin J2 (15-d-PGJ_2), and PGA_1 (15, 18, 30). As for PPARα, these endogenous ligands indicate that PPARγ also play a role in regulation of inflammatory responses (15). Several synthetic agonists have been developed throughout the years, such as the glitazones that will be discussed in the next sections.

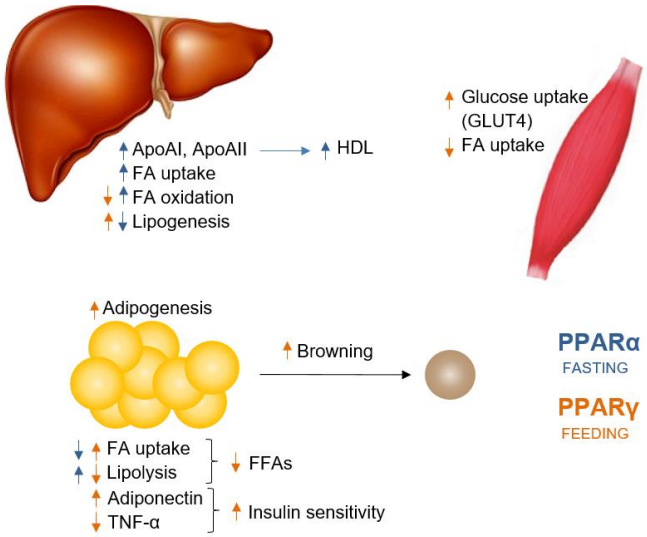

Figure 6: Metabolic effects of PPARα and -γ activation. PPARγ actions during feeding states, are represented by orange arrows. PPARα actions during fasting states, are represented by blue arrows.

1.4 Diabetes Mellitus

1.4.1 Background and definitions

Disruption of the metabolic homeostatic balance may lead to pathological conditions, commonly referred to as metabolic diseases. Diabetes Mellitus is a group of such metabolic diseases, characterized by prolonged, elevated blood glucose levels. The majority of diabetics are affected by the type 2 Diabetes Mellitus (T2DM), defined as a chronic disease that results from inefficiency of the body's utilization of insulin. The insulin resistance observed with T2DM could be due to defects in insulin action, secretion or both, and leads to hyperglycaemia (37-39). Prolonged hyperglycaemia brings about glycosylation of various cellular components. Therefore, untreated T2DM leads to micro-vascular and macro-vascular complications, e.g. nephropathy and cardiovascular disease, respectively (37).

Insulin resistance is defined as inadequate cellular responses to insulin. *Insulin deficiency* is defined as inadequate insulin secretion, and can be absolute or relative. Absolute insulin deficiency is seen in type 1 Diabetes Mellitus, an autoimmune disorder in which pancreatic β-cells are attacked and destroyed, leading to reduced or absent production of insulin. Relative insulin deficiency most commonly involves the pancreatic β-cells being stressed by prolonged excessive energy intake. The β-cells must continuously produce insulin in response to the increased blood glucose

levels. Eventually, the β-cells are exhausted. Simultaneously peripheral cells no longer respond properly to insulin. These metabolic disruptions are characteristic for T2DM, in which the patients very often suffer from a relative insulin deficiency in combination with insulin resistance (2, 37).

T2DM and is not an inherited disease, although increased prevalence is observed within families, and genetic predisposition may contribute to the development (37). Nevertheless, T2DM is closely associated with comorbidities such as overweight/obesity, cardiovascular disease (CVD), dyslipidaemia and hypertension (39, 40). In a newly published study it was reported that close to 80 % of patients with T2DM were overweight/obese (40). The strong risk factors of overweight/obesity, inactivity and unhealthy diet, can be modified through lifestyle changes (37).

1.4.2 Metabolic consequences

Clearly, when knowing the essential role of insulin in energy homeostasis, the lack of insulin and/or insulin response is an obvious driver disrupting several key metabolic processes. T2DM is recognized as a result of dysregulated energy metabolism initiated by prolonged status of excess energy (5). The main explanation of why obesity and T2DM are so strongly linked is outlined below, and the dysregulated pathways in the two disorders overlap in many aspects (**Figure 7**). So far, dysregulated pathways that has been linked to T2DM include adipokine signaling, inflammatory states and the PPAR pathway, all of which are also dysregulated in obesity (5).

Little or no BAT is associated with obesity, possibly caused by insulin resistance with subsequent apoptosis of brown adipocytes and/or damage of their progenitors (6). In most cases of obesity both adipose hypertrophy and hyperplasia is observed, as well as increased abdominal and visceral WAT depots (2). As previously mentioned, abdominal and visceral WAT depots are associated with larger influence on metabolic dysfunction than adipose depots elsewhere. An explanation to this may be that FFAs and signal molecules released from these depots enter the portal vein and have direct access to the liver where they may lead to increased hepatic synthesis of TAG (2).

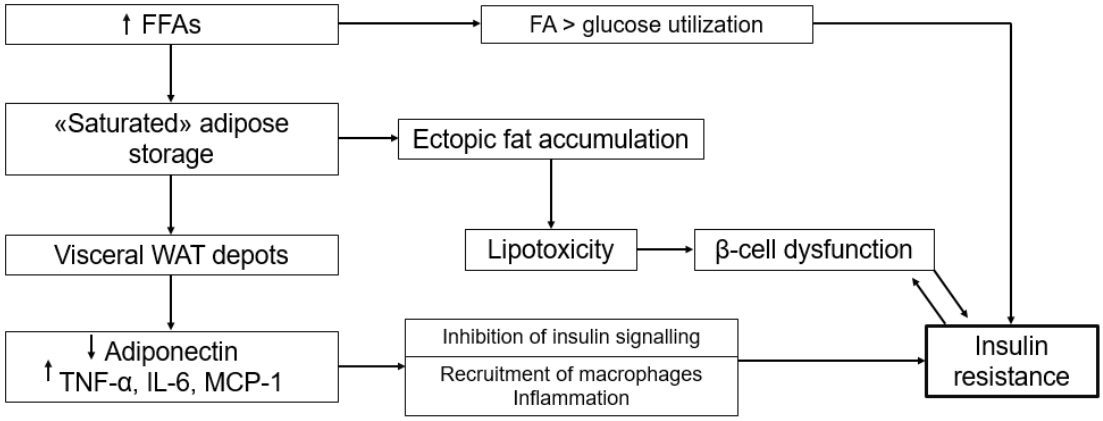

Figure 7: Simplified scheme for the pathophysiology of Type 2 Diabetes Mellitus.

Increased levels of FFAs in the circulation force the tissues in the body to utilize FFAs rather than glucose for energy production. Chronic hyperglycaemia induces pancreatic β-cell exhaustion, leading to T2DM. If the excess energy intake proceeds to an extent in which adipocytes ability to store TAG is exceeded, the excess FAs are stored in other tissues, such as muscle and liver. This ectopic fat accumulation is highly associated with insulin resistance. This is partly due to the lipotoxic effect of lipids stored in pancreatic β-cells, causing their dysfunction and apoptosis (1, 2, 20). Another aspect is that excess lipids can overwhelm the capacity of mitochondria to fully catabolize the FAs, and therefore lead to incomplete β-oxidation. Partially oxidized lipid metabolites are also associated with insulin resistance (11).

Chronic low-grade inflammation, as often observed accompanying obesity, is characterized by abnormal adipokine production and secretion, such as increased levels of leptin, resistin, MCP-1, TNF-α and IL-6. These factors favors inhibition of insulin signaling (5, 41). Normally, leptin production increases with increased adipose tissue, and the body respond with increased utilization of energy and decreased appetite. However, upon prolonged, exaggerated energy intake and increased adipose mass, the individual may develop resistance to leptin and so this important pathway for regulation of body weight is disrupted (2).

Another adipokine, adiponectin, inversely correlates to both obesity and insulin resistance, an effect that may partly be explained by adiponectin-induced AMPK activation (5, 9). AMPK activates cellular uptake of glucose through translocation of GLUT4. AMPK also inactivates acetyl-CoA carboxylase, leading to reduced malonyl-

CoA concentrations. As malonyl-CoA is an effective inhibitor of CPT1, the ultimate effect is increased mitochondrial β-oxidation of FAs in myocytes (42). Through these mechanisms, adiponectin contribute to insulin sensitization. Genetic factors has also been shown to contribute to adiponectin levels (9).

1.4.3 Current therapeutic approaches

The overall aims for the treatment of T2DM are symptom relief, and prevention and delay of complications. T2DM treatment includes lifestyle changes such as change in diet and physical activity, and medical therapy with anti-diabetic drugs. Anti-diabetic drugs currently used for T2DM management includes sulfonylureas, biguanides (e.g. metformin), meglitinides, dipeptidyl peptidase-4 inhibitors, α-glucosidase inhibitors, and the PPARγ agonists Thiazolidinediones (TZDs) (e.g. Rosiglitazone and Pioglitazone), commonly known as glitazones (43). Glitazones are highly specific PPARγ agonists, with no effect on other PPARs. Through activation of PPARγ, glitazones increase adipocyte proliferation and differentiation, and by such means, safely stores FAs in adipose tissue. Along with increased secretion of beneficial adipokines such as adiponectin, this brings about an insulin sensitizing effect of glitazones. However, PPARγ activation also increase body weight due to elevated rates of FA storage in adipose tissue (17, 20).

As T2DM often is accompanied by comorbidities such as hypertension, overweight/obesity, dyslipidaemia and CVD, treatment of these additional disorders must subsequently be provided. Lifestyle changes, including improved dietary composition, weight control and physical activity, is the recommended primary management. For individuals at high risk for developing CVD, and for whom lifestyle changes alone is not sufficient, medical treatment of comorbidities are often required. Therapeutical anti-obesity medication, anti-hypertensive medication, and lipid-lowering agents such as statins and fibrates are often useful in this context (44-46). Fibrates are fibric acid derivatives that have received a lot of attention due to their lipid-lowering and potentially insulin sensitizing effects. Fibrates are PPARα agonists, with marginal effects on other PPARs. Fibrates require high micromolar concentrations to activate human PPARα, and must therefore be provided in high

doses (300-1200 mg/day) in clinical use (47). Treatment with fibrates is reported to reduce elevated plasma TAG and LDL, as well as increase HDL (48). A number of previous studies have also reported an insulin-sensitizing effect with fibrates and other synthetic PPARα agonists (49-51).

1.5 The rationale behind the present project

Due to their role in metabolism and inflammation, PPARs are attractive targets for pharmacological intervention in conditions such as T2DM. Currently, several synthetic PPAR ligands, such as glitazones and fibrates, are in clinical use for the management of T2DM and related conditions (17). However, many of the medications used today often show adverse side-effects and are contraindicated for patients with specific comorbidities. As mentioned, drugs targeting PPARα must be administered in high doses, and side-effects of these drugs includes liver damage, myopathy and renal failure (52). Several of the drugs targeting PPARγ have been withdrawn from the market due to adverse side effects. Side effects such as increased cardiovascular risk, risk of pulmonary and macular edema, as well as weight gain have limited the use of glitazones in diabetic patients with high lipid levels and cardiovascular instabilities (17, 20). For example, the European Medicines Agency withdrew the approval of the PPARγ agonist Rosiglitazone (Avandia™, Avandamet™ and Avaglim™) in 2010 due to cardiovascular concerns (53, 54).

The prevalence of diabetes amounted to more than 415 million individuals in 2015 and is steadily increasing, with the majority affected by T2DM (39). Consequently, there is an urgent need for new, effective anti-diabetic agents which are able to overcome the limitations of the current therapeutic agents. In recent years, dual PPARα/γ agonists have been pointed out as a novel, interesting direction for the development of new anti-diabetic agents. By combining the effects of PPARα on lipid oxidation and PPARγ on lipid storage and secretion of beneficial signal molecules, an improvement of insulin resistance without the side-effects observed with each agonist alone, especially the PPARγ agonists, have been hypothesized (32).

The current project is a follow-up of the Anti-Diabetic Activity from Marine lipids (ADAM) bioprospecting project. The ADAM project is a collaboration between the

University of Oslo (UiO), the Arctic University of Norway (UiT) and the Arctic Biodiscovery Centre (ABC), formerly known as MabCent – SFI, aiming to develop a new generation of effective PPAR targeting anti-diabetic drugs with limited side effects. In 2014, two oxo-FAs were identified in the microalgae *Chaetoceros karianus* (55). These oxo-FAs, 9-oxohexadec-7-enoic acid [(7E)-9-OHE] and 9-oxohexadec-10-enoic acid [(10E)-9-OHE], exhibited modulatory effect on human PPARα and PPARγ. By nuclear magnetic resonance (NMR) spectroscopy analysis, the structures of the oxo-FAs were determined. These analyses revealed that the two oxo-FAs were isomeric and differed only in the position of one double bond (**Figure 8**) (55).

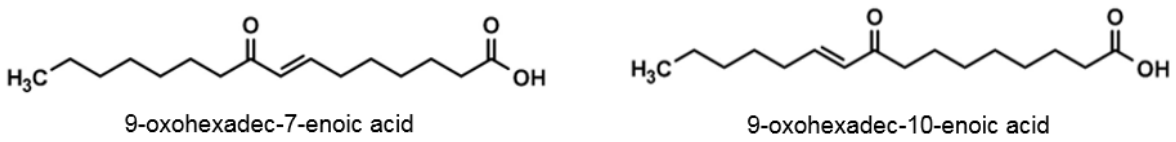

Figure 8: Chemical structures of the two isolated oxo-fatty acids Reproduced from Moldes-Anaya et al. (55) with permission from the authors.

The two oxo-FAs were synthetized in collaboration with the School of Pharmacy (UiO). *In vitro* cell studies revealed that the synthetic oxo-FAs exhibited the same activity-specificity profile as the natural compounds. However, they demonstrated cytotoxicity at or above the half maximal effective concentration (EC_{50}), which was not satisfying for proceeding with animal studies. Hence, a modified version of one of the most promising oxo-FA was designed and synthetized.

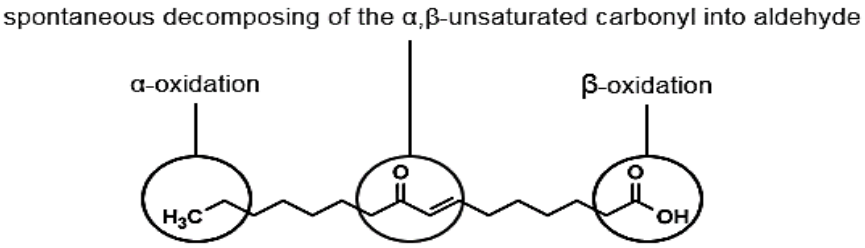

Figure 9: Areas of chemical modifications.

This synthetic oxo-FA analogue, hereby named ADAM1, was structurally stabilized in an attempt to decrease its cytotoxicity. Chemical modifications were made in the ketogroup to prevent spontaneous decomposing of the α,β-unsaturated carbonyl into aldehyde (**Figure 9**). Moreover attempts were made to introduce changes to the β-group and ω-end to prevent β- or ω-oxidation, respectively. *In silico* 3D modelling

were applied to predict molecular stability and PPAR binding activities. For future publishing and intellectual property reasons, the chemical formula for this first generation analogue cannot be presented here.

1.6 Aims of the present project

Prior *in vitro* analysis of the synthesized oxo-FAs showed a half maximal effective concentration (EC_{50}) in the 10^{-5} molar range, where the cytotoxic effects also began to appear. The new, modified analogue to be studied in the current project was hypothesized to be a potent dual PPARα/γ agonist exhibiting low cytotoxicity. By *in vitro* cell studies, ADAM1 was analyzed with respect to activation profile and specificity, cytotoxicity, effect of hepatic and adipocyte target genes, as well as effect on adipocyte differentiation.

The aims of the present project can be divided into three objectives:

1) Investigate the nuclear receptor agonist activity and specificity of ADAM1, particularly with respect to human PPARα and -γ.
2) Investigate the cytotoxic effects of ADAM1.
3) Explore the effects of ADAM1 on expression levels of a selection of PPAR target genes in hepatocytes and adipocytes, as well as on adipocyte differentiation.

Ideally, this analogue could serve as a “proof-of-principle”, showing that constructing analogues of these natural occurring oxo-FAs is the way to proceed to develop new, safe anti-diabetic drugs.

2 Methods

This section describes the laboratory techniques and procedures carried out in this project. Details about reagents, kits, equipment and software are listed in **Appendix I**, and preparation of buffers and reagents is outlined in **Appendix II**.

2.1 Mammalian cell culturing

Development of cell lines from a single cell enables continuous growth of cell cultures consisting of genetically identical cells. This is a valuable tool to study biological processes in a simplified model system. Immortalized cell lines are transformed through stable transfections or naturally occurring mutations or to evade cellular senescence and are therefore able to grow and divide for prolonged periods *in vitro* (56). Primary cells are, in opposition to cell lines, isolated directly from human or animal tissue and have a limited lifespan.

Three distinctive mammalian cell lines were used for the *in vitro* experiments of this project; COS1, HuH7 and SGBS. These cell lines are further described in the following **sections 2.1.1-2.1.3**. COS1 cells were used for the study of nuclear receptor activity and cytotoxicity assays. HuH-7 and SGBS cells were used in gene expression assays. SGBS cells were also used for the adipocyte differentiation assay with Oil Red O staining, described in **section 2.2**. All cells were cultured in disposable, sterile polystyrene culture flasks (Corning Inc., Falcon™). For down-stream applications to diverse assays, the cells were seeded in single-use sterile polystyrene culture plates (Corning Inc., Falcon™). Cell line work were under all circumstances executed in biological safety cabinets in the cell lab, where the working area was washed with ddH_2O and 70 % ethanol (EtOH) prior to use.

All mammalian cell lines undergo a growth cycle ending in a plateau phase where they either stop dividing or start to differentiate. The densities of cells are estimated by confluence level, which denotes the percentage of the culture vessel surface area covered by cells. If the cells are kept in the same environment, the culture medium will be exhausted, and the cells will decease. Therefore, once a cell culture is

initiated, it must be sub-cultured, or passaged, periodically to maintain growth. Most cell lines can undergo a limited number of sub-cultures determined by intrinsic factors regulating cell cycle and shortening of telomeres on the chromosomes (57). The sub-culturing process involves washing cells, detaching cells from the culture vessel using the proteolytic enzyme trypsin, and transfering cells in dilution to new vessels with fresh culture medium. The procedure for sub-culturing of the cell lines applied in the current project is described in **section 2.1.4**.

2.1.1 COS1

CV-1 cells are fibroblast cells derived from African green monkey kidney. The COS1 cell line is derived from CV-1 cells transformed by an origin-defective mutant of SV40 encoding wild-type large T antigen. The SV40 large T antigen is involved in promoting DNA replication and by such means make COS1 cells susceptible to uptake and incorporation of foreign DNA. COS1 cells are adherent and substrate dependent (58). In the current project, culture medium for the COS1 cells was composed by high glucose Dulbecco's modified Eagle's medium (Sigma-Aldrich, #D6546) enriched with 10 % heat-inactivated FBS (Sigma-Aldrich, #F7524), 4 mM L-Gln (Sigma-Aldrich, #G7513), and 50 U/mL penicillin/50 µg/mL streptomycin (Sigma-Aldrich, #P4458).

2.1.2 HuH7

HuH-7 is an immortal cell line commonly used as an *in vitro* hepatocyte model. The HuH-7 cell line was established by Nakabayashi et al. (59) in 1982 from cells derived from the hepatocellular carcinoma tissue of a 57 year old Japanese male. HuH7 cells are epithelial-like, adherent cells that typically grow in monolayers. They contain several mutations, such as a point mutation in p53 (59). In the current project, culture medium for the HuH7 cells was composed by high glucose Dulbecco's modified Eagle's medium (Sigma-Aldrich, #D6546), 10 % heat-inactivated FBS (Sigma-Aldrich, #F7524), 4 mM L-Gln (Sigma, #G7513), 50 U/mL penicillin/50 µg/mL

streptomycin (Sigma-Aldrich, #P4458), and ITS (10 ng/mL insulin, 5.5 ng/mL transferrin, 5 pg/mL selenium) (Sigma-Aldrich, #I3146).

2.1.3 SGBS

In 2001, Wabitsch et al. (60) established the human Simpson-Golabi-Behmel Syndrome (SGBS) pre-adipocyte cell line. This cell line was derived from subcutaneous white adipose tissue of a patient with SGBS. SGBS cells are neither transformed nor immortalized, and they show high capacity for adipocyte differentiation (60, 61). *In vitro* differentiated SGBS adipocytes are not distinguishable from human adipocytes differentiated in primary culture in regards of expression of adipocyte-specific genes and functional characteristics (60, 62). Therefore, SGBS cells compose a valuable tool for the study of adipocyte function and development in a human model (60).

Preparation of the different media for SGBS cultivation are listed in detail in **Appendix III.** Culture medium for SGBS cells was composed by Dulbecco's modified Eagle's medium/Nutrient Mix F12 Ham (Sigma-Aldrich, #D6421), 10 % non-heat inactivated FBS (Sigma-Aldrich, #F7524), 4 mM L-Gln (Sigma-Aldrich, #G7513), and 50 U/mL penicillin/50 µg/mL streptomycin (Sigma-Aldrich, #P4458), supplemented with vitamin mix of 8 mg/L biotin (Sigma-Aldrich, #B4639) and 4 mg/L D-pantotenate (Sigma-Aldrich, #P5155). To induce differentiation to adipocytes, SGBS cells were cultivated in culture medium without FBS (0F medium), supplemented with human 0.01 mg/mL apo-transferrin (Sigma-Aldrich, #T4382), 20 nM human insulin (Sigma-Aldrich, #I2643),0.2 nM triiodythyronine (Sigma-Aldrich, #T6397), 100 nM hydrocortisol (Sigma-Aldrich, #H0396), 500 µM IBMX (Sigma-Aldrich, #I5879) and 25 nM dexamethasone (Sigma-Aldrich, #D2915), with or without addition of a PPARγ agonist (25 µM ADAM1 or 2.0 µM Rosiglitazone (RSG, BRL-49653) (60).

2.1.4 Cell cultivation procedures

All cell lines used in this project were cultivated at 37°C in a humidified atmosphere of 5% CO_2 in air.

Procedure for sub-culturing of cells

The volumes and concentrations listed in the following procedure are appropriate for one 75 cm^2 (T-75) culture flask. For larger culture flasks, make adjustments correspondingly.

First, remove the culture medium from the culture flask. Carefully wash the cells twice with 5 mL PBS. Gently remove all fluid before trypsinizing the cells by adding 2.5 mL trypsin/EDTA. Incubate the cells at 37°C until they are almost detached (3-4 min for COS1, 1-2 min for HuH7, 2-3 min for SGBS). Knock the flask gently against your wrist to detach the rest of the cells. Add 7.5 mL culture medium containing FBS to inactivate trypsin. Sub-culture the COS1 and HuH7 cells 1:5 (2×10^6/T-75) or 1:10 (1×10^6/T-75), and SGBS cells 1:2.5 (0.8×10^6/T-75) or 1:4 (0.5×10^6/T-75), in new culture flasks, depending on the number of days before next sub-culturing. Adjust medium to 12 mL. Sub-culture the cells and/or renew the medium three times per week, and ensure cell concentrations are not exceeding 8×10^6 cells/T-75 (COS1/HuH7) or ~2×10^6 cells/T-75 (SGBS).

Procedure for thawing cells

Ampullas of cells are stored in liquid nitrogen (N_2) tanks. Before thawing cells, equilibrate 15 mL appropriate cell culture medium in a T-75 culture flask at 37 ºC and 5 % CO_2 for two hours. Thaw tubes of cells quickly in water bath (37 ºC). Transfer the fluid to the culture flask containing equilibrated culture medium. For SGBS cells, change the medium approximately 24 hours later to remove the DMSO.

Procedure for freezing cells

First, make freezing medium according to **Table 1**. Wash the cells with PBS and trypsinize as described previously. Count the cells as described in **section 2.1.5**, and calculate how many tubes to freeze. The concentration of cells should be 1×10^6 in 1 mL medium per ampulla. Spin down the cells at 1300 rpm for three minutes, and discard the supernatant. Re-suspend the cells in to a concentration of 1×10^6/mL in freezing medium. For SGBS cells, re-suspend the cells in medium 1 and add equal amount of medium 2 while mixing gently before aliquoting the cells in 1 mL per freezing tube.

Table 1: Freezing media

Cell line	Freezing medium composition
COS1	5 % DMSO, 95 % heat inactivated FBS
HuH7	5 % DMSO, 95 % heat inactivated FBS
SGBS	Medium 1: FBS-containing medium Medium 2: 90 % FBS-containing medium + 10 % DMSO

Freeze the cells for 24 hours in -80 ºC freezer using a cryogenic freezing container with isopropanol (-1 ºC/min). Do not move or disturb the cells before they are frozen. After 24 hours, transfer the ampullas of cells to the liquid N_2 storage tank.

2.1.5 Cell counting

To be able to sub-culture or seed cells at the desired concentrations, the cells must be counted in advance. A quick and simple method to count cells is to use an automatic cell counter such as Countess™ Automated Cell Counter (Invitrogen™). When Tryphan Blue Stain is mixed in 1:1 ratio to cell suspension, dead cells will absorb the blue staining. By such mean the automatic cell counter are able to distinguish between viable, un-stained cells and dead cells which are stained blue.

Procedure for cell counting

After trypsinization of the cells and addition of culture medium with FBS to inactivate the trypsin, make a representative aliquot of 30-50 µL for cell counting. Mix 10 µL of the cell suspension with 10 µL 0.4 % Tryphan Blue Stain solution (Invitrogen #T10282) in a 1.5 mL micro tube. Transfer 10 µL of the mixture onto a cell counting chamber slide and insert the slide into the Countess™ Automated Cell Counter (Invitrogen™). Through the microscope, the cells can be seen on the screen. Adjust the focus so that live cells are white and dead cells are clear blue before pressing count. The concentration of total, live and dead cells are displayed on the screen.

2.2 Adipocyte differentiation assay

The techniques described in this section were performed to assess the effects of ADAM1 on adipocyte differentiation in the SGBS adipocyte model.

In the current project, SGBS cells were seeded in 12-well plates in concentration of 0.8×10^5/1.5 mL culture medium with FBS, and incubated for 3 days. **Figure 10** outlines the experimental setup. The differentiation program was initiated by changing medium to differentiation medium (Quickdiff medium, Appendix III) supplied with either 0.1 % DMSO in combination with Bovine Serum Albumin (BSA), 25 µM ADAM1 in combination with BSA, or 2 µM RSG. From day 4, all cells were treated equally switching to a general serum-free adipogenic medium (3FC medium, Appendix III) that was changed every fourth day.

Cell lysates were collected for RNA isolation and Oil Red O staining before initiation of the differentiation program, and on day 4, 8 and 12 of differentiation. RNA was extracted from the cell lysates and utilized for cDNA synthesis with subsequent qPCR for gene expression analysis, as further described in **section 2.4**.

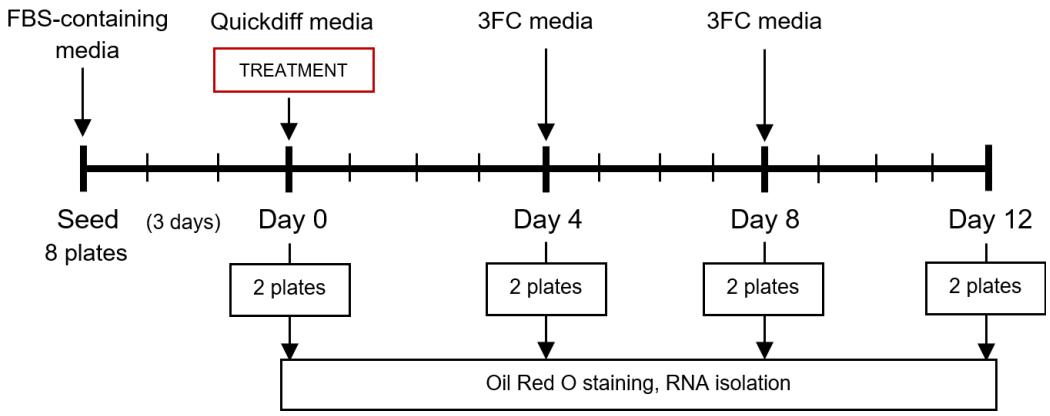

Figure 10: Flow-chart the adipocyte differentiation assay. Preparation of the various culture media is described in section 2.1.3 and Appendix III.

Procedure for differentiation of SGBS cells

Seed the cells in FBS-containing media on 12 well culture plates. Let the cells grow >95 % confluent before initiating the differentiation program. This increases the degree of differentiating cells substantially. To start the differentiation process, first remove all medium from the wells. Wash the cells carefully twice with 750 µL 0F medium. Prepare differentiation medium (Quickdiff, Appendix III) with preferred treatment agents and add 1.5 mL of this to each well. The cells are then incubated for 4 days before the procedure of washing and adding 3FC medium is repeated. The 3FC medium is thereafter replenished every 3-4 days for as long as the experiment persists.

2.2.1 Oil Red O staining

Oil Red O is a fat-soluble diazol dye which stains neutral lipids and cholesteryl esters, but not biological membranes. Oil Red O is minimally soluble in aqueous solutions, and the solubility is further decreased by dilution of Oil Red O in distilled water before appliance. The hydrophobic Oil Red O dye will therefore move from the solvent to hydrophobic environments and associate with lipids within cells or in tissue sections (63, 64).

Procedure for Oil Red O staining

Start by making a 0.5 % solution of Oil Red O (Sigma-Aldrich, #O0625) in 100 % isopropanol. This solution should be kept at 4 ˚C. Make a working solution of 60 % Oil Red O solution and 40 % dH_2O. Prepare the working solution prior to each staining, as precipitates will form during prolonged storage.

Prior to staining, the cells must be fixated to stabilize the cell structures. For cells grown in 12-well plates, carefully wash the wells once with 2 mL PBS before fixating the cells in 1 mL 4 % paraformaldehyde in PBS for 15 min. Wash the cells twice with 1 mL PBS, and twice with 1 mL dH_2O. Stain the cells by adding 0.8 mL Oil Red O working solution to each well and incubate at room temperature for 15 minutes. Oil Red O crystal complexes will form in the solution. Swirl the dish to get the complexes into the solution and off the cell layer. Wash off the Oil Red O solution by slowly adding dH_2O to the well with a pipette while swirling the plate. Remove the Oil Red O complexes in solution by using a vacuum suction. Try to avoid letting the Oil Red O crystals to come in contact with the cell layer. Continue to add dH_2O while removing the complex in solution. Do not drain the well completely until all unwanted crystals are removed. This will reduce the possibility that Oil Red O complexes attach to the cell layer. Finally, wash the cells with 1 mL PBS and store the cells in PBS at 4 ˚C.

The cells can now be inspected under a microscope. We took pictures using an Olympus CKX41 inverted microscope (Olympus®, #CKX41) with ColorView IIIu light microscope CCD camera (Olympus®) and cell* imaging software v.3.4 (Olympus® Soft Imaging Solutions GmbH). Before taking pictures, normalize the white balance in the software settings to a culture well without cells, filled with 1000 µL PBS. Use the same setup and colour settings for every picture taken. Take pictures within days after the staining, as the color will fade after a while. Do not let the samples dry out as this will change the shape of the stained cells.

2.3 Activity Assays

The techniques described in this section were performed to assess the NR agonist activity and specificity of ADAM1, as well ADAM1's ability to activate natural PPARα and -γ regulated promoters.

2.3.1 Transfection

Introduction of genetic material into mammalian cells is known as transfection. There are several methods for transfection (e.g. chemical transfection and electroporation). The method of choice depends on the type of cells and the purpose of the transfection, amongst other factors. All types of transfection can be broadly divided into two categories; stable or transient. Stable transfection is applied to enable introduced genetic material to persist in the cells and their progenies long-term, and it is therefore a beneficial strategy for studies of long-term effects of genetic alterations. In transient transfection, the introduced genetic material is not integrated into the genome, neither passed on to the next generation. The genetic material only exists in the cells for a limited period of time, and transient transfection are therefore useful in studies of shorter-term effects (65).

In the current project, COS1 cells were transiently transfected with DNA plasmids containing reporter and expression plasmids, in a dual-luciferase reporter assay system described in **section 2.3.2**. DNA plasmids and construction of them are described in further detail in **section 2.3.4**. Lipofectamine® 2000 reagent (Invitrogen, #11668-019) were used to facilitate delivery of DNA plasmids into COS1 cells. Lipofectamine is a cationic lipid with a positively charged surface that interacts with the negatively charged genetic material, forming a transfection complex. The positive surface charge of the cationic lipid allows fusion with the negatively charged cell membrane, and the transfection complex enters the cell through endocytosis. The cationic lipid also mediates DNA condensation and interactions inside the cell to facilitate further transport of the genetic material to the cell nucleus (66).

Procedure for transfection of COS1 cells

Seed the COS1 cells in enriched DMEM (with 10% FBS) in 24-well culture plates at a concentration of 0.7×10^5/500 µL per well. Incubate the cells for 24 hours. Inspect the cells under a light microscope to ensure the cultures have reached acceptable confluence, which for COS1 cells prior to transfection is 80-95 %.

Prepare mixes of DNA plasmids in 1:10 TE buffer appropriate for the experimental setup and purpose. The particular plasmids and the amount of them used in the assays of the present project are highlighted in **Table 2**. A full overview of the plasmids used in the current project is given in **Appendix IV**.

Table 2: Amounts of the DNA plasmids included in the nuclear receptor activity assays.

Ligand-dependent activation of NRs		
DNA plasmid		**Amount (µg)**
Reporter	pGL3-5XUAS-SV40	0.20
Effector	pSG5-GAL4-PPARα-LBD / -PPARγ-LBD / -hPPARδ-LBD / -LXRα-LBD / -LXRβ-LBD / -RXRα-LBD / pSG5-GAL4	0.10
Control	pRL-CMV	0.05
Total		**0.35**
PPAR/PPRE-dependent activation of natural promoters		
DNA plasmid		**Amount (µg)**
Reporter	pGL3-CPT1A-Int / pGL3-CPT1A-Int PPREmut pGL3-PLIN1-3'del / pGL3-PLIN1-3'del PPRE3mut	0.20
Effector	pCDNA3.1-hPPARα-FLAG / pCDNA3.1-hPPARγ2-FLAG	0.20
Effector	pCDNA3.1-hRXRα	0.20
Control	pRL-CMV	0.05
Total		**0.65**

Pre-warm DMEM (without FBS) in a 37 ˚C water bath, and equilibrate Lipofectamine at room temperature. Prepare a master mix of DMEM (50 µL/well) and Lipofectamine and pipet carefully up and down twice to mix. Incubate at room temperature for 5 min. For an optimal transfection complex use a DNA:Lipofectamine ratio between 1:2 and 1:3. Mix DMEM (50 µL/well) and DNA (Table 2) before adding the Lipofectamine master mix to the DNA suspensions. Incubate the mixtures at room temperature for 20 min. Add the transfection complex mixtures to the cells dropwise to avoid injuring the cells, and gently shake the culture plate to distribute evenly. Incubate cells for 4-6 hours at 37 ˚C. After 4-6 hours prepare PPAR agonists for the stimulation experiments. Dilute the agonists in DMSO and DMEM enriched with FBS to a final concentration of 0.1% DMSO. Add 50 µL of this treatment suspension per well,

dropwise. Incubate cells for 18-24 hours at 37 ˚C before collecting cell lysates for down-stream application as described in **section 2.4.1**.

2.3.2 Dual-Luciferase reporter assay system

The Dual-Luciferase reporter assay system is a bioluminescence reporter gene assay based on the use of luciferase reporters coupled to gene promoters of interest. The interactions between light-producing luciferases and its substrates lead to production of light that can easily be measured by a luminometer (67). In dual reporter gene assays, two individual reporters are included. An experimental reporter will correlate with the response of a specific treatment, while a co-transfected control reporter will function as an internal control of background response (68).

Luciferase is a light-producing enzyme found in different organisms, such as in firefly (*Photinus pyralis*), sea pansy (*Renilla reniformis*) and deep sea shrimp (*Oplophorus*) (67). The Renilla luciferase uses a different substrate than firefly luciferase, and the two can therefore be distinguished by the sequential provision of their substrates. This makes them suitable for a dual reporter assay. The two luciferase reactions are illustrated in **Figure 11,** and they both lead to photon production through chemiluminescence (67).

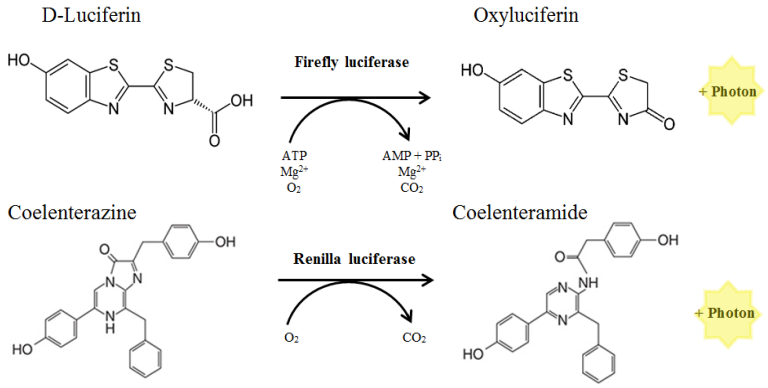

Figure 11: Simplified illustration of the firefly and renilla luciferase reactions. The luciferases' respective substrates and known co-factors are presented. Modified from (67).

The dual-luciferase reporter assay is performed by sequentially adding two reagents to each sample and measuring the luminescence following each addition. The first reagent contains a firefly luciferase substrate which activates the firefly luciferase

reaction, while addition of the second reagent quenches the firefly luciferase activity and initiate renilla luciferase activity (67).

In the curent project, cells were transfected with a pSG5-GAL4 empty vector expression plasmid, pSG5-GAL4 plasmids expressing Gal4 DBD fused to LBD of human NRs, a GAL4-responsive firefly luciferase (LUC) reporter, and a CMV-driven renilla luciferase (RLUC) co-reporter. The pSG5-GAL4 expression plasmid contains DBD of the yeast transcription factor Gal4, and a Simian virus (SV40) early promoter that together with other regulatory element ensures a strong transcription in mammalian cells. The Gal4-responsive LUC reporter contain five upstream activating sequences (5×UAS) that contains the cannonical binding sites for Gal4, not found in mammalian genomes. The GAL4-DBD-NR-LDB fusion protein will induce transcription of the reporter when the proper ligand is bound to the LBD. pSG5-GAL4 without any LBD will also bind UAS, but not activate transcription due to the lack of an activation domain. The RLUC co-reporter is driven by a cytomegalocirus (CMV) promoter ensuring constitutive expression of RLUC, which therefore function as an internal control of transfection efficiacy.

Procedure for measurement of luciferase activity

In the current project, the dual-luciferase reporter assays were performed using Dual-Luciferase® Reporter Assay System kit (Promega, #E1960). The firefly luciferase substrate, LARII, and the renilla luciferase substrate, Stop&Glo® reagent, supplied in the kit must be prepared according to manufacturer's manual (2009)(69) prior to assay application. The prepared substrates were kept in the dark in aluminum wrapped tubes. The prepared substrates can be stored at -20 °C for about a month.

After 24 hours of incubation, inspect the cells in a light microscope to ensure that the transfection or treatments had not affected cell numbers or viability in any way. Remove medium from the wells and wash the cells twice with 0.5 mL PBS. Remove all fluid from the wells before adding 100 µL passive lysis buffer (1x) per well. Passive lysis buffer (5x) is supplied in the kit and must be diluted 1:5 prior to use. Incubate the cell lysates on an orbital shaker for 15 minutes before transferring 30 µL

of the lysates to a 96-well white polystyrene microplate (Thermo Fischer Scientific, #136101).

Proceed with reading the plate on a plate reader. In the current project, we used the Synergy 2 Multi-Mode Reader (Bio-Tek® Instruments). This is a plate reader validated for use with the assay (5, 6), which also have reagent injectors. Before reading the plate, prime and purge the dispensers of the plate reader with ddH_2O. Prime both dispensers with 1.5 mL substrate. Read the plate using a protocol where the plate reader injects 30 µL of LARII to each well of the microplate, measure firefly luciferase activity, and then injects 30 µL of Stop & Glo® Reagent to each well of the microplate, and measure renilla luciferase activity. Apply a 2 second delay between adding of substrate and measurement of light, and a 10 second light integration time. Prime and purge the dispensers with 70 % EtOH and subsequently with ddH_2O after the reading.

2.3.3 Processing of activity data

Data was normalized through several steps using Excel. First, the firefly luciferase activity (LUC), in RLU, was divided by the background renilla luciferase (RLUC) activity, in RLU, to attain the relative luciferase signal. Then, data from different biological replicates were normalized to each other using a normalization factor. To identify the optimal normalization factors mean, SD, and relative standard deviation (RSDs) were calculated for all sets of data according to the following formula: RSD = SD / mean. The Solver Excel add-in was then applied to identify the normalization factors that would yield the lowest sum of relative standard deviations. Furthermore, sample means were normalized to their respective controls; vehicle/DMSO or Gal4 empty vector. The vehicle/DMSO and Gal4 sample means were set to 1.

2.3.4 DNA cloning

DNA plasmids are circular, extrachromosomal, double stranded DNA-molecules which occur naturally in prokaryotes, yeast and some higher eukaryotes. By recombinant DNA technology, DNA plasmids containing genetic information of

interest can be constructed by amplifying and cutting DNA from different sources using PCR and specific restriction enzymes, and joining the fragments with DNA ligase (70). Essential components of DNA plasmids are 1) a replication origin (ORI), 2) a drug-resistance gene, and 3) a multiple cloning site into which DNA fragments can be inserted. The ORI is a specific DNA sequence to which the host cell polymerases bind and initiate replication. This is crucial for the DNA plasmid to replicate. Apart from the essentials, plasmids contain additional elements depending on its type and experimental application (70).

DNA plasmids can be introduced to and replicated in a competent host through the process of transformation. Transformation is in this context a term used to denote the uptake of foreign genetic material in a host cell, causing replication of the foreign material by the host cell's own DNA replicating machinery. Depending on the purpose of the study, transformation can be used to produce large amounts of specific proteins, genetically modify the host, or to amplify DNA plasmids. The latter is the case in the current project.

Escherichia coli (*E. coli*) strains are commonly used for transformation because of its rapid growth rate and abilities to grow on chemically defined medium. During the exponential phase of its growth in rich medium, *E. coli* doubles every 20-30 minutes (71). The competent *E.coli* strains currently used for transformation of DNA plasmids are genetically manipulated to optimally replicate DNA plasmid. After an overnight incubation period on an agar dish containing the appropriate antibiotics, only the transformed cells containing the antibiotic-resistance gene will have survived and yielded colonies. Positive clones of the DNA plasmid can then be isolated and purified.

The majority of the DNA plasmids used in the current project (Appendix IV) were cloned and transformed at Department of Nutrition, University of Oslo during the period 2012-2017. Stock solutions were stored at -20˚C. The DNA plasmids were transformed using heat shock competent, ampicillin-resistant DH5α *E.coli*. Important features of the DH5α *E.coli* strain are mutations ensuring elimination of endonuclease activity and reduced homologous recombination (72). The pSG5-GAL4-DBD-hRXRα-LBD chimeric construct was cloned, transformed, and purified as a part of the current project, by the procedures described below.

Procedure for cloning and sub-cloning of DNA plasmid

Start with amplifying the desired plasmid insert using PCR. First of all, dilute PCR reaction solutions to appropriate concentrations. Mix 5.0 µL of the DNA template (5 ng/µL) with 2.5 µL forward primer (10 µM), 2.5 µL reverse primer (10 µM), 5.0 µL PfuUltra reaction buffer (10×) (Agilent, #600670), 2.5 µL dNTPs (10 mM), 1.0 µL PfuUltra II Fusion HotStart DNA Polymerase (2.5 U/µL)(Agilent, #600670), and adjust to a total volume of 50 µL with ddH_2O. PfuUltra II Fusion HotStart DNA Polymerase is a thermostable enzyme that catalyzes polymerization of nucleotides into DNA strand in 5´→3´ direction. Run the reaction mix on a thermal cycler. We used a Veriti™ 96 Well Thermal Cycler (Applied Biosystems™) following the program delineated in **Figure 12**.

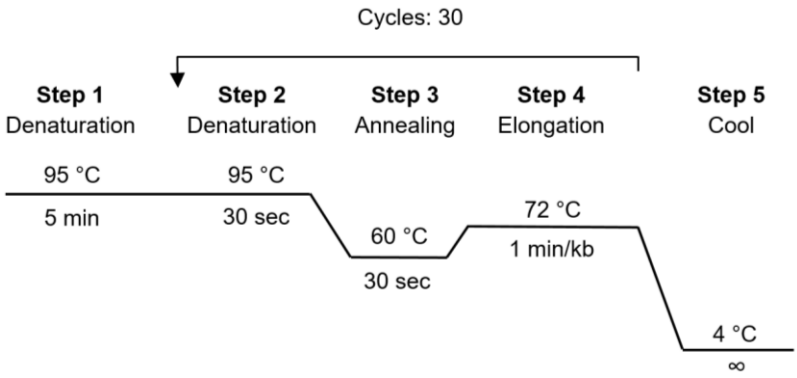

Figure 12: PCR amplification program. Kb, kilobase (1000 bp).

Verify that the PCR product has the correct size by running an aliquot on an agarose gel. Mix 5 µL of the PCR product with 15 µL ddH_2O and 5 µL loading dye. Run the PCR sample along with a DNA ladder (Invitrogen, #10787018) on an 0.8% agarose gel in TEA buffer at 100V for 30 min using Sub-Cell® GT Horizontal Electrophoresis System (Bio-Rad® laboratories, #1704401) and PowerPac™ Basic Power Supply (Bio-Rad® laboratories, #1645050). As DNA is negatively charged, it will migrate towards the anode. The procedure for preparation of agarose gels is described in further detail at the end of this section.

After verifying the PCR product, perform a PCR clean-up using the NucleoSpin® Gel and PCR Clean-up kit (Macherey-Nagel #740609) according to manufacturer's manual (2017)(73) with the following adjustment: Incubate for 1 min. when binding DNA before washing, and when eluting DNA after washing. Elute DNA in 25 µL 1:10

TE buffer and measure concentration on NanoDrop® ND-1000 spectrophotometer (NanoDrop Technologies).

Prepare the vector and PCR product for sub-cloning by cutting open the vector and trimming the ends of the template with appropriate restriction enzymes. Prepare the cutting reaction mixes of template/vector, restriction enzymes and buffers, and incubate for 2 hours at 37 ˚C.. The particular conditions used in this project are given in **Table 3**. Perform a new PCR cleanup of the trimmed template and opened vector as described earlier in this section and measure concentrations at NanoDrop® ND-1000. Store the samples at -20 ˚C until proceeding with ligation reaction.

Table 3: Cutting reaction of DNA template and DNA vector.

Reagents	Volume (µL)	
	Template	Control
Template (hRXRα-LBD)	23.0	
Vector (pSG5-GAL4) (10 µg)		10.0
SacII (New England Biolabs #R0157S)	2.0	3.0
KpnI (New England Biolabs #R0142S)	2.0	3.0
NEBuffer 2 (New England Biolabs #B7002S)	4.0	10.0
BSA (100×) (New England Biolabs #B9001S)	0.5	1.0
1:10 TE	8.5	73.0

Ligate the template into the vector using T4 DNA ligase (New England Biolabs #M0202S/L), T4-DNA ligase buffer and 1:10 TE. Set up ligation and control reaction in a total volume of 20 µL as outlined in **Table 4,** and incubate in room temperature for 30 min. Make sure to add the 3-5 fold molar excess of the insert using any online ligation calculator (e.g. http://2011.igem.org/Team:UT_Dallas/ligation)

Table 4: Ligation and control reactions.

Reagents	Volume (µL)	
	Ligation	Control
Vector (200 ng/ µL)	5	5
Insert (50 ng/µL)	10	-
T4-DNA ligase buffer (10×)	2	2
T4-DNA ligase	1	1
1:10 TE	2	12

Procedure for transformation

After the ligation the plasmid can be used to transform *E.coli* DH5α. First, thaw two tubes of competent DH5α on ice. Mix 5 µL of the ligation and control mix with 200 µL of bacteria each. Pipette up and down a few times before incubating on ice for 30 min. Heat shock the bacteria at 42 ˚C for exactly 90 seconds before cooling the tubes on ice for 2 min. Seed 50 µL of each bacterial suspension onto two separate LB plates with the appropriate antibiotics, in this case Ampicillin. Incubate over night at 37˚C.

Identification of positive clones

Pick colonies and re-streak on fresh LB-Ampicillin dishes. Incubate the dishes at 37˚C overnight before keeping them at 4 ˚C until proceeding with maxi preparation of plasmids. Inoculate and incubate 3 mL cultures of the same candidate clones at 37 ˚C, with shaking (250 rpm). Run mini plasmid preparations using the Nucleospin® Plasmid kit (Macherey Nagel #740588) according to manufacturer's manual (2015) (74). Measure the plasmid concentrations. For this, we used a NanoDrop® ND-1000 spectrophotometer. To verify that the clones picked have the desired insert, test cut them by mixing appropriate reagents. In the current project, we test cut by mixing 4.0 µL of the DNA (100 ng/µL), 1.0 µL SacII, 1.0 µL KpnI, 2.0 µL NEB-buffer 2 (10×), 0.2 µL BSA (100×) and adjust to a total volume of 20 µL with 1:10 TE.

Include uncut controls for all samples using a mix of 4 µL of the DNA and 16 µL 1:10 TE. Add 5 µL loading dye to each solution before loading the cut and uncut plasmids (25 µL) as well as a DNA ladder (15 µL) on 0.8 % agarose gel and perform electrophoresis in TAE buffer at 100V for 30 min.

Send off to two or three clones with the correct insert size for sequencing. In the current project, we sent off clones to GATC biotech for light-speed Sanger sequencing with the custom-designed pSG5-GAL4 forward and reverse primers. Prior to shipping, the guidelines from GATC must be followed. These include dilution of the plasmid DNA to 80-100 ng/µL, and mixing of 5 µL plasmid DNA and 5 µL

forward or reverse primer in 1.5 mL tubes. Based on sequence integrity, choose one positive clone for maxi preparation of the plasmid.

Maxi preparation of plasmids

Preform a maxi preparation of the positive clone using Nucleobond ® Xtra Maxi Plus kit (Macherey Nagel, #740416) according to manufacturer's manual (2016) (75). Start a bacterial culture with a volume of 200 mL. Inoculate the culture with bacteria from the re-streaked plates. Incubate overnight at 37 ˚C, with shaking (250 rpm).

Procedure for preparation of agarose gel

For a 0.8% agarose gel, mix 0.8 g agarose (Lonza, #50181) with 100 mL TAE in an Erlenmeyer flask. The higher agarose concentration, the better separation of small DNA molecules. Boil the solution for 3 minutes in a microwave oven. Pay attention to the solution and ensure it doesn't boil over. Cool the solution under running water to reach a temperature of about 70 ˚C. Add 10 µL SYBR™ safe DNA Gel Stain (Invitrogen™ # S33102) and gently swirl the flask until the solution is homogenous. Pour the solution into a gel tray and place a comb into the gel solution. Ensure the top of the well comb is above the fluid. Wait for about 20 min until the gel has polymerized before loading and running the samples in an electrophoresis cell.

2.4 Gene expression assays

The techniques described in this section were performed to assess the effects of ADAM1 on endogenous PPAR target gene expression in HuH7 hepatocyte and SGBS adipocyte models.

2.4.1 Total RNA isolation

As mRNA is the transcribed copy of DNA used for synthesis of proteins according to the genetic code, it provides information about which genes are expressed, that is, shall be transcribed to protein products. To analyze the genetic response of a cell or tissue to a specific treatment, RNA from the cell or tissue is extracted and purified. The isolated RNA is, through down-stream techniques, utilized to represent the gene expression of the cell or tissue.

Procedure for collection of cell lysates

Prior to RNA isolation, cell lysates must be collected from the cell cultures. First, inspect the cells in a light microscope and ensure preferred confluence level is reached. Prepare lysis buffer of 10 β-ME per 1 mL buffer RLT supplied in the RNEasy Mini kit (Qiagen, #74104). Remove medium and wash the cells carefully with 1 mL PBS. Remove all fluid before adding 400 µL of the lysis buffer per well. Scrape the cells off the plastic with a rubber cell scraper. Transfer the lysate to a 15 mL tube and homogenize by passing the lysate through a 21G cannula. Ensure no clumps are visible. If the lysates are not immediately used for down-stream applications, keep them frozen at -80 °C.

Procedure for total RNA extraction

Total RNA was extracted from cell lysates using the RNEasy® Mini kit (Qiagen® #74104) according to the manufacturer's manual (2011) (76, 77) with following modifications:

For samples with expected high fat content, add a high salt solution (prepared as described in Appendix II) in 70 % EtOH to the cell lysate in a 1:1 ratio and mix well by pipetting. Follow the steps for DNase digestion, and elute samples twice in 30-50 µL, depending on the expected RNA yield. Measure RNA concentrations on NanoDrop® ND-1000 spectrophotometer.

2.4.2 Complementary DNA (cDNA) synthesis

Reverse transcription is a process where an enzyme, reverse transcriptase (RT) generates complementary DNA (cDNA) from an RNA template. Primers are short DNA sequences that anneal to the RNA template and provide the RT enzymes with starting points for synthesis. Selection of primers for reverse transcription is dependent on type of experiment and setup, but in this case we used random hexamers (5'-NNNNNN-3'). The RT synthetize cDNA from the RNA template, resulting in one DNA:RNA hybrid.

Ribonucleases (RNAses) are nucleases catalyzing degradation of RNA. RNases are found in practically every cell type, bacteria and fungi. They are extremely stable and abundant in skin, hair, saliva etc. Therefore, precautions must be made when working with RNA to avoid degradation of the RNA by RNAses. Gloves must be worn at all times when working with RNA. All RNA work in the current project was carried out on a bench designated for RNA work, and the bench was washed with RNAse Away (Molecular BioProducts) prior to use.

Procedure for cDNA synthesis

The High Capacity cDNA Reverse Transcription Kit (AppliedBiosystems™ #4368814) was utilized to synthetize cDNA from extracted total RNA according to manufacturer's manual (2016)(78). This kit includes deoxynucleotides (dNTPs), random primers, RT buffer and MultiScribe RT.

Dilute the RNA samples to 50 ng/µL in 10 µL RNAse-free water, and preform the reverse transcription reaction in a total volume of 20 µL per reaction. Per RT reaction, include 2.0 µL RT Buffer (10×), 2.0 µL Random primers (10×), 0.8 µL dNTPs (100 mM), 4.7 µL RNAse-free dH_2O, and 10.0 µL RNA template.

Run the reverse transcription reaction in PCR strips on a Veriti™ 96 Well Thermal Cycler (AppliedBiosystems™) under conditions optimized for use with the High-

Capacity cDNA Reverse Transcription kit, as outlined in **Figure 13**. Store the cDNA at -20˚C until further use.

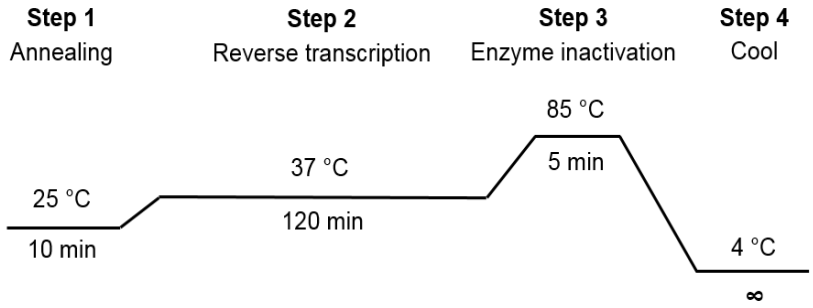

Figure 13: Reverse transcription protocol. Step 1-4 illustrates the reaction steps with the thermal cycling conditions.

In the current project, samples without reverse transcriptase (no RT) and without RNA (no template control, NTC) were included and run as cDNA/qPCR quality controls to reveal contamination of genomic DNA in the cDNA preparations or in any of the reagents used, as well as primer-dimer formation.

2.4.3 Quantitative Polymerase Chain Reaction (qPCR)

In a Polymerase Chain Reaction (PCR), copies of a DNA template are generated exponentially. Quantitative PCR (qPCR) is a method to detect and measure the generation of copies of a DNA product during each cycle of a PCR reaction. The products are directly proportional to the amount of template added to the reaction mixture. Primers for qPCR are short forward and reverse complementary oligonucleotides that can anneal to the gene of interest represented as cDNA. The primers direct the DNA polymerase enzymes to the starting point for synthesis of the given gene. Primers should be gene specific and if possible anneal to at least one exon-exon border. This will eliminate amplification of the same gene from genomic DNA. The primers used in this project was designed using Primer-BLAST from NCBI (https://www.ncbi.nlm.nih.gov/tools/primer-blast/), or by using primer sequences found in literature (**Appendix V**). Reverse transcription qPCR (RT-qPCR) is a common term used for the entire procedure from cDNA synthesis from isolated RNA by reverse transcriptase, to the qPCR reaction.

To measure the amount of amplified DNA, termed amplicons, in a qPCR reaction a reporter dye is applied. There exists many different reporter dyes for qPCR, but the common principle is that the amplicons are dyed, and a detectable signal is emitted when the molecules are excited by monochromatic light. The choice of reporter dye depend on experimental setup and compatibility with the qPCR instrument used. In the current project, SYBR Green® were applied as reporter dye. SYBR Green® is a fluorescent dye that binds double-stranded DNA molecules by intercalating between the DNA base pairs. Unbound SYBR Green® emits limited fluorescence, while binding of SYBR Green® to double-stranded DNA greatly enhances the fluorescent signal (79).

The endpoint for qPCR is the threshold cycle (Ct), which is a numerical value of the PCR cycle when the reporter dye signal crosses the threshold value in the exponential phase of amplification. The Ct is inversely related to the amount of amplicons in the reaction (80). To examine whether the signal from the reporter dye represents the DNA of interest, a melting curve can be applied in the end of a qPCR protocol. Melting curves are fluorescence plotted as a function of temperature, and will distinguish an amplicon with known melting temperature (Tm) from potential amplification artifacts that melts at other temperatures (79).

Procedure for qPCR

First, prepare a master mix corresponding to 5.0 µL KAPA SYBR® FAST qPCR Master Mix (2X) Universal (KAPA Biosystems, #KK4601), 2.3 µL ddH_2O and 0.1 µL of respectively forward (10 µM) and reverse (10 µM) target gene primers per qPCR reaction.

Pipette 7.5 µL from a given master mix into the wells of a PCR plate according to the experimental setup. Dilute cDNA samples 1:5 with qPCR water and pipette 2.5 µL of each cDNA sample into the corresponding wells of the PCR plate, using a multichannel pipette, so that the total volume per qPCR reaction is 10 µL. Remember to include the NTC and no RT control samples. Seal the PCR plate with an optical seal. Use a rubber spatula to remove bubbles from the cover and ensure the PCR

plate is tightly sealed around the edges. Spin down the PCR plate at 1400 rpm for 1 min. Run the qPCR reaction on a CFX96 Touch™ Real-Time PCR Detection Systems (Bio-Rad Laboratories), using a protocol suitable for KAPA SYBR® FAST qPCR Master Mix (2X) Universal, supplied by KAPA Biosystems (81), as outlined in **Figure 14.** To analyze the specificity of the qPCR reaction and identify potential primer-dimers, a subsequent melt curve analysis should be included.

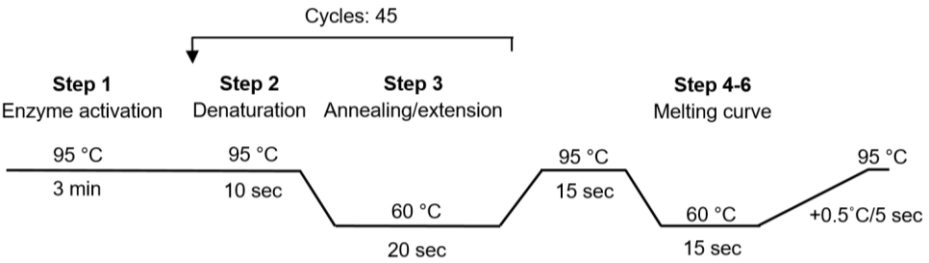

Figure 14: qPCR protocol. Step 1-3 illustrates the qPCR reaction cycle with the thermal cycle conditions, while step 4-6 shows the recommended melting curve analysis.

2.4.4 Processing of qPCR data

The qPCR data were normalized to the reference gene TATA-binding protein (TBP). The comparative threshold method ($2^{-\Delta\Delta Ct}$ method) was applied to calculate relative mRNA expressions levels. In this mathematical equation, ΔCt is the Ct of the target gene subtracted from the Ct of the reference gene, and ΔΔCt is the ΔCt of a given treatment or study object subtracted from ΔCt of the control. In this project the control samples refers to cells treated with vehicle/DMSO, or as for the adipocyte differentiation assay, cells at time zero. The relative amount of target gene mRNA in a sample is given by $2^{-\Delta\Delta Ct}$ (80). This will automatically set the control/T0 samples to 1. Ct > 32 were considered negligible expression, and Ct values exceeding 32 were set to 32.

2.5 Cell viability assays

Microculture tetrazolium assays are calorimetric assays that can be used to study cell death, proliferation and overall cell viability. Such assays are widely used in drug discovery studies. In the current project, effects of ADAM1 exposure on cell damage

and cell function was assessed using two microculture tetrazolium assays, namely LDH cytotoxicity assay and XTT-based cell viability assay. The principles of these methods are described in this section.

2.5.1 Lactate Dehydrogenase (LDH) Cytotoxicity Assay

Lactate Dehydrogenase (LDH) is an enzyme present in all cell's cytoplasm. LDH catalyzes the conversion of lactate to pyruvic acid. Upon damage of the plasma membrane, LDH is rapidly released into the cell culture medium. The LDH Cytotoxicity Assay is a calorimetric method for quantification of cell lysis and leakage, based on measurements of LDH activity in cell culture medium. The LDH activity is determined in this assay by two enzymatic steps. First, LDH-catalyzed conversion of lactate to pyruvate reduces NAD^+ to $NADH+H^{+.}$ Second, $2H^+$ is transferred from $NADH+H^+$ to a tetrazolium salt (INT) by a catalyst, diaphorase, and reduces the INT to a highly colored formazan compound. The reactions are illustrated in **Figure 15**. The formazan is water-soluble with an absorbance of 490 nm. The tetrazolium salt INT shows no significant absorption at this wavelength (82).

Rupture of plasma membrane with following leakage of LDH indicates that the cell is dead or dying, either from apoptosis or necrosis. LDH is relatively stable in culture medium, and an increase in LDH enzyme activity in the medium correlates with the amount of colored formazan formed during a given time period. Therefore, the colored formazan is proportional to the relative level of cell death.

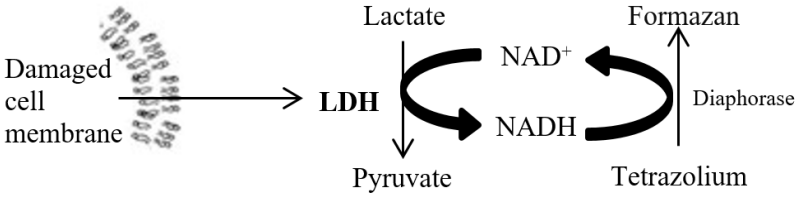

Figure 15: Principle of the LDH Cytotoxicity assay. LDH, Lactate Dehydrogenase.

Procedure for LDH Cytotoxicity Assays

In the current project, the LDH Cytotoxicity Assays were performed in COS1 cell media from the dose-response assays, using the Cytotoxicity Detection Kit (LDH) (Roche, #11644793001).

Half an hour prior to collection of the cell media, add triton X-100 to a final concentration of 2 % to two wells with untreated cells. This will lyse all cells and generate medium that can be used as a positive control. After 30 min. collect a minimum of 150 µL medium from all wells in separate, marked micro tubes and keep them refrigerated (4 °C) until the assay are to be run. Remember to also collect negative control samples (media from untreated, non-transfected cells). Spin down the cell media at 300×rcf for 10 min in room temperature. Pipet 90 µL dH_2O into the desired number of wells in a 96-well plate. Transfer 10 µL of each sample supernatant to the 96-well plates. Prepare the reaction mix of solutions supplied in the kit according to manufacturer's manual (2011) (82). Transfer 100 µL reaction mix to each well, and remove any bubbles using a cannula. Incubate the plate at room temperature for 20-25 min before measuring absorbance at 492 nm and 750 nm using Synergy H1 Hybrid Multi-Mode Microplate Reader (BioTek® Instruments).

Use the 750 nm measurements as reference controls for unrelated absorbance. Use the measured absorbance from the triton X-100 treated samples as positive control for maximal LDH activity from the cells used in the assay, and the absorbance of the untreated samples as negative control for spontaneous LDH release.

2.5.2 XTT-Based Cell Viability Assay

The XTT Cell Viability assay is a method based on measurements of active metabolic processes in viable cells. As illustrated in **Figure 16**, the intermediate electron acceptor Phenazine Methosulfate (PMS) accept electrons produced in trans-membrane electron transport of viable cells. PMS transfers electrons and reduces the XTT tetrazolium to the highly colored, water-soluble XTT formazan that can be measured at an absorbance of 450 nm (83, 84).

Because the electron transport chain is broken at cell death, the Ubiquinone cycle comes to a halt and XTT formazan can no longer be generated. The amount of XTT formazan generated is therefore a good measure of cell viability (84).

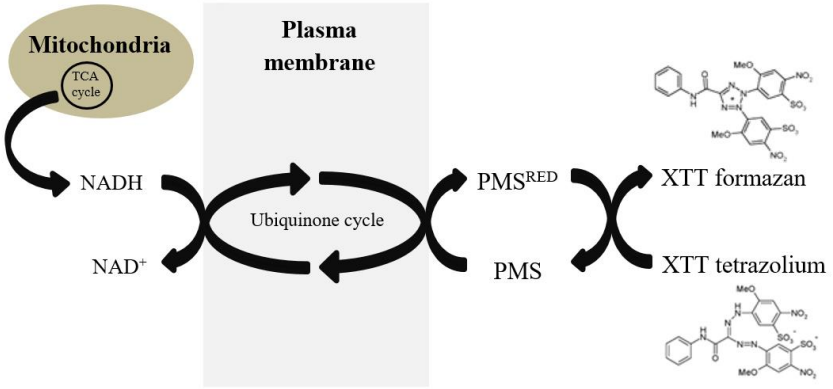

Figure 16: Principle of the XTT-based Cell Viability assay. PMS, Phezaine metosulfate.

Procedure for XTT-based Cell Viability Assays

In the current project, the XTT Cell Viability Assay was performed using the In Vitro Toxicology Assay Kit (XTT based) (Sigma-Aldrich, #TOX2-1KT).

On day one, COS1 cells were seeded in concentration 0.12×10^5/0.1 mL/well in a 96-well culture plate. Final cell number should not exceed 10^6 cells/cm^2, i.e. 3.2×10^5 cells/well (83). Incubate the cells at 37 ˚C for 24-30 hours. On day two, treat the cells with concentrations of ADAM1 with or without BSA, or DMSO with or without BSA for control, and incubate at 37 ˚C for 18-20 hours. On day three, thaw XTT-PMS and mix 5 mg with 5 mL PBS to yield a 1 mg/mL XTT-PMS solution. The XTT-PMS solution should be kept in a tube wrapped in aluminum foil to avoid exposure to light. Ensure the XTT-PMS is fully dissolved by warming the solution in a 56 ºC water bath. The solution should become clear before it is used. Add 28 µL (~20 % of culture medium volume) of the XTT-PMS solution to the wells and incubate at 37 ˚C for 4 hours. Measure absorbance at 450 nm and 690 nm using Synergy H1 Hybrid Multi-Mode Microplate Reader (BioTek® Instruments). Use the 690 nm measurements as reference controls for unrelated absorbance.

2.5.3 Processing of cell viability data

LDH Cytotoxicity data was first normalized against the 750 nm reference, positive and negative control using the equation below. By application of this equation, the positive control will correspond to 0 % and the negative control to 100 % viability.

Cell viability = 100 - $\left(\frac{\text{sample } \left(\frac{492\text{ nm}}{750\text{ nm}}\right) - \text{mean neg. ctrl } \left(\frac{492\text{ nm}}{750\text{ nm}}\right)}{\text{mean pos. ctrl } \left(\frac{492\text{ nm}}{750\text{ nm}}\right) - \text{mean neg. ctrl } \left(\frac{492\text{ nm}}{750\text{ nm}}\right)} \times 100 \right)$ (82).

XTT Cell viability sample means were normalized against the corresponding negative controls; DMSO or DMSO:BSA. The DMSO/DMSO:BSA samples were then set to 1, and all means were multiplied by 100 to obtain relative values as percent viable cells. Furthermore, the same procedure with multiplication with normalization factors, and RSD, as described in **section 2.3.3** was applied to normalize assembled data from the different biological replicates.

2.6 Statistical analysis

IBM® SPSS® Statistics (v. 24) and GraphPad Prism 6 was used for the statistical analysis and designing figures, respectively. Alpha levels were set to 0.05 for all analyses if not otherwise is specified. The distribution and variance of data analyzed by Shapiro-Wilk normality test, and Brown-Forsythe and Bartlett's test, respectively. For Gaussian distributed data with equal variances, statistical differences were analyzed using independent samples t-test, or one-way ANOVA with Bonferroni's correction for multiple comparisons. For non-Gaussian distributed data, the data was log-transformed to attain normality. If normality was not attained by log-transformation, statistical differences were analyzed using Mann Whitney U Test, or Kruskal-Wallis test with post hoc Mann Whitney U Test and Bonferroni's correction for multiple comparisons.

3 Results

3.1 Physicochemical properties of ADAM1

ADAM1 is a monounsaturated C16 fatty acid mimetic with an approximate molecular weight of 281.4 g/mol. In solid form, ADAM1 is a yellow wax. ADAM1 was not soluble directly in the water or DMEM, and formed oil and crystalloid phases of yellowish color in these aqueous solutions. By dissolving ADAM1 in DMSO, the solubility was increased. ADAM1 was soluble in 0.1 % DMSO up to concentrations of 100 µM. 1 % DMSO was sufficient for dissolving ADAM1 at concentrations above 100 µM. Cells treated with 1 % DMSO exhibited no difference in morphology compared to 0.1 % treated cells (data not shown), indicating these concentrations of DMSO is appropriate for facilitating solubility without affecting the cells directly.

3.2 Dose-response and cytotoxicity

In order to address the agonist activity and specificity of the ADAM1 compound we performed dual-luciferase assays with so-called Gal4 tethering constructs where the ligand-binding domain (LBD) of different human nuclear receptors (NRs) had been fused in-frame to the yeast Gal4 DNA-binding domain (DBD), enabling us to compare the ADAM1 agonist activity from different NRs on the same Gal4-responsive luciferase reporter.

The two marine oxo-fatty acids, (7E)-9-OHE, and (10E)-9-OHE, and parent compounds of the ADAM1 analogue, were prevously shown to have PPARα and PPARγ agonist activity (55). Therefore, the dose-response relationships of ADAM1 with respect to activation of human PPARα and -γ were analyzed in COS1 cells transfected with a plasmid expressing Gal4 DBD fused to human PPARα or -γ LBD, and a Gal4-responsive reporter. Surprisingly, the dose-response experiments revealed that ADAM1 activates PPARα with an EC_{50} value of 23 µM, while little or no activation of PPARγ was detected (**Figure 18**). For concentrations lower than 10^{-4} M ADAM1 displayed a sigmoidal dose-response curve with respect to PPARα agonist activity. However, with ADAM1 concentrations above 100 µM, a sudden decrease of PPARα activity was observed. In parallell with this decrease, we observed an

increased number of rounded cells, hovering just above the culture surface, as depicted in **Figure 17**.

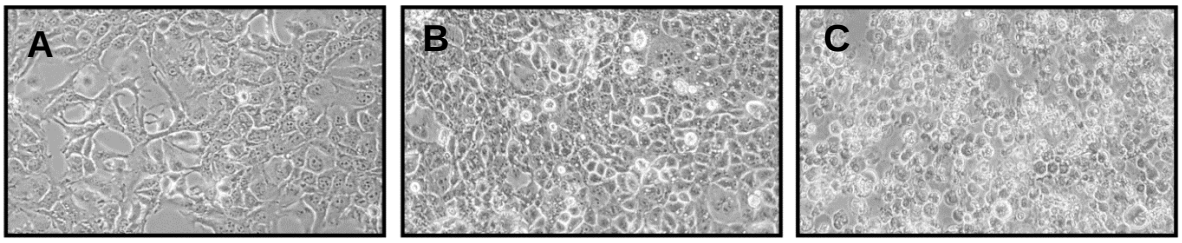

Figure 17: Microscopic photographs of COS1 cells. The pictures were taken after 18 hours treatment with (**A**) 0 M ADAM1; (**B**) 10^{-9} M ADAM1; (**C**) 10^{-3} M ADAM1. 10× enlargement.

Compared to (7E)-9-OHE and (10E)-9-OHE, no pronounced changes in efficacy of PPARα activation was observed with ADAM1 (**Table 5**). However, the ability to activate PPARγ seem to have dissappeared completely or been dramatically compromised due to the modifications made to the parent compound.

Cytotoxicity was analyzed in LDH and XTT based cytotoxicity/cell viability assays in COS1 cells. ADAM1 exhibited similar cytotoxicity as (7E)-9-OHE and (10E)-9-OHE, with a decreased cell viability starting in concentration of about 10^{-4} M (100 µM) (**Figure 19**). However, the reduction in cell viability appeared steeper with ADAM1 compared to (7E)-9-OHE and (10E)-9-OHE (previous studies; unpublished data). In the LDH assay, cell viability drops to around 60 % upon treatment with 10^{-3} M ADAM1, compared to just 90 % upon treatment with (7E)-9-OHE or (10E)-9-OHE in the same concentration (previous studies; unpublished data). Cell viability at ADAM1 EC_{50} were somewhat lower compared to cell viability at EC_{50} for the (7E)-9-OHE and (10E)-9-OHE (Table 5).

Table 5: PPARα/γ agonism and cytotoxicity of relevant compounds

Compound	PPARα agonism EC_{50} (µM)	PPARγ agonism EC_{50} (µM)	Viability at EC_{50} LDH (%)	Viability at EC_{50} XTT (%)
ADAM1	23.0	n/a	>95	80-85
(7E)-9-OHE[1]	20.0	10.0	>95	90-93
(10E)-9-OHE[1]	26.0	8.5	>95	85-90
PA	39.0	n/a	>95	>95
RSG	n.d.	0.2	>95	93

n/a, not available.

[1] unpublished data obtained from prior analysis and not as a part of the current project

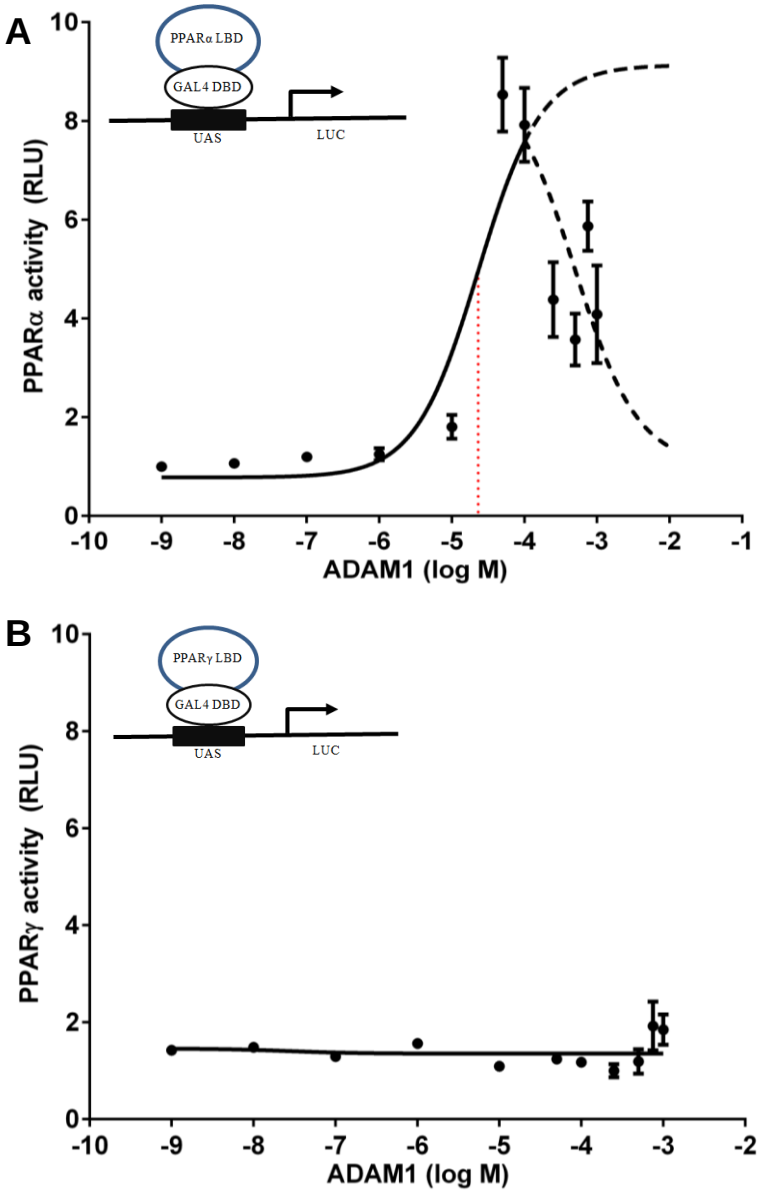

Figure 18: Dose-response curves. COS1 cells were transfected with a 5×UAS-driven LUC reporter, plasmids expressing Gal4 DBD fused to human PPARα or PPARγ LBD, and a CMV-driven RLUC co-reporter. The graphs show the dose-response relationship for ADAM1 with respect to human PPARα (**A**) and PPARγ (**B**) activity. The graphs represent relative luciferase activity normalized to DMSO control. The data represents three biological replicates analyzed in quadruplicates, presented as mean ± SEM. EC_{50} is indicated as a red, stapled line. RLU, Relative light units.

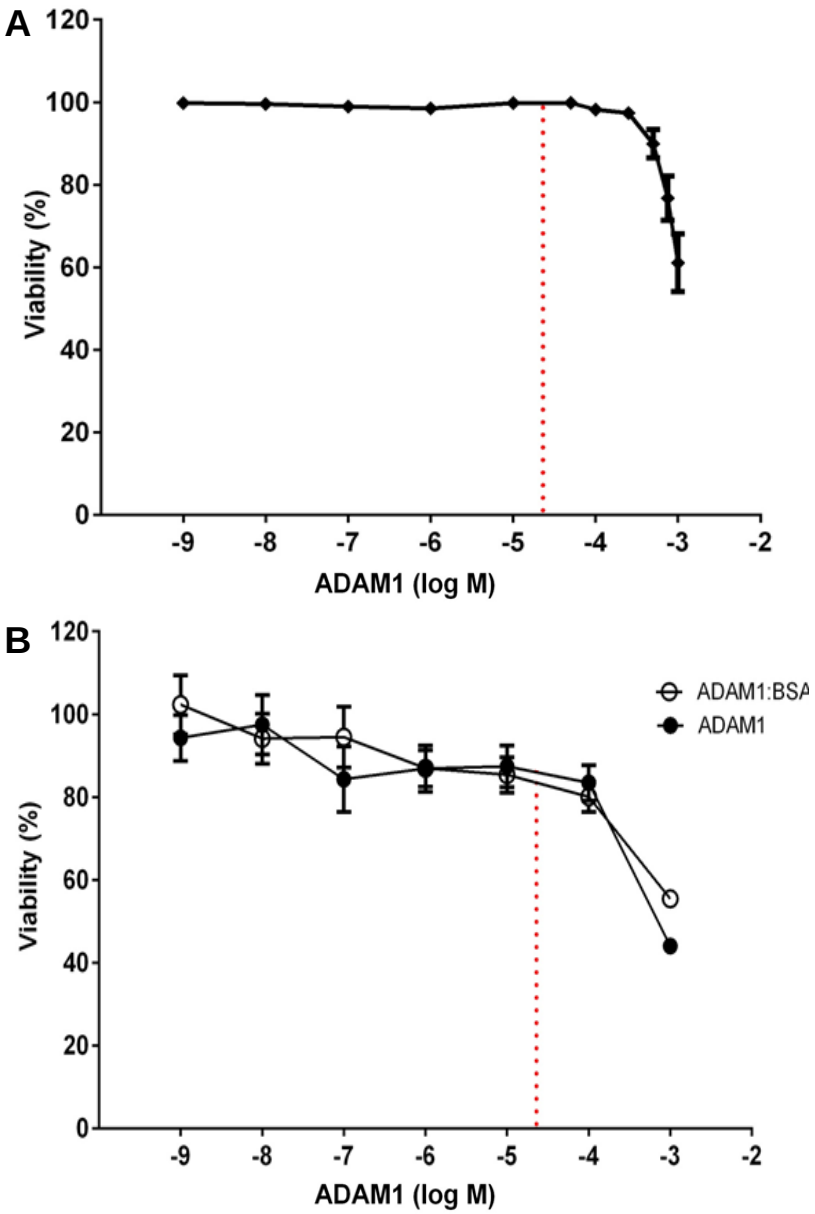

Figure 19: Effect of ADAM1 treatment on COS1 cell viability. The data is obtained by (**A**) measurements of LDH activity in media of COS1 cells treated with 10^{-3}-10^{-9} M ADAM1, 0.1/1.0 % DMSO, or 2 % triton X-100. The graphs represents mean percent viable cells ± SEM, normalized to untreated cells (negative control), triton X-100 treated cells (positive control) and respective DMSO controls. The data is representative for three biological replicates analyzed in quadruplicates. (**B**) Measurement of XTT-formazan formation in media of COS1 cells treated with 10^{-3}-10^{-9} M ADAM1 bound or unbound to 24 µM BSA, or 0.1/1.0 % DMSO bound or unbound to 24 µM BSA. The graphs represents mean percent viable cells ± SEM, normalized to respective DMSO or DMSO+BSA controls. The data is representative for three biological replicates analyzed in duplicates. EC_{50} for PPARα activation are presented as red, stapled lines.

3.3 Cloning of a GAL4-RXRα-LBD expression construct

After examining the agonist activity of ADAM1 with respect to PPARα and -γ, we also wanted to address the ability of ADAM1 in activating other nuclear receptors. Prior to this work the catalogue of Gal4-LDB fusion plasmids in the lab included human PPARα, -δ and -γ, as well as human LXRα and -β. These constructs had been used for the bioprospecting campaign. To increase the diversity, we decided to sub-clone human RXRα LBD into the GAL4-DBD expression plasmid pSG5-GAL4. RXRα LBD was amplified from the template plasmid (pCDNA3.1-hRXRα) using specific primers. To confirm whether the PCR amplification was successful, the PCR product was separated by electrophoresis on agarose gel and visualized using SYBR-safe. The electrophoresis resulted in one DNA fragment of size between 650 and 850 bp, corresponding to hRXRα-LBD which should have the size of 795 bp (**Figure 20**).

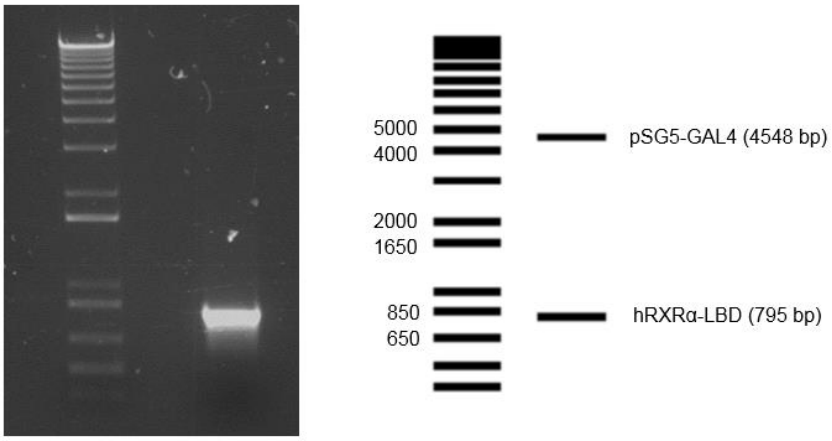

Figure 20: Verification of PCR product on agarose gel. The product of PCR amplification of human RXRα LBD from a pCDNA3.1-hRXRα template was verified on 0.8 % agarose gel. The standard reference is modified from restriction analysis of pSG5-GAL4-hRXRα-LBD cut with SacII and KpnI, using Serial Cloner v.2.5 (Serial Basics).

After trimming of the hRXRα-LBD using the restriction enzymes SacII and KpnI, the PCR product was sub-cloned into the pSG5-GAL4 vector using the same enzymes, and transformed in *E.coli* DH5α. Similar colony growth was observed on both ligation reaction plate and control plate, and six colonies were selected for plasmid mini preparation. These six plasmid clones were test cut with SacII and KpnI and verified on agarose gel.

Upon test cutting with SacII and KpnI, two plasmid clones yielded two fragments of approximately 800 bp and 4500 bp, corresponding to hRXR-LBD (795 bp) and pSG5-Gal4 vector (4548 bp), respectively (**Figure 21**). The remaining plasmid clones showed only one fragment of 4548 bp in the double cut reaction, indicating that the ligation of hRXRα-LBD into the pSG5-GAL4 vector had been unsuccessful for these clones. The two positive plasmid clones were sent for sequencing, and both showed 100% sequence identity in the coding region. Plasmid clone number 2 were chosen for maxi preparation and its sequence chromatogram is given in **Appendix VI** aligned to the pSG5-GAL4-hRXRα-LBD plasmid between bp position 1500- 2300, covering the full open reading frame.

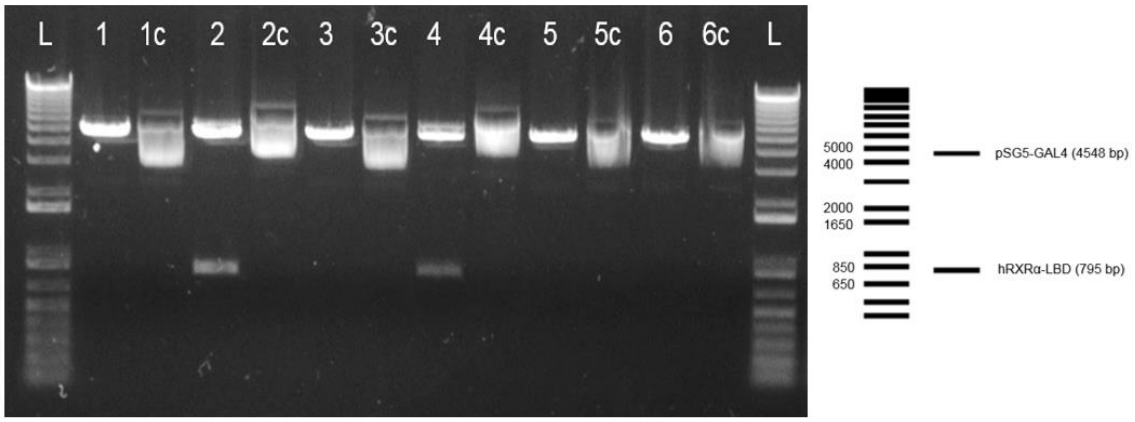

Figure 21: Verification of DNA plasmid clones on agarose gel. hRXRα-LBD was cut with SacII and KpnI, sub-cloned into pSG5-GAL4 vector, and transformed in E.coli DH5α. After mini preparation of the clones, the plasmids were test cut with SacII and KpnI and verified on 0.8 % agarose gel along with uncut plasmids for control. Numbers designate the ID for plasmids isolated from separate colonies. L, ladder; c, uncut plasmid. The standard reference is modified from restriction analysis of pSG5-GAL4-hRXRα-LBD cut with SacII and KpnI, using Serial Cloner v.2.5 (Serial Basics).

In order to validate the function of the cloned pSG5-GAL4-hRXRα-LBD, its response to a known RXRα agonist, 9-cis Retinoic acid (9-cis RA) was analyzed in COS1 cells transfected with a plasmid expressing Gal4 DBD fused to human RXRα LBD, and a Gal4-responsive reporter. A 9-cis Retinoic acid-dependent activation of hRXRα was observed, while no activation was observed with DMSO or with the Gal4 empty vector (**Figure 22**).

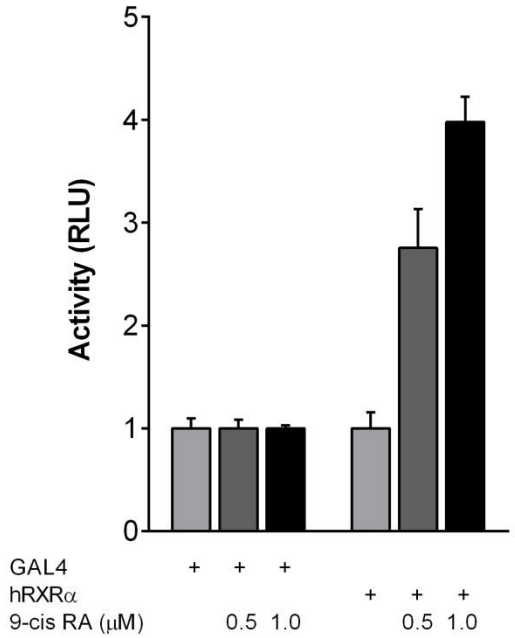

Figure 22: Human RXRα-specific transactivation by 9-cis Retinoic acid. COS1 cells were transfected with a 5×UAS-driven LUC reporter, plasmids expressing Gal4 DBD empty vector or fused to human RXRα LBD, and the CMV-driven RLUC co-reporter. For 18 hours, the cells were treated with 9-cis Retinoic acid (RA) dissolved in 0.1 DMSO, while 0.1 % DMSO was used as control. The columns represents relative luciferase activity normalized to DMSO controls, presented as mean ± SD. Cells transfected with Gal4 empty vector, as well as DMSO controls were set to 1. The data represent one biological replicate analyzed in quadruplicates. RLU, Relative light units.

3.4 Specificity

We could now analyze this NR specificity of ADAM1 in COS1 cells transfected with plasmids expressing Gal4 DBD fused to different NR LBD, and a Gal4-responsive reporter. The concentrations of ADAM1 applied in this experiment were chosen based on the empirical EC_{50} values determined previously (Figure 18). As expected, human PPARα activity was significantly induced upon ADAM1 treatment both with 25 µM and 50 µM compared to DMSO control (**Figure 23**). Human PPARγ activity was also significantly induced upon ADAM1 treatment of 25 µM (p=0.021) and 50 µM (p=0.034). However, the fold induction of hPPARγ was minimal compared to that of hPPARα (Figure 23). None of the other NR-LBD fusion proteins were activated by ADAM1 under these conditions and concentrations.

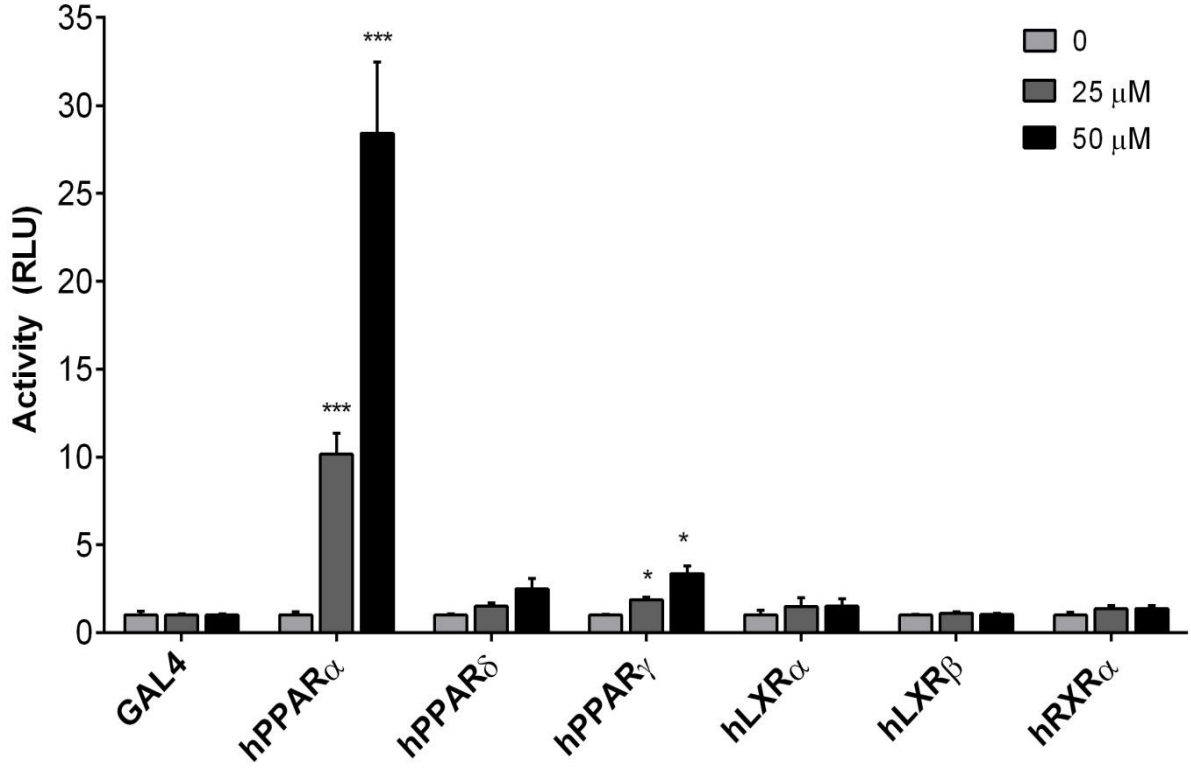

Figure 23: Nuclear receptor-specific transactivation by ADAM1. COS1 cells were transfected with a 5×UAS-driven LUC reporter, plasmids expressing Gal4 DBD empty vector or fused to LBD of human PPARα, PPARδ, PPARγ, LXRα, LXRβ or RXRα, and a CMV-driven RLUC co-reporter. For 18 hours, the cells were treated with 25 or 50 µM ADAM1 dissolved in 0.1 % DMSO, while 0.1 % DMSO was used as control. The columns represents relative luciferase activity normalized to DMSO controls, presented as mean ± SEM. Cells transfected with Gal4 DBD empty vector, as well as DMSO controls were set to 1. The data represents six biological replicates analyzed in quadruplicates for Gal4 and hPPARα, and three biological replicates analyzed in quadruplicates for the remaining NRs. RLU, Relative light units. *p≤ 0.05, ***p≤ 0.001 compared to DMSO control.

The *in vitro* cell-based reporter assays revealed that ADAM1 behaves as a specific PPARα agonist (Figure 18 and 23). Therefore, the potency of ADAM1 with respect to activating PPARα at EC_{50} was compared to the potency of a known PPARα agonist, Pirinixic acid (PA, WY-14643). The results presented in **Figure 24** demonstrate that ADAM1 result in approximately 2.5-fold greater PPARα activity compared to PA in both 25 and 50 µM. These differences are significant with p=0.011 and p=0.040, respectively.

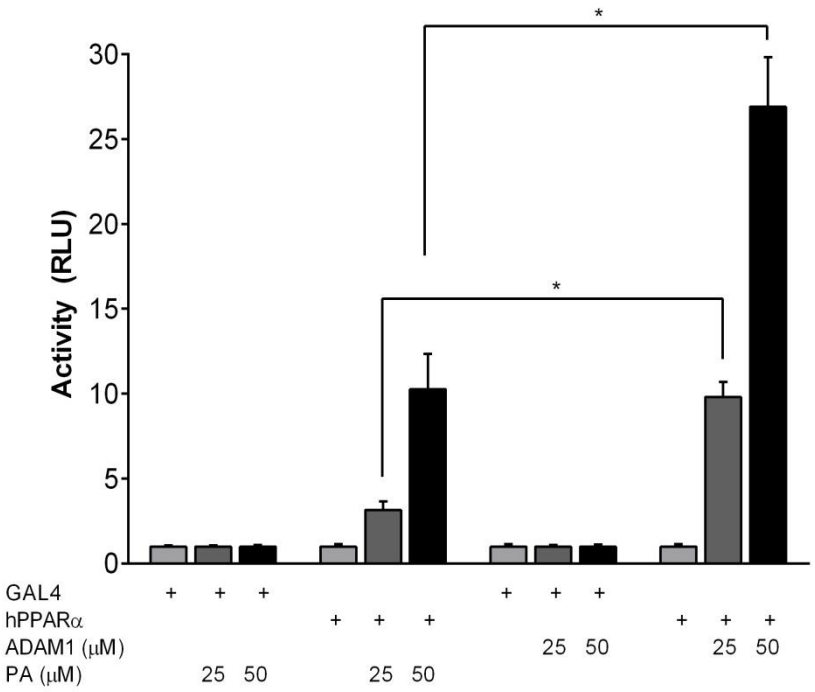

Figure 24: Human PPARα transactivation by PA and ADAM1. COS1 cells were transfected with a 5×UAS-driven LUC reporter, a plasmid expressing Gal4 DBD fused to LBD of human PPARα, and a CMV-driven RLUC control reporter. For 18 hours, the cells were treated with 25 or 50 µM ADAM1 or PA dissolved in 0.1 % DMSO, while 0.1 % DMSO was used as control. The columns represents relative luciferase activity normalized to DMSO controls, presented as mean ± SEM. Cells transfected with Gal4 DBD empty vector, as well as DMSO controls were set to 1. The data represents four biological replicates analyzed in quadruplicates for PA, and six biological replicates analyzed in quadruplicates for ADAM1. RLU, Relative light units. *p≤ 0.05, adjusted for multiplicity

3.5 Activation of natural promoters

To evaluate the ability of ADAM1 in activating natural PPARα and PPARγ-regulated promoters, COS1 cells were transfected with LUC reporters driven by the human *CPT1A* promoter or *PLIN1* promoter for PPARα and PPARγ-mediated activation, respectively. The *CPT1A*-reporter contained an intronic PPARα-responsive promoter (bp position +2290 to +5110 relative to TSS), while the PLIN1-reporter contained the PPARγ-responsive proximal promoter (bp position -3918 to +231 relative to TSS). Both reporters came in two flavors; either as wild-type with functional PPREs, or mutated PPREs with non-functional recognition elements. The *CPT1A*-driven reporters (pGL3-hCPT1AInt and pGL3-hCPT1AInt-PPREmut) were gifts from Prof. Diego Haro and has been described previously (85), while the *PLIN1*-driven reporters (pGL3-hPLIN1-3′del and pGL3-hPLIN1-3′del-PPREmut) were constructed at Dept. of Nutrition, University of Oslo, as previously reported by Dalen et al. (86). To be able to activate these reporters the COS1 cells were transfected with full-length human PPARα or -γ and their required heterodimerization parther RXRα.

Cells transfected with full-length human PPARα and RXRα, along with the *CPT1A*-driven wild-type reporter induced transcription 2.5-fold when treated with ADAM1, compared to cells that were not transfected with PPARα ($p<0.001$), or cells that were not treated with ADAM1 ($p<0.001$) (**Figure 25A**). This transactivation was not seen with the PPRE-mutated reporter. Together these results indicate that ADAM1 activates full-length human PPARα in a ligand and PPRE-dependent fashion.

Cells transfected with full-length human PPARγ and RXRα, along with the *PLIN1*-driven reporter with functional PPRE induced a minor signal upon ADAM1 treatment (**Figure 25B**). However, this induction did not differ significantly from the gene induction seen in cells transfected with PPRE-mutated reporter, not transfected with PPARγ or not treated with ADAM1, indicating that ADAM1 do not activate full-length human PPARγ.

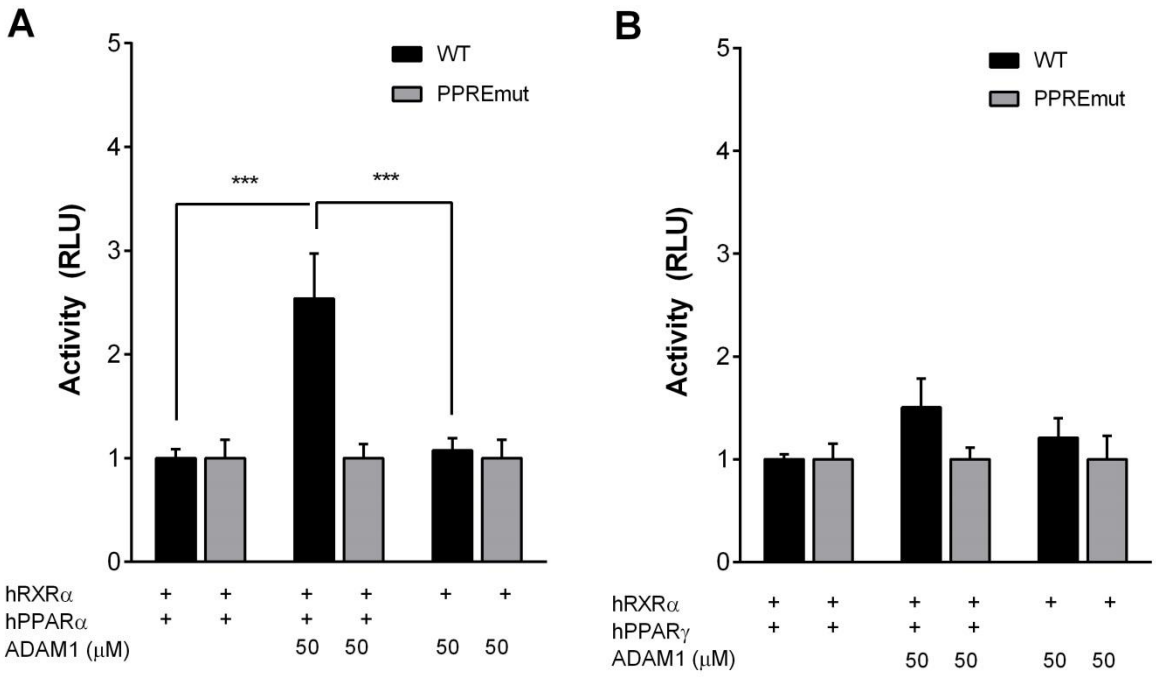

Figure 25: Activation of natural PPARα and -γ regulated promoters by ADAM1. COS1 cells were transfected with plasmids expressing **(A)** full-length hPPARα, the heterodimerization partner hRXRα, a *CPT1A*-driven reporter, as wild-type or with mutated PPRE, and a CMV-driven RLUC co-reporter, or **(B)** full-length hPPARγ, hRXRα, a *PLIN1*-driven reporter, as wild-type or with mutated PPRE, and a CMV-driven RLUC co-reporter. For 18 hours, the cells were treated with 50 µM ADAM1 dissolved in 0.1 % DMSO, while 0.1 % DMSO was used as control. The columns represents relative luciferase activity normalized to DMSO controls, presented as mean ± SEM. Cells transfected with reporters with mutated PPREs, as well as DMSO controls were set to 1. The data is representative for three biological replicates analyzed in quadruplicates. RLU, Relative light units. ***p≤ 0.001, adjusted for multiplicity.

3.6 Endogenous target gene expression in hepatocytes

To investigate the effects of ADAM1 on endogenous, chromatinized PPAR target genes in a hepatocyte model, we isolated total RNA from harvested HuH7 cells that had been treated with either 50 µM ADAM1, 50 µM PA, 1 µM RSG or 0.1 % DMSO. cDNA synthesis was performed with 500 ng total RNA, and diluted 1:5 before gene expression analyzes was performed using qPCR with specific primers (Appendix V). The genes analysed included PPAR target genes such as *ACOX1* encoding Acyl-CoA Oxidase 1, *ACSL1* and *ACSL3* encoding Acyl-CoA Synthetase Long-Chain 1 and 3, *ANGPTL4*, encoding Angiopoietin-like protein 4, *CPT1A* encoding carnitine palmitoyltransferase α (CPT1α), *FABP1* encoding Fatty-acid binding protein 1, *PLIN1* encoding perilipin 1, and *SCD1* encoding stearoyl-CoA desaturase 1. In addition, *NR1H3* encoding Liver X Receptor α, *PPARA* encoding PPARα, *PPARG* encoding PPARγ, and *SREBF1* encoding sterol regulatory element-binding transcription protein (SREBP) 1 were included in the analysis.

Of all genes analyzed, the induction of *CPT1A* expression was the most prominent. The induction was significant with all three treatments compared to the DMSO control (**Figure 26**). PA induced expression to a higher level than ADAM1 and RSG. However, these internal differences were not statistically significant.

The relative expression of *FABP1* was also significantly induced with all three treatments compared to the DMSO control (ADAM1, $p=0.008$; PA, $p=0.003$; RSG, $p<0.001$). Moreover, treatment with PA and RSG significantly induced *ACSL3* expression ($p=0.019$ and $p=0.041$, respectively). *PLIN1* expression was undetectable in this assay, while relative expressions of *PPARG* and *SREBF1* were unaffected by any of the treatments (data not shown).

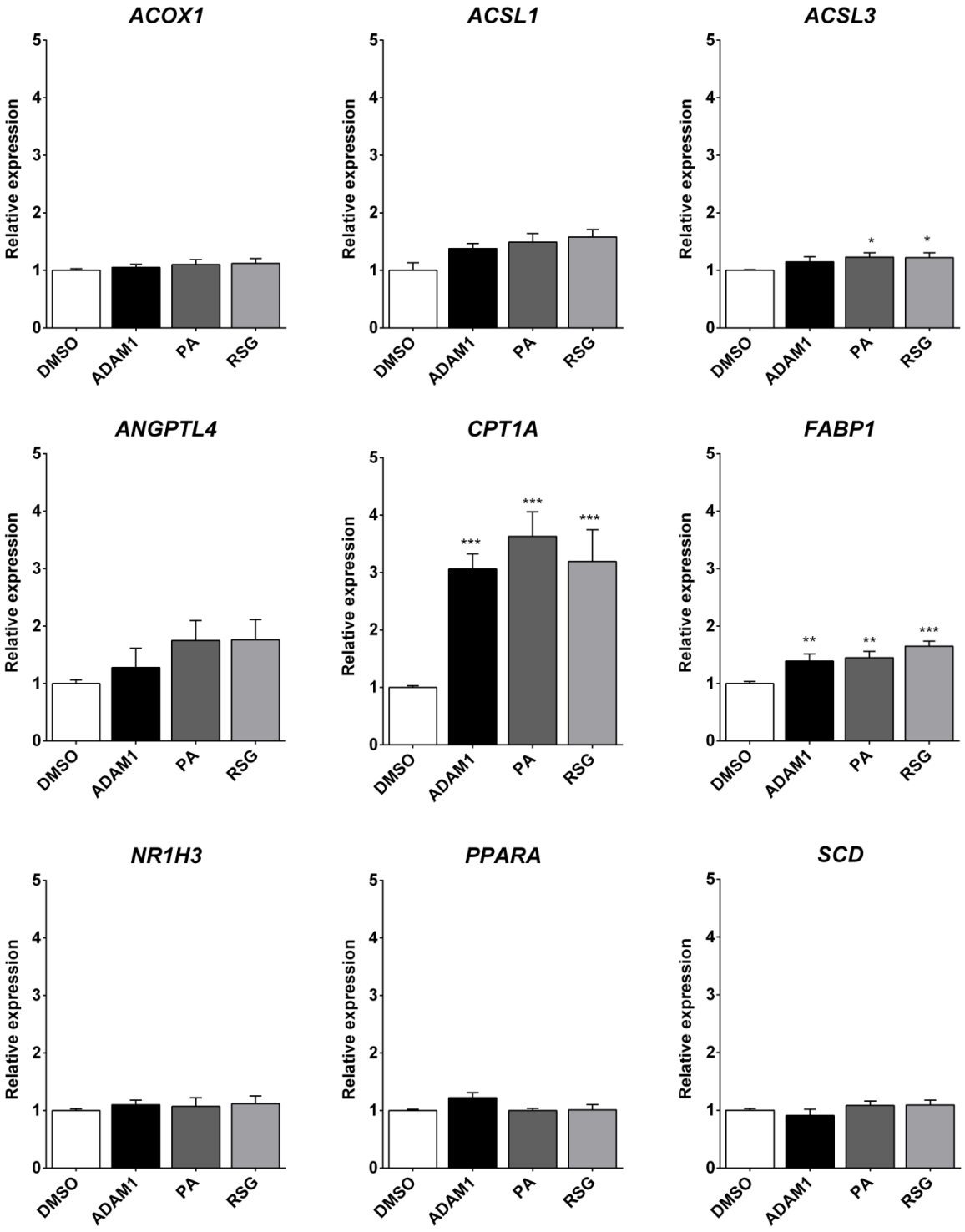

Figure 26: Relative expression of endogenous PPAR target genes in HuH7 cells. Huh7 cells were grown in high glucose media (25 mM glucose) supplemented with ITS. The cells were treated with 50 µM ADAM1, 50 µM PA, or 1 µM RSG for 18 hours before harvested for qPCR analysis. The data represents three biological replicates analyzed in triplicates. Relative expression is normalized to the respective DMSO control samples, presented as mean ± SEM. *p≤ 0.05, **p≤ 0.01, and ***p≤ 0.001 compared to DMSO control.

Table 6: Target gene expression in HuH7 cells

Target gene	ADAM1 50 µM	(7E)-9-OHE 50 µM[1]	(10E)-9-OHE 50 µM[1]
ACSL1	ns	n/a	n/a
ACSL3	ns	+	ns
ACOX1	ns	-	ns
ANGPTL4	ns	+	+
CPT1A	+	+	+
FABP1	+	-	-
NR1H3 (LXRA)	ns	-	-
PPARA	ns	ns	ns
PPARG	ns	-	-
PLIN1	n/a	ns	+
SCD	ns	n/a	n/a
SREBF1	ns	n/a	n/a

Significant induction (**+**; p≤ 0.05) or reduction (**-**; p≤ 0.05) of target gene expression compared to DMSO control. ns, not significant; n/a, not available.
[1] unpublished data obtained from prior analysis and not as a part of the current project.

Even though a direct comparison of the effects of ADAM1 and the oxo-fatty acids cannot be made at this point, as the compounds have not yet been analyzed side-by-side in the same assays, we have chosen to compare the regulatory trends in **Table 6**. *CPT1A* was the only gene induced by all three compounds (Table 6). ADAM1 induced *CPT1A* expression 3-fold compared to DMSO, while a 4-fold induction was observed upon PA treatment (Figure 26). In comparison, a 2.5-fold induction of *CPT1A* was detected in prior analysis of (7E)-9-OHE and (10E)-9-OHE, compared to a 4-fold induction upon PA treatment (previous studies; unpublished data).

ADAM1 induced *ANGPTL4* expression approximately 10 %, while PA treatment induced *ANGPTL4* expression close to 2-fold (Figure 26). However, the standard error is large, and no significant differences were detected. Previously, a 2-fold induction of *ANGPTL4* was observed with (7E)-9-OHE and (10E)-9-OHE compared to about 3.5-fold upon PA treatment (previous studies; unpublished data).

ADAM1 did not induce *ACSL3* expression in this analysis, while PA treatment induced *ACSL3* expression significantly. However, the increase in gene expression was less than 10 % (Figure 26). Prior analysis revealed a 1.5-fold induction of *ACSL3* expression when stimulating the cells with (7E)-9-OHE and no induction with PA or (10E)-9-OHE (previous studies; unpublished data).

ACOX1, *PPARG* and *NR1H3* expression was not affected by any of the treatments in this analysis, while FABP1 was significantly induced by all treatments. Previous analysis of the natural compounds (7E)-9-OHE and (10E)-9-OHE revealed a statistically significant downregulation of *ACOX1, FABP1, PPARG and NR1H3* expression, although the reduction was rather small, corresponding to less than a 10 % drop (previous studies; unpublished data). No effect was observed upon PA treatment.

3.7 Endogenous target gene expression in adipocytes

To examine the effects of ADAM1 on PPAR target genes in adipocytes and how their regulation might affect adipocyte differentiation we took advantage of the SGBS preadipocyte cell line. By exhanging the PPARγ-agonist RSG, which is an essential component in the differentiation mix, with ADAM1 we could compare the two compounds effect on target gene activation and cell morphology changes. The SGBS cells were harvested before initiation of differentiation, and on day 4, 8 and 12 after differentiation was initiated. cDNA synthesis was performed with 300 ng total RNA, and diluted 1:5 before gene expression analyzes was performed using qPCR with specific primers (Appendix V). The genes analyzed were the same as listed in section 3.6, in addition to adipocyte specific genes such as *ADIPOQ*, *FABP4*, *CD36*, *CEBPA*, *LEP* and *UCP1*.

As expected, RSG treatment induced the expression of most PPARγ target genes during the course of differentiation (**Figure 27**). For ADAM1-treated cells, a pattern of increased expression by day 4 was observed, followed by a decrease by day 8 and a second boost of expression by day 12. This was detected for most of the genes examined.

Due to the low number of biological replicates we had to compile part of the data to be able to perform statistics. Time effects were analyzed by comparing day 0 with day 4 to 12 for the corresponding treatment. This was done using the Mann-Whitney U test or independent samples t-tests, depending on distribution. The results are summarized in **Table 7**. Furthermore, the compound effect was analyzed by comparing the mean of day 4-12 for each treatment with the other treatments. For

this we used the Kruskal-Wallis, post hoc Mann Whitney U test with Bonferroni's correction. The test results are presented in Figure 27.

As can be seen in Table 7 nearly all genes were significantly different expressed from day 0 to day 4-12 with a couple of exceptions. *ACOX1*, *CD36* and *SREBF1* was not regulated upon DMSO-treatment, and *ACSL3* and *PPARA* upon ADAM1-treatment, although a p-value close to significance (p=0.056) was detected for *PPARA*. *CPT1A* was the only target gene significantly downregulated from day 0, irrespective of treatment (DMSO, p=0.04; ADAM1, p=0.03; RSG, p=0.03).

Table 7: Target gene expression in SGBS cells

Target gene	**DMSO 0.1 %**	**ADAM1 25 µM**	**RSG 2 µM**
ACOX	ns	+	+
ADIPOQ	+	+	+
ACSL1	+	+	+
ACSL3	+	ns	+
ANGPTL4	+	+	+
CEBPA	+	+	+
CD36	ns	+	+
CPT1A	-	-	-
FABP4	+	+	+
LEP	+	+	+
LXRA	+	+	+
PPARA	+	ns	+
PPARG	+	+	+
SREBF1	ns	+	+
UCP1	+	+	+

Significant induction (**+**; p≤ 0.05) or reduction (**-**; p≤ 0.05) of target gene expression on day 4 to 12 compared to day 0. ns, not significant.

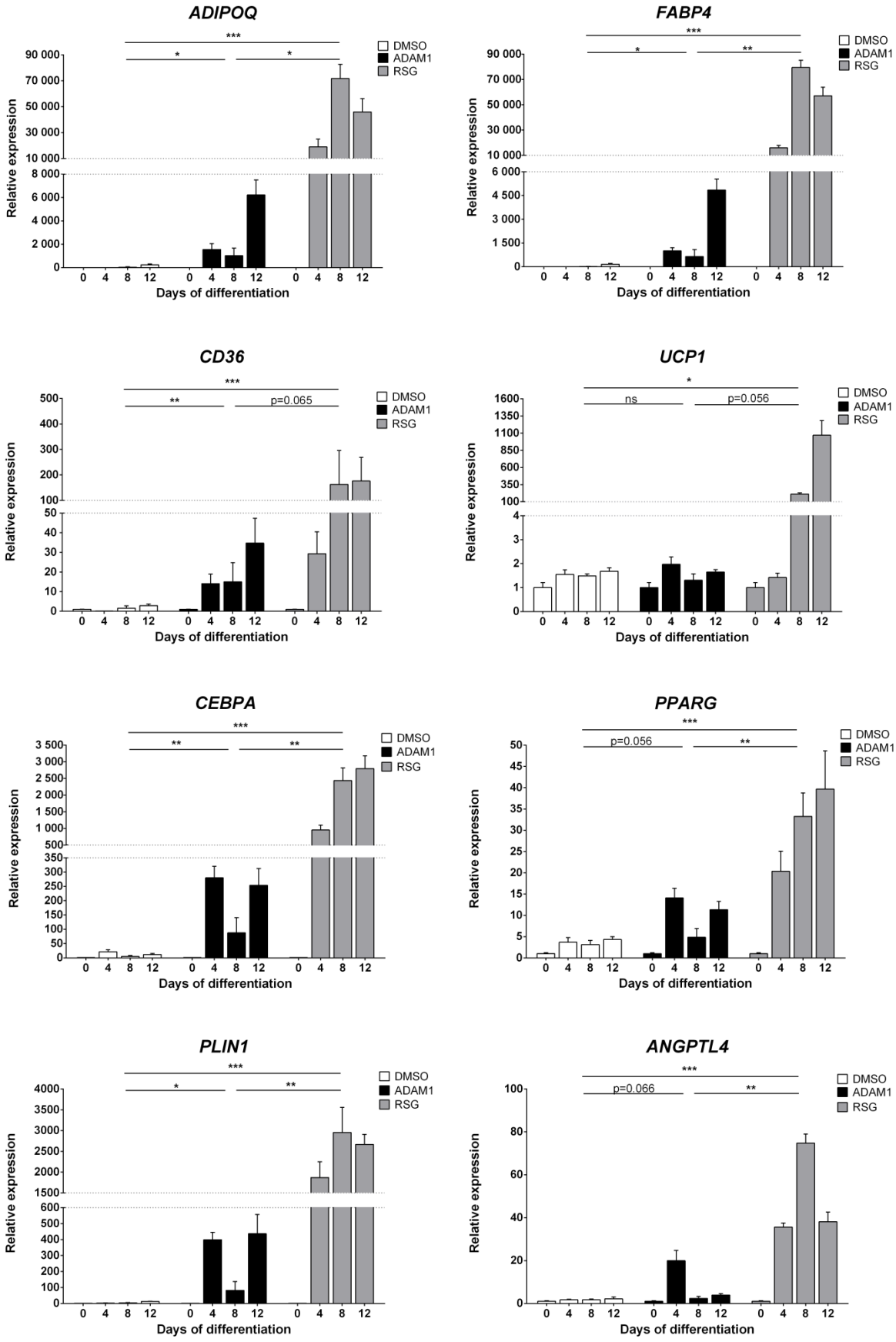
ADIPOQ
FABP4
CD36
UCP1
CEBPA
PPARG
PLIN1
ANGPTL4
DMSO
ADAM1
RSG
Relative expression
Days of differentiation
0 4 8 12 0 4 8 12 0 4 8 12
***
*
**
p=0.065
ns
p=0.056
p=0.066

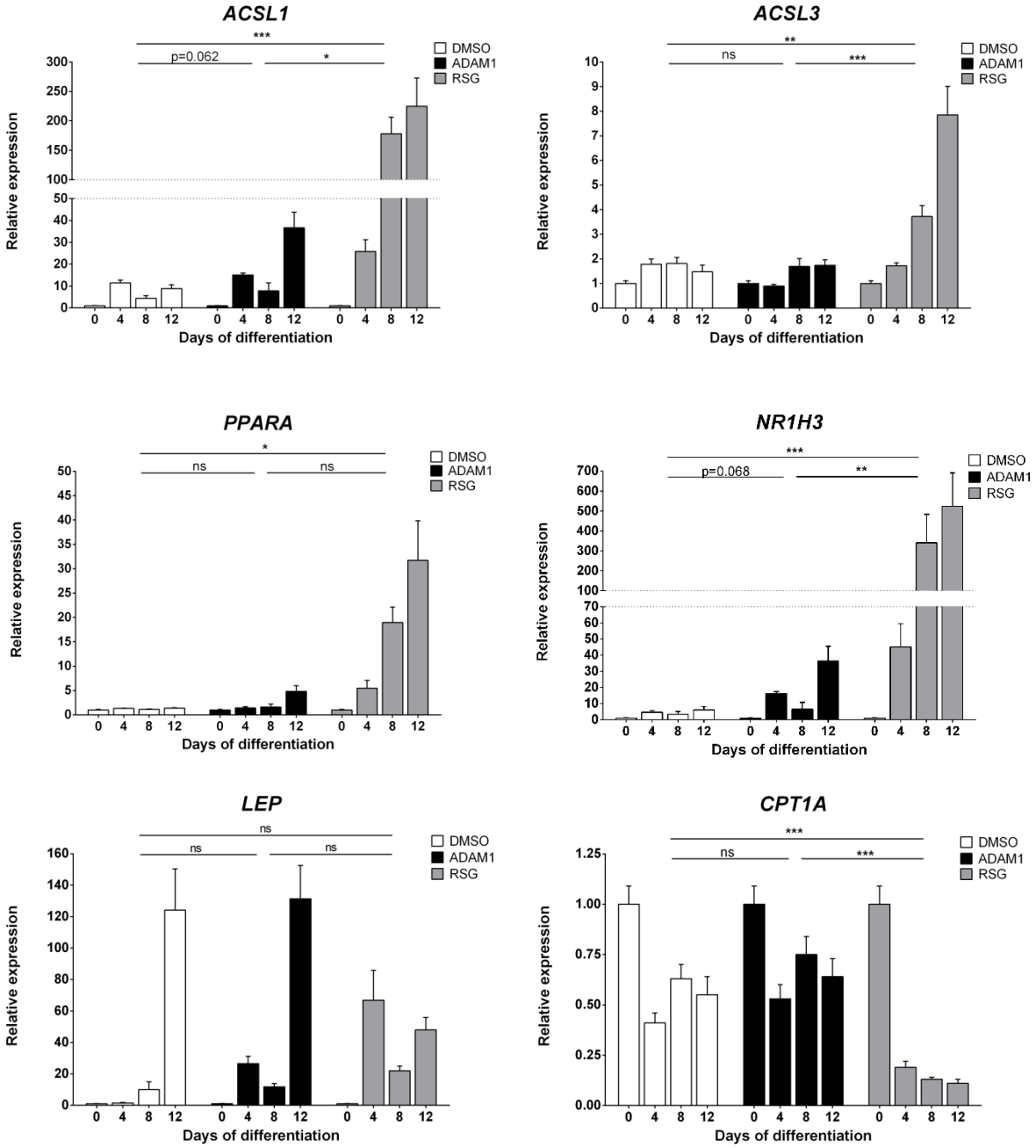

Figure 27: Relative expression of endogenous PPAR target genes in SGBS cells. Differentiation of SGBS cells were initiated with differentiation medium supplied with either 0.1 % DMSO, 25 µM ADAM1 or 2 µM RSG from day 0 to 4. Media was changed to a general serum-free adipogenic medium at day 4, and from that point all cells were treated the same. Cells were harvested and analyzed before initiation of differentiation, and 4, 8 and 12 days after. The data represent two biological replicates analyzed in duplicates, normalized to TBP and day 0, presented as mean ± SD. ns, not significant; *p<0.05; **p<0.01; ***p<0.001, adjusted for multiplicity.

When comparing the treatment to each other, significant differences in relative expression were detected between DMSO and ADAM1 treatment for *ADIPOQ*, *CEBPA*, *CD36*, *FABP4*, and *PLIN1*. Close to significant differences were found for *ACSL1* (p=0.062), *ANGPTL4* (p=0.066), *PPARG* (p=0.056), and *NR1H3* (p=0.068). Significant differences in relative expression were detected between DMSO and RSG treatment for all target genes, except from *LEP*. Significant differences were detected between ADAM1 and RSG treatment on relative expression of most of the target genes, except from *LEP*, *PPARA*, *CD36* and *UCP1*, although close to significant differences were detected for the two latter (p=0.065 and p=0.056, respectively). As we can see from Figure 27, differences at day 12 were considerable for these genes, although no statistical significance were detected upon analysis of the means of day 4 to 12 together.

The effect of ADAM1 on the relative *CPT1A* expression is very similar to the effect of the DMSO control, and no significant difference were detected between the two. Yet, a significant difference between RSG and DMSO-treatment ($p<0.001$), as well as between RSG and ADAM1 treatment ($p<0.001$) could be obsrved.

For most target genes, the relative expression levels were generally lower upon ADAM1 treatment compared to (7E)-9-OHE when related to the effects prompted by RSG (previous studies; unpublished data).

3.8 Adipocyte differentiation

To evaluate the effects of ADAM1 on adipocyte differentiation at the morphological level, we stained SGBS cells with Oil Red O (ORO). The cells were treated as in the previous experiment. Mirroring what could be observed at the gene expression level, ADAM1 promotes adipocyte differentiation compared to DMSO control, but to a lesser extent than RSG (**Figure 28**). ADAM1-treated cells show less noticeble adipocyte-like cell structure, as well as less prominent lipid droplets on day 8 and day 12 compared to RSG treated cells. Pictures taken prior to the ORO staining show profound lipid droplets in both ADAM1 and RSG treated cells, although fewer in ADAM1 treated cells (**Figure 29**)

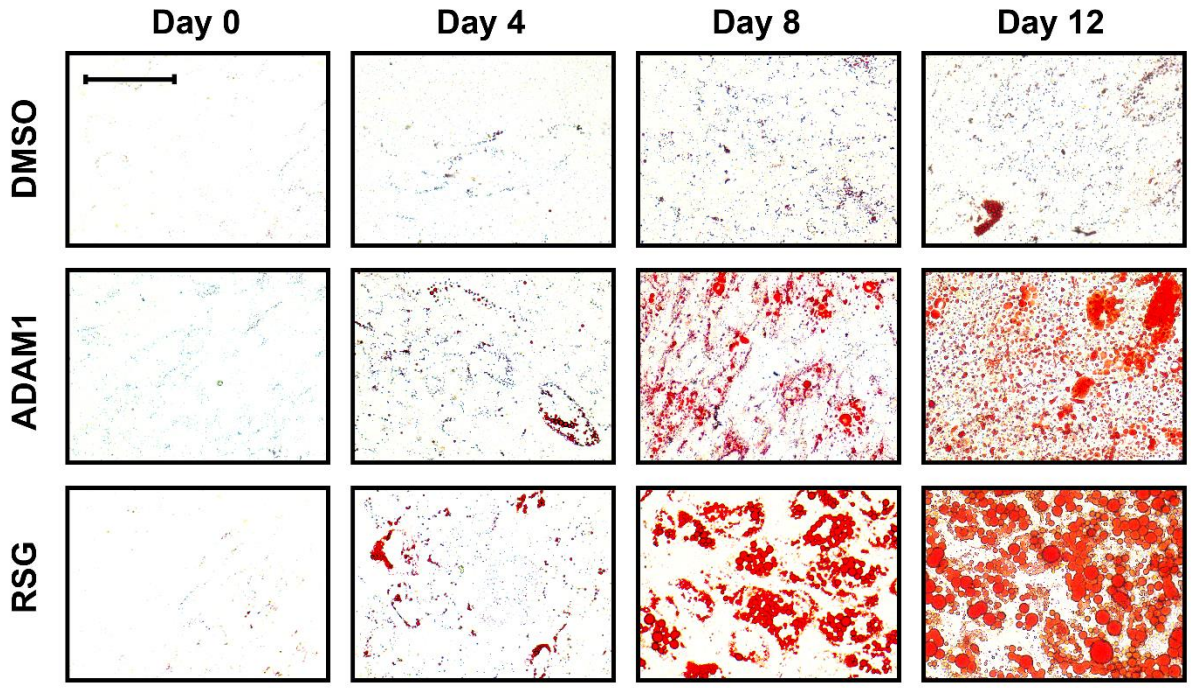

Figure 28: Neutral lipid accumulation in SGBS cells. Differentiation of SGBS cells were initiated with differentiation medium supplied with either 0.1 % DMSO+BSA, 25 µM ADAM1+BSA, or 2 µM RSG from day 0 to 4. . Media was changed to a general serum-free adipogenic medium at day 4, and from that point all cells were treated the same. **T**he pictures show representative areas of wells with treated cells before initiation of differentiation, and 4, 8 and 12 days after, captured with ColorView IIIu light microscope CCD camera. 40× enlargement, bar represents 100 µm.

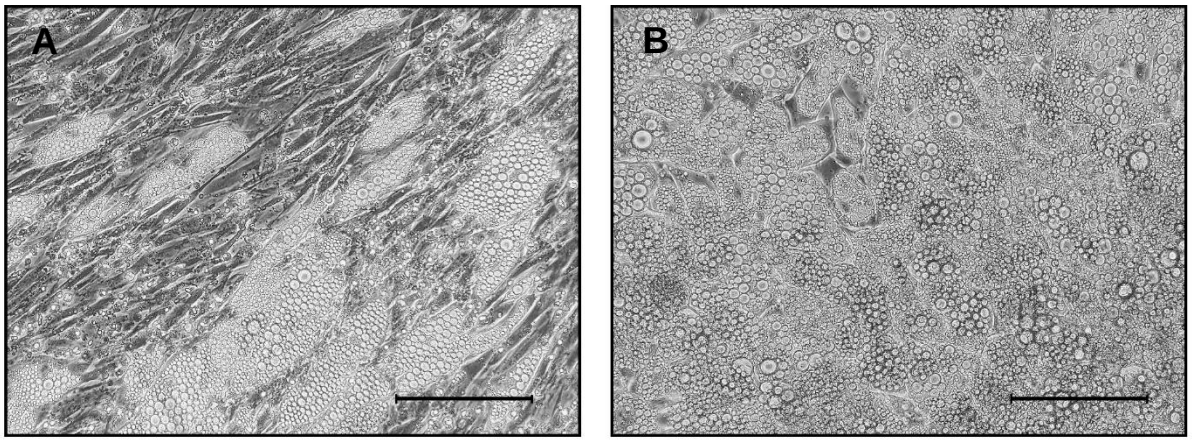

Figure 29: Microscopic photographs of SGBS cells. Pictures were taken at day 12 post-differentiation after treatment with (**A**) 25 µM ADAM1+BSA and (**B**) 2 µM RSG, prior to ORO staining. 40× enlargement, bars represent 100 µm.

4 Discussion

The prevalence of diabetes is expected to reach over 640 million individuals by 2040. As T2DM accounts for 85-95 % of all cases of diabetes worldwide, the increase in diabetes prevalence is predominantly attributed to T2DM (39). In most cases, T2DM can be prevented, and even reversed, primarily by weight control, physical activity and improved diet quality (87). However, primary prevention interventions are difficult to implement, and will not affect incidence of T2DM short term. Aggressive risk factor management, especially of blood glucose, lipid levels, and body weight, is crucial to quickly alleviate the complications associated with T2DM (87). To offer an effective, holistic treatment to individuals with T2DM, a combination of lifestyle interventions and medical therapy is often necessary (87). Therefore, the increasing prevalence of T2DM is demanding new and safe anti-diabetic agents.

Several approaches have been explored in the search of new pharmaceutical agents in treatment of T2DM and its associated comorbidities. ADAM1 is a newly developed FA mimetic with yet unknown characteristics. FA mimetics are molecules that structurally resemble naturally occurring FAs and consequently their actions in the human body. Accordingly, FA mimetics obtain great pharmaceutical opportunities as they function as ligands for a spectrum of proteins important in metabolic and inflammatory processes (88). FA mimetics targeting PPARs have been widely studied in relation to T2DM, obesity and inflammation, such as lipid-lowering PPARα agonists and insulin-sensitizing PPARγ agonists (20, 31). However, as the side-effects of some of these agonists have limited their use (20, 52, 53), combined PPARα and -γ agonists can be suggested to attenuate the side effects associated with each agonist alone, especially PPARγ agonists. In this perspective, we have investigated ADAM1 as a potential dual PPARα/γ agonist in treatment of T2DM.

4.1 Methodological considerations

4.1.1 *In vitro* cell lines as model systems in biomedical research

A drug development process typically include three main steps. The first step is the discovery and development of the drug. This step includes *in vitro* and *in vivo* characterizing the relevant molecular compound with respect to activity, specificity, absorption, distribution, metabolism and excretion. Preferentially the compounds are first tested in cell models, thereafter in animal models. The second step involves systematic preclinical assessments of the compounds dosage and toxicity levels. When these basic questions are satisfactory answered, step three is initiated. This step involves human clinical trials that typically expand over four phases.

Immortalized cell lines are often a first-choice for projects in basic biomedical research. Immortalized cell lines ensures a continuous supply of almost identical cells, and their use in biomedical research avoids the challenges of inter-individual variation (56). However, as these are transformed or genetically modified cells, great caution must be taken in generalizing the study of biological processes in these cells to normal human cells *in vivo*. For example, although the SGBS cell line is considered an appropriate model for the study of human adipocyte differentiation, it has to be kept in mind that SGBS cells are derived from an individual with a specific syndrome. It is reported that the Simpson-Golabi-Behmel syndrome may be owed to mutations in the glypican 3 gene (*GPC3*) as well as other, presently unknown genes, that may impact the cellular mechanisms (62). Primary cells are the closest model for physiological responses *in vivo*, though there are also disadvantages tied to their use. For example, primary cells obtain a very limited lifespan, and are subjects to large phenotypic and genotypic variability.

Immortal cell lines that are grown continuously over time, or exchanged between laboratories with subsequently exposure to different environments, will exhibit genotypic and phenotypic variation, as fast-growing and less representative cells may be selected. By avoiding indefinite passaging, and not uncritically distribute them between laboratories, immortal cell lines are stated to be relatively stable in respect of genotypic and phenotypic variation (56). In the current project, COS1 and HuH7 cell lines were not allowed to exceed 30 passages in total, and SGBS cells

were propagated no longer than to passage 10, and differentiated for no longer than 12 days.

The culture media used in the current project contains phenol red as a pH indicator, causing a color change as pH in the media changes. pH in cell cultures changes due to metabolites released by cells, consumption of bicarbonate (HCO_3^-), and atmospheric CO_2 dissolving in the media. Optimal pH for most mammalian cell lines are 7.4, where the culture media obtain a bright red color. At lower pH levels, the phenol red exhibit a gradual transition to a yellow color. Precautions should be made to minimize pH changes in the environment affecting the cells. As well as changing cell culture media routinely, prepared stocks of culture media kept in refrigerator were discharged every third week, and fresh media prepared. For HuH7 culture medium, ITS was added to aliquots of media prior to their application.

4.1.2 Ligand-dependent activation studies

Luciferase reporter gene assays can be applied in many different experiments for various purposes, as luciferase does not require any post-translational modification for activity. Luciferase is solely a stable, easy-to-measure reporter, and its use depends on the location in a DNA plasmid of which the luciferase gene is incorporated. In the current project, a promoter-reporter approach was used to assess information about compounds abilities to activate nuclear receptors (NRs) through ligand-dependent transactivation. The luciferase gene was cloned downstream of human NR-activated promoters or target gene sequences, placing the transcription of luciferase under strict NR and target gene promoter control. Promoter activation, and thus activation of luciferase gene transcription, would lead to production of luciferase through translation. Light produced by luciferase is measured quantitatively, and so the level of luciferase would correlate with activation of the promoter. This provides information about the activation of promoters and the transcriptional control of genes, as opposed to qPCR which quantitatively measures the amount of transcripts.

Luciferase reporter gene assay is subject to variability caused by differences in transfection efficiency and cell viability. The inclusion of a co-reporter in a dual

luciferase reporter gene system minimizes such variabilities by allowing normalization of the experimental reporter to the activity of a constructively expressed co-reporter – an internal control. Nearly all energy put into the luciferase reactions is converted to light. A light is easily detected using photometers, thus allowing observation of even small changes in transcription.

Several factors are essential in modulation of NR response upon ligand binding, and are therefore important to consider in the assays implemented in the current project. Alternative splicing, use of alternative promoters, and cross-talk between NR mediated pathways and other signaling pathways, are examples of ways results from ligand-dependent activation studies may be misinterpret (13). The assays performed in the current project are dependent on ligand binding, leading to remodeling of the NR 3D-structure necessary for activation of AF2. However, no binding assays were performed, meaning it is not 100 % certain that the ligand binds the LBD, but activates the promoter in other manners. Still, the high degree of specificity, as observed in Figure 23 with Gal4-fusion proteins differing only in the nature of LBD, strongly suggested that the effects observed are propagated through the PPARα LBD.

4.1.3 RNA analysis

Quantitative PCR analysis gives a snapshot of the amount of a particular gene transcript. For calculation of qPCR results, absolute or relative quantification can be used. In absolute quantification, a standard curve prepared from samples of known quantity is used to determine the quantity of transcripts in an unknown sample. The relative quantification method is based on comparing gene expression in a sample to that of a control sample, e.g. untreated cells, and normalizing to a reference gene (89). In the current project, the relative quantification method was used. Absolute quantification would not provide any profitable information in the context of this project, as we have been interested in the effect of ADAM1 on gene expression compared to the basal gene expression in a non-treated control sample.

In the current project, the starting material for RT-qPCR was total RNA. Total RNA contains ribosomal RNA, transfer RNA, and small, non-coding RNA which may exhibit different regulatory functions. Therefore, the use of mRNA as template may provide more sensitivity. However, in most cases, total RNA is more suitable because additional purification steps are avoided, meaning the quantity of RNA is generally higher. In addition, as the relative quantification method was used for determining gene expression, absolute sensitivity for detection was not required.

Assessment of RNA quality and integrity is crucial to obtain reliable gene expression data. The accuracy of qPCR analysis of gene expression is highly influenced by the quality and quantity of the starting RNA (90). Optimally, the starting RNA should be free of proteins, genomic DNA, RT inhibitors, and other contaminants. In the current project, genomic DNA was removed by DNAse treatment prior to cDNA synthesis. Quality and quantity of starting RNA was assessed by measurements of absorbance at 230 nm, 260 nm and 280 nm using Nanodrop® ND-100 spectrophotometer. These wave lengths represents background absorbance and possible contaminants (230 nm), nucleic acids (260 nm), and proteins (280 nm) present in the sample. An absorbance of 260/280 nm ratio between 1.8 and 2.0 is generally considered an indicator of adequate RNA quality (90). In the current project, all samples used displayed a 260/280 ratio between 1.7 and 2.1. RNA integrety was not assessed in the samples used in this project and thus represent a potential source of error. However, RNA isolated from cell cultures systematically show high integrity, and >99 % of all samples measured in our laboratory show a RNA integrity number (RIN) value of > 9.7 using BioAnalyzer (unpublished data).

qPCR chemistry

Different chemistry is available for detection of qPCR products, where the most commonly used are TaqMan® and SYBR® Green. A TaqMan® probe contains a 5’ end fluorescent reporter dye and a 3’ end quencher dye, and has a specific sequence complementary to a target sequence. When intact, this probe emits no fluorescence. When the target sequence is amplified, the probe is digested by the polymerase, and the reporter dye is separated from the quencher. This is repeated

with each extension cycle. Once separated from the quencher, the reporter dye emits a specific fluorescent signal. This methods require little optimization, as the probes are sequence-specific and optimized by the vendor (91). However, as different TaqMan® probes are required for different target sequences, this method is expensive, and calls for more complex assay setups. SYBR® Green is a low-cost, efficient alternative that were implemented in the current project. It can be applied to assess amplification of any dsDNA sequence. Yet, SYBR® Green is more susceptible to unspecific, fluorescent signals caused by primer-dimers and amplification of non-specific products (79). This may generate false positive results, and thereby lead to overestimation of target gene expression. To control for this, NTC and no RT samples were implemented in the qPCR assays, and melt curve analysis were performed for all target genes.

More than one melt curve peak indicates that there is more than one product in the sample (79). This could be a specific amplification, i.e. that the qPCR primers have picked up other targets, or a non-specific amplification, i.e. hybridization of the two primers, so-called primer-dimer formation. A fluorescent signal of an NTC sample and/or no RT sample may also indicate primer-dimer formation, or amplification of genomic DNA, respectively. Contamination by genomic DNA can be caused by random contamination of samples, or by contamination of the reagents used. Clean working regimes and working stations were employed to avoid such problems. Samples with abnormal melt curves, or melt curve signals with NTC and/or no RT samples of Ct-values <32 were excluded from further analysis, as they were considered contaminated and not reliable.

Selection of reference gene for normalization

The basic assumption is that a proper reference gene for qPCR should be characterized by a permanent expression in all samples that are tested, and that the reference gene expression should be independent of and unaffected by any experimental factors. However, in real life there is always some sort of variance in expression of reference genes (92). Even in cell lines, variance can be observed, e.g. due to ageing of the cells. The key is to select genes that exhibit the most stable

expression and least variability. The general recommendations are choosing a reference gene whose expression is neither very low, nor very high, ideally with a Ct-value between 30 and 15 (91, 92).

The TATA-box binding protein (TBP) is commonly applied as a reference gene for *in vitro* cell based studies of gene expression, due to its stable endogenous expression that is unaffected by differing nutritional or hormonal conditions. As the cell lines used in the current project are immortalized, clonal cells, and the relative quantification method was applied to calculate qPCR results, TBP was considered a suitable reference gene. Previous studies of reference gene selection have also appointed TBP as a suitable reference gene for studies of gene expression in human cells (93). Another reason for choosing TBP as a reference gene in this project was for the data to be as comparable as possible to the results from prior analysis of (7E)-9-OHE and (10E)-9-OHE.

Selection of target genes

The PPARα and -γ target genes assessed in the gene expression analysis included a spectrum of previously characterized PPARα target genes involved in different aspects of FA metabolism (19, 23), and PPARγ target genes representing the adipocyte phenotype (20, 34, 35, 86), and adipocytes browning (6, 7). The target genes were essentially matching those assessed in the prior analysis of (7E)-9-OHE and (10E)-9-OHE, to be able to compare the responses.

4.2 General discussion

The hydrocarbon chain length is the main determinants of a FA's solubility in water. The shorter hydrocarbon chain, the greater is its solubility. ADAM1 with its 16 carbon atoms is a long-chained FA, and poor solubility could be predicted (2). DMSO is therefore required to facilitate solubility. In aqueous solutions, FAs tend to associate, forming micelles. The increased number of rounded and detached cells observed with concentrations of ADAM1 may be due to formation of micelles that separate the structures in the cell culture, e.g. separate the plastic and the cells adhesion molecules, causing the loosening of cells from the culture vessel (Figure 17C). This effect is often termed soap effect. Another possibility is that these cells are apoptotic. However, it is important to acknowledge that the loosening of cells does not automatically mean they are lysed. As the cytotoxicity assays implies, a percentage of the cells treated with 1000 µM ADAM1 was viable.

4.2.1 Nuclear receptor agonist activity of ADAM1

In this project, we characterized what initially was hypothesized to be a dual PPARα/γ agonist, alternatively a selective PPARγ agonist, based on 3D docking studies. Instead, ADAM1 turned out to be a specific PPARα agonist, with little or no effect on other lipid-activated, metabolic nuclear receptors. ADAM1 activates PPARα with an EC_{50} value of 23 µM, similarly to the EC_{50} values determined in prior analysis of (7E)-9-OHE and (10E)-9-OHE. Only a negligible activation of PPARγ was observed with ADAM1 making calculation of an EC_{50} impossible. This is in stark contrast to the EC_{50} values of 8-10 µM seen with (7E)-9-OHE and (10E)-9-OHE.

The overall results points towards ADAM1 reaching a plateau of human PPARα agonism around 50-100 µM. The efficacy seen with 250 µM ADAM1 is already highly affected by cytotoxicity, and the drop in activity level from 100 µM to 250 µM is steep. These observations indicate that the ADAM1 concentrations should be further titrated between 100 and 200 µM to better identify the plateau. The rapid decrease in activity observed with ADAM1 concentrations above 100 µM are likely caused by cytotoxicity, detached cells and formation of precipitate opposing the activity. These

high concentrations are difficult to work with, and minor technical errors will greatly affect the data. Indeed, cell cultures treated with ADAM1 concentrations of over 100 µM exhibited increased rates of detached cells and changed morphology (Figure 17), indicating that the toxic effects of ADAM1 had affected the cells to such a degree that the responses observed are not representative.

As the level of cytotoxicity exhibited by ADAM1 in COS1 cells is similar to, or even higher, than that observed with (7E)-9-OHE and (10E)-9-OHE, this suggests that the chemical modifications made to design ADAM1 did not result in the anticipated reduced cytotoxicity. The modifications may have been inappropriate to prevent decomposing of ADAM1 into cytotoxic aldehydes. Alternatively, the cytotoxicity observed with (7E)-9-OHE and (10E)-9-OHE, as well as ADAM1, was not caused by aldehyde formation at all, but other toxic metabolites or simply by soap effects. To get a deeper insight into the metabolism of the three compounds in the cell, mass spectrometry studies of isotopically labeled equivalents is needed.

Several factors influence the absorption, distribution, metabolism and clearance of FA analogues. The challenge in designing FA mimetics lies in generating a desirable pharmacokinetic profile, as poor permeability, rapid metabolism and formation of toxic and reactive metabolites are among important concerns (88). Introduction of bioisosteres or replacement of functional groups with substitute structures are classical strategies in the construction of improved analogues in chemical medicine and drug development. The modifications can improve metabolic stability, toxicity, diffusion across biological membranes, and functional properties of the compound (88, 94). *In silico* approaches have been pointed out as novel tactics to predict selectivity and off-target activities of potential FA mimetics (88).

Bioisosteres are chemical structures introduced to, or exchanged with, a part of a molecule to enhance the compound's physical or biological properties without generating substantial changes in its chemical structure. For example, commonly used strategies to prevent rapid oxidation of FAs and eventual formation of reactive metabolites are replacement of the carboxylic acid functional group the β-carbon (88), and substitution of a methylene group on the carbon chain with a Sulphur atom (95). Strategies to stabilize an FA molecule to stop spontaneous decomposition of a α,β-unsaturated ketogroup into an aldehyde is currently not well known. However, the

results obtained in the current project suggests that the modifications have disrupted the analogue's ability to activate PPARγ, rater than making the compound less toxic. As the PPARα agonism is conserved, the loss of PPARγ agonism of ADAM1 are not likely due to changes in stability, but rather altered affinity for the PPARγ ligand-binding site. For future publishing and intellectual property right reasons, the exact modifications made design ADAM1 will not be further discussed as a part of this thesis.

4.2.2 ADAM1 and the regulation of PPAR target genes in hepatocytes

In hepatocytes, the target genes whose expression was induced upon treatment with ADAM1 or the PPARα agonist, pirinixic acid (PA), was also induced to approximately the same levels by rosiglitazone (RSG). This observation was quite surprising, especially for the well-characterized PPARα target gene *CPT1A*, as RSG is a selective PPARγ agonist with no ability to activate PPARα. A possible explanation to this may be that the PPRE of the PPAR target genes are responsive to more than one PPAR isoform. The affinity of the target genes to PPAR isoforms are largely determined by the strength of ligand binding, strength of the PPRE in interacting with PPARs, and co-factor availability. Also, PPARγ is moderately expressed in hepatocytes (33), providing another explanation to the increased expression of target genes in HuH7 cells. Activation of PPARα by RSG have also been reported in previous studies (29).

Generally, we would have expected higher expression of most of the target genes in response to the ADAM1 and especially PA treatments. The absence of responses may be due to the high oxidative capacity of these hepatocytes, and that the compounds may have been metabolized or decomposed before some of the effects could be detected. The results might also be affected by the cells general ability to express various genes. Genetic profile and liver-specific gene expression levels have previously been studied in HuH7 cells, and reported to be poorly preserved compared to primary human hepatocytes (96). Thus, we have recently moved on to

study the effect of ADAM1 in primary mouse hepatocytes and so far the results seem promising.

Another explanation to the low responses may be that ADAM1 in concentration of 50 µM is somehow cytotoxic to the HuH7 cells. Although the cell viability assays indicate that ADAM1 should not cause any cytotoxic effects at 50 µM, the cell viability assays were performed with COS1 cells, while target gene expression was assessed in HuH7 cells. COS1 cells are more robust than HuH7, and the cytotoxicity of ADAM1 investigated in COS1 cell models may be lower for human cell lines such as HuH7, and also SGBS. Still, the liver is the major detoxifying organ in our body, with a high oxidative and drug metabolizing capacity. And so a loss of ADAM1 activity, rather than cytotoxic effect is more likely.

4.2.3 ADAM1 and the regulation of PPAR target genes in adipocytes

The effects of ADAM1 treatment on regulation of target genes in adipocytes further emphasize its PPARα specific agonism. Although PPARα is expressed at low levels in adipocytes, some effects were observed upon ADAM1 treatment compared to the control treatment, indicating a role for PPARα in these cells. Similar effects may be observed for many FAs (29, 97), but are likely not strong enough to provoke any clinical effects. We found that most of the target genes, e.g. *ADIPOQ*, *CD36*, *PLIN1* and *FABP4*, were induced by ADAM1 in the SGBS adipocyte model, but to a much lower extent than by RSG. Several of these genes correspond to genes considered to be PPARγ responsive. Thus, the results were a bit surprising given that ADAM1 seemed to be a relatively specific PPARα agonist.

At day 4, all the PPAR agonist were removed from the cell media and replaced by a general serum-free adipogenic medium (3FC medium, Appendix III), containing DMEM/nutrient mix, biotin, D-pantothenate, transferrin, insulin, cortisol and T3. The continuous increase in relative expression for most of the PPAR target genes observed upon RSG treatment in our study, and as reported in numerous papers, is likely attributable to RSG's ability to induce production of endogenous ligands. Such mechanism of PPAR agonists have been suggested in previous studies (29, 98).

PPARγ-mediated induction of genes involved in metabolic processes may lead to production of metabolites that again activate PPARγ, resulting in an automated feed-forward loop. To exemplify this point, one can consider the PPARγ target gene *CD36*. *CD36* encodes the CD36 scavenger receptor, which mediates uptake of lipid particles, including oxidized LDL (oxLDL). OxLDL activates PPARγ, as well as PPARα, possibly via hydroxyoctadecadienoic acids (HODEs) and hydroxyeicosatetraenoic acids (HETEs) components of oxLDL, or through overexpression of the rate limiting enzyme in prostaglandin synthesis, COX2 (30).

Under normal conditions, the concentrations of endogenous ligands such as HODEs and HETEs are likely too low to function as PPAR ligands (29). However, when increased concentrations of exogenous PPAR ligands are available, this might initiate an automatic self-reinforcing production of these endogenous ligands. For example, Limor et al. (99) reported an upregulation of 12- and 15-LOX in vascular smooth muscle cells upon treatment with RSG. Subsequently, increased concentration of their products, 13-HODE, and 12- and 15-HETE was observed. 13-HODE and 15-HETE have previously been reported to be endogenous PPARγ ligands (100).

The moderate increases in relative gene expression at day 4 of the ADAM1 treatment followed by a dip at day 8, illustrates that ADAM1 may have a weak effect combined with the adopogenic substances (dexamethasone and IBMX) in the differentiation media. An example of this is *ANGPTL4* expression which was detected only at day 4, but not at day 8 or 12. For many of the other PPAR target genes, e.g. *ADIPOQ*, *PLIN1* and *CEBPA*, the dip at day 8 was transient, and an increase in expression was again observed by day 12. This pattern was not observed for RSG, and not seen in the previous analysis with (7E)-9-OHE and (10E)-9-OHE. One possible explanation is that ADAM1 lack the ability to activate PPARγ to the extent necessary to initiate the feed-forward loop as early as RSG, and that there is a delayed induction of gene expression.

PA can activate PPARγ as well as PPARα, and even the most specific PPARα agonists, such as GW-7647, holds some potency for activating PPARγ (101). It is possible that ADAM1 also has a weak ability to activate human PPARγ in adipocytes. Thus, it cannot be precluded that the effects on gene expression observed in the

current project are in fact PPARγ-mediated. Another explanation could be interactions and cross-regulation of these adipogenic genes over time. Yet another possibility is that metabolites produced as a result of PPARα-mediated processes may activate PPARγ. It has been reported that FAs can increase their own elimination through activation of PPARα. As activated PPARα leads to upregulation of CYP4A which mediates ω-hydroxylation, metabolites produced during catabolism of PPARα ligands may in turn activate PPARγ (102).

It should be mentioned that the relative expression of the genes in these assays are normalized to the TBP expression levels and pre-differential expression levels of the specific genes. As DMSO is also normalized this way, a minor induction with ADAM1 treatment will result in a great relative expression number. It is therefore necessary to consider these data in relation to RSG, and not solely compared to T0 and DMSO. Data from these experiments should be evaluated with respect to relative expression patterns rather than their numerical values.

4.2.4 Effects of ADAM1 on adipocyte differentiation

The effects of ADAM1 on the morphological level, assessed by Oil Red O (ORO) staining of the cells, mirrored the effects on gene expression. The ORO-stained SGBS cells treated with RSG showed a massive increase in accumulation of neutral lipids, reflecting up-regulation of adipocyte specific genes. ADAM1 also showed a clear increase in the level of neutral lipids, both as a function of days in culture and when compared with DMSO. However, when inspecting the culture wells more carefully a lipid smear and diffuse cell structures was observed in addition to the classical mature adipocytes, as if the culture was dominated by cell remnants rather than living cells. A possible explanation to this is that the ADAM1 concentration (25 µM) is toxic for the SGBS cells, as previously pointed out for HuH7 cells.

Another possibility is that ADAM1 is able to drive TAG synthesis in the preadipocytes without inducing the proper adipocyte differentiation steps, leaving the preadipocytes lipid-laden, but without the protecting layer of perilipin and other lipid droplet coating proteins. Proper protein coating of lipid droplets is necessary for accurate ORO staining. The fixation step cross-links the proteins coating lipid droplets while the

ORO dyed neutral lipids are kept inside. Thus, the prominent lipid droplets observed with RSG (Figure 28) can be said to reflect both the induction of TAG synthesis and upregulation of *PLIN1*. Less distinct droplets were observed with ADAM1 treated cells, which exhibited only modest upregulation of *PLIN1*.

An interesting hypothesis is therefore that the lipid droplets in the ADAM1 treated cells are more unstable due to a lack of proteins coating the droplets, and therefore ruptures during ORO staining, leaving a lipid smear. Such an hypothesis can find support in previous studies demonstrating the importance of perilipins in controlling lipid storage. Perilipin is reduced in obese rodents (86), and perilipin knock-out models show increased level of lipolysis, but also increased levels of leptin, insulin, glucose and TAG levels in plasma (103). During adipocyte differentiation, a transition from small lipid droplets, coated by more ubiqiously expressed proteins, e.g. adipophilin, to large lipid droplets in WAT, coated by adipocyte specific perilipin, occurs. This shift is important, as perilipin is presumably more robust in controlling lipolysis (86, 104). The pictures of SGBS cells taken prior to the ORO staining (Figure 29) show profound lipid droplets in ADAM1 treated cells, which also adds to this hypothesis.

Nevertheless, although SGBS adipogenic differentiation is known as a PPARγ dependent process (60), the current project demonstrates that a PPARα agonist, like ADAM1, may induce expression of adipogenic genes and to some degree promote differentiation in SGBS cells. The role of PPARα in WAT are still not fully understood, but growing evidence points towards a role of PPARα in WAT metabolism and differentiation (105). Previous studies have reported induction of *ADIPOQ* expression in human (106) and mouse (106, 107) WAT with PPARα agonists. Goto et al. (108) have shown that PPARα activation induced adipocyte differentiation with limited lipid accumulation in 3T3-L1 adipocytes as well as in mice WAT. Further, they hypothesized that PPARα are involved in driving adipocyte hyperplasia but not hypertrophy, a hypothesis also stated in other studies (105, 109). In hindsight, it would have been beneficial to include a known PPARα agonist in this project's adipocyte differentiation assay, e.g. PA, to be able to compare the adipogenic potential of ADAM1 to both PPARα and -γ agonists.

4.2.5 Anti-diabetic effects of PPARα and -γ activation

Prolonged excess energy consumption, resulting in chronic hyperglycaemia, inflammation, and ectopic fat accumulation is important drivers of insulin resistance. The insulin-sensitizing effects of PPARγ, and to a certain extent PPARα, agonists have been attributed to normalization of these factors. PPARγ mediates storage of FFAs as TAGs in adipose tissue through up-regulation of a plethora of genes encoding proteins involved in cellular uptake of FFAs (e.g. *FABP4*)(35), packing and organizing of lipid droplets (e.g. *PLIN1*)(110), beneficial adipokine production (e.g. *ADIPOQ*)(107, 111), and adipocyte differentiation and maturation (e.g. *CEBPA*)(34). This contributes to a shift where peripheral tissues start utilizing glucose rather than FAs for energy production. This also reduces the likelihood of ectopic accumulation of fat in other tissues, such as liver, skeletal muscle and pancreas, minimizing the potential lipotoxic effect associated with T2DM.

PPARα and -γ agonists are also reported to reduce biomarkers of inflammation (112, 113), which if left untreated adds to insulin resistance. As one of the most widely studied pro-inflammatory cytokines, TNF-α is reported to be overexpressed in obese mice, and through interfering with insulin-signaling cause systemic insulin resistance (114). This effect correlates with reduced adiponectin levels, suggesting there is an inverse relationship. Several studies have reported reduced plasma adiponectin levels in insulin-resistant states, such as T2DM and obesity (115, 116). PPARγ agonists have shown to directly activate the *ADIPOQ* promoter both *in vivo* and *in vitro* (111), an effect associated with insulin sensitization. Adiponectin is reported to attenuate inflammatory signaling (111, 117), as well as increase AMPK activity (118), all of which may contribute to the insulin-sensitizing effect of increased circulatory levels of adiponectin. AMPK is a major regulator of cellular glucose uptake via translocation of GLUT4. AMPK activity also suppress FA synthesis and promote β-oxidation (42).

GLUT4 is encoded by *SLC2A4*, and is an insulin-dependent transmembrane glucose transporter expressed in adipocytes, skeletal and cardiac myocytes. In response to insulin, GLUT4 translocate from intracellular vesicles to the cell membrane where it facilitates cellular uptake of glucose (1). Reduced GLUT4 levels is a common feature

of conditions of insulin-resistance, and have been observed in animal models of diabetes and obesity (119). The role of GLUT4 in adipocytes in relation to insulin resistance, and the mechanisms behind the PPARγ effects on *SLC2A4* expression remains unclear. However, unbound by ligand, PPARγ has been shown to repress transcription of *SLC2A4*, a repression that is reversed upon ligand binding (120). Although skeletal muscle is the main site for blood glucose regulation via insulin-dependent GLUT4, and ADAM1 is likely not directly regulating GLUT4, it would have been interesting to assess *SLC2A4* as a target gene in this project.

An insulin-sensitizing effect have also been reported with PPARα agonists in rodents (49, 51, 107). Tsuchida et al. (107) reported that PA treatment significantly ameliorated serum hyperglycaemia, hyperinsulinemia and hyperlipidaemia in obese, diabetic mice. In this study, RSG also reduced blood glucose and plasma insulin levels, but increased serum lipid levels. These effects are perhaps secondary to the lipid-lowering effects of PPARα agonism. An important note is that the studies reporting anti-diabetic effects with PPARα agonists, have used various fibric acid derivates also obtaining modest abilities to activate PPARγ. This means the effects might be PPARγ-mediated.

4.2.6 Properties of new, anti-diabetic drugs targeting PPARs

Previous studies have shown that even though sustained activation of PPARα by synthetic agonists may reduce obesity and improve insulin sensitivity, it is also reported to increase the risk for development of liver cancer, in part due to excess energy combustion. Increased hepatic FA oxidation increases the generation of reactive oxygen species, which contributes to oxidative stress including genotoxic stress (52, 121). Together with the high doses of PPARα agonists that must be provided to obtain clinical effects, this may account for some of the side-effects associated with PPARα agonist treatment. PPARγ agonists may improve the adverse effects of such excess energy combustion, although there are conflicting reports of PPARγ agonists concerning liver damage (122, 123). Vice versa, PPARα agonist, fenofibrate, have been reported to ameliorate RSG induced obesity (124). Although this might be attributable to the PPARγ binding action of PA, there still are many

strong arguments that a combination of PPARα and -γ agonism seems beneficial to outweigh the negative side-effects of the separate agonists. Another additional argument for this might be that one can reduce the dosage of the individual agonists and still retain the combined beneficial effect.

Several promising dual PPARα/γ agonists have reached clinical trials, e.g. Chiglitazar, Muraglitazar, Tesaglitazar and Aleglitazar (20). Of these compounds, Chiglitazar is the only one still in phase III trials for T2DM treatment (125). The clinical trials of the remaining compounds have been terminated due to safety concerns (20). Analysis of Aleglitazar have argued against the benefits of combining PPARα and -γ agonist features within one single molecule, as the effects were no different than those achieved by combining separate agonists (112). The anti-diabetic effects of RSG have also been reported to be enhanced when RSG is applied in combination with PA (107). Thus, it can be questioned whether there exist intramolecular, synergistic effects of dual PPARα/γ agonists, or if the combined effect of the separate agonists is just as efficient. In either case, combining ADAM1 with a PPARγ agonist, or even the parent oxo-FAs, separately or in one fused molecule, might result in competent dual PPARα and -γ agonism. It can be hypothesized that the effective dose of such combination will be much lower than that of each compound separately, and that the cytotoxicity observed with the separate compound may no longer be an issue.

As a result of cancelled clinical trials and adverse effects reported with discovered dual PPARα/γ agonists, several alternative strategies for development of PPAR-targeting anti-diabetic drugs have been tested. These include pan-agonists, partial agonists, and selective PPAR modulators (SPPARMs), among others (17, 20). Non-agonist PPAR ligands blocking phosphorylation of PPARγ have also been proposed (17, 126). In addition, down-stream effects of PPAR activation have recently gained more attention. Activation of non-PPAR-targets such as AMPK is suggested as an alternative mechanism to the effects of PPARα and -γ agonists (17). In this aspect it is worth considering whether some of the effects on gene expression levels seen with ADAM1-treatment in the current project may be due to activation of PPAR-independent pathways. Kinase activity assays and transcriptome profiling with pathway analyses may be two independent strategies to employ to dig deeper into

this matter. Still, the performance of controlled dose-response and specificity assays supports the idea that PPAR-activation is the underlying mechanism for much of the ADAM1 effects. However, as the expression of the receptors assayed mainly is controlled through transfections, and the endogenous effects in e.g. human cell are far more complex, *in vivo* studies are needed to strengthen the conclusions.

5 Conclusions

Through cell based studies we have characterized ADAM1 and found it to be a semi-potent PPARα agonist with an unexpected low to no potency for activating PPARγ. Although more data are needed to draw final conclusions from these assays, the activation profile, cytotoxicity and target gene repertoire of ADAM1 was considered unsatisfactory for a dual PPARα/γ agonist. ADAM1 may have the ability to bind PPARγ, but this affinity is likely to be very weak. High doses of this compound might have evoked greater PPARγ-mediated responses, but the relatively high cytotoxicity prevents such doses from being administered to humans. Overall, the properties of ADAM1 were in this project found to be unacceptable for proceeding with e.g. animal studies. Finally, the results of this project demonstrate the challenges in utilizing FA mimetics as pharmaceutical agents, and the limitations in using modern *in silico* 3D modeling as a method to predict a molecule's stability and potency of agonism.

5.1 Future perspectives

A long-term goal for researchers in this field is to acquire a detailed understanding of the multiple physiological effects and interactions elicited by natural and synthetic PPAR ligands. Reflecting the increased prevalence of T2DM, there is, without a doubt, an urgent need for new, safe anti-diabetic pharmaceuticals. As drug development processes are long and intricate processes, there is a need to continue to apply proactive tactics in the development of new, safe anti-diabetic pharmaceuticals. In the meantime, the most effective approach to prevent and improve T2DM, is to eat healthy and stay physically active.

6 References

1. Frayn K. *Metabolic Regulation: A Human Perspective*. 3rd ed: Wiley-Blackwell; 2010.

2. Ferrier DR. *Lippincott Illustrated Reviews Biochemistry*. 7th ed. Magee S, Fahey C, editors. Philadelphia, PA, USA: Wolters Kluwer; 2017.

3. Saltiel AR, Kahn CR. *Insulin signalling and the regulation of glucose and lipid metabolism*. Nature. 2001;414(6865):799-806.

4. Wanders RJ, Komen J, et al. *Fatty acid omega-oxidation as a rescue pathway for fatty acid oxidation disorders in humans*. FEBS j. 2011;278(2):182-94.

5. Li H, Li H, et al. *Dysregulated pathways in type 2 diabetes*. Biomed Res. 2017;28(3):1426-43.

6. Bartelt A, Heeren J. *Adipose tissue browning and metabolic health*. Nat Rev Endocrinol. 2014;10(1):24-36.

7. Wang W, Seale P. *Control of brown and beige fat development*. Nat Rev Mol Cell Biol. 2016;17(11):691-702.

8. Kusminski CM, Bickel PE, et al. *Targeting adipose tissue in the treatment of obesity-associated diabetes*. Nat Rev Drug Discov. 2016;15(9):639-60.

9. Kadowaki T, Yamauchi T, et al. *Adiponectin and adiponectin receptors in insulin resistance, diabetes, and the metabolic syndrome*. J Clin Invest. 2006;116(7):1784-92.

10. Cristancho AG, Lazar MA. *Forming functional fat: a growing understanding of adipocyte differentiation*. Nat Rev Mol Cell Biol. 2011;12(11):722-34.

11. Johnson AR, Milner JJ, et al. *The inflammation highway: metabolism accelerates inflammatory traffic in obesity*. Immunol Rev. 2012;249(1):218-38.

12. Metallo CM, Heiden MGV. *Understanding metabolic regulation and its influence on cell physiology*. Mol Cell. 2013;49(3):388-98.

13. Gronemeyer H, Gustafsson JA, et al. *Principles for modulation of the nuclear receptor superfamily*. Nat Rev Drug Discov. 2004;3(11):950-64.

14. Aagaard MM, Siersbaek R, et al. *Molecular basis for gene-specific transactivation by nuclear receptors*. Biochim Biophys Acta. 2011;1812(8):824-35.

15. Glass CK, Ogawa S. *Combinatorial roles of nuclear receptors in inflammation and immunity*. Nat Rev Immunol. 2006;6(1):44-55.

16. Li T, Chiang J. *Bile Acid Signaling in Metabolic Disease and Drug Therapy*. Pharmacol Rev. 2014;66(4):948-83.

17. Ahmadian M, Suh JM, et al. *PPARgamma signaling and metabolism: the good, the bad and the future*. Nat Med. 2013;19(5):557-66.

18. Bishop-Bailey D, Wray J. *Peroxisome proliferator-activated receptors: a critical review on endogenous pathways for ligand generation*. Prostaglandins Other Lipid Mediat. 2003;71(1-2):1-22.

19. Contreras AV, Torres N, et al. *PPAR-alpha as a key nutritional and environmental sensor for metabolic adaptation*. Adv Nutr. 2013;4(4):439-52.

20. Mansour M. *The roles of peroxisome proliferator-activated receptors in the metabolic syndrome*. Prog Mol Biol Transl Sci. 2014;121:217-66.

21. Braissant O, Foufelle F, et al. *Differential expression of peroxisome proliferator-activated receptors (PPARs): tissue distribution of PPAR-alpha, -beta, and -gamma in the adult rat*. Endocrinology. 1996;137(1):354-66.

22. Kersten S, Seydoux J, et al. *Peroxisome proliferator-activated receptor alpha mediates the adaptive response to fasting*. J Clin Invest. 1999;103(11):1489-98.

23. Rakhshandehroo M, Knoch B, et al. *Peroxisome Proliferator-Activated Receptor Alpha Target Genes*. PPAR Research. 2010;2010:20.

24. Ntambi JM, Miyazaki M. *Regulation of stearoyl-CoA desaturases and role in metabolism*. Prog Lipid Res. 2004;43(2):91-104.

25. Furuhashi M, Hotamisligil GS. *Fatty acid-binding proteins: role in metabolic diseases and potential as drug targets*. Nat Rev Drug Discov. 2008;7(6):489-503.

26. Barbera MJ, Schluter A, et al. *Peroxisome proliferator-activated receptor alpha activates transcription of the brown fat uncoupling protein-1 gene. A link between regulation of the thermogenic and lipid oxidation pathways in the brown fat cell*. J Biol Chem. 2001;276(2):1486-93.

27. Forman BM, Chen J, et al. *Hypolipidemic drugs, polyunsaturated fatty acids, and eicosanoids are ligands for peroxisome proliferator-activated receptors α and δ*. Proc Natl Acad Sci U S A. 1997;94(9):4312-7.

28. Wolfrum C, Borrmann CM, et al. *Fatty acids and hypolipidemic drugs regulate peroxisome proliferator-activated receptors alpha - and gamma-mediated gene expression via liver fatty acid binding protein: a signaling path to the nucleus*. Proc Natl Acad Sci U S A. 2001;98(5):2323-8.

29. Krey G, Braissant O, et al. *Fatty acids, eicosanoids, and hypolipidemic agents identified as ligands of peroxisome proliferator-activated receptors by coactivator-dependent receptor ligand assay*. Mol Endocrinol. 1997;11(6):779-91.

30. Taketa K, Matsumura T, et al. *Oxidized low density lipoprotein activates peroxisome proliferator-activated receptor-alpha (PPARalpha) and PPARgamma through MAPK-dependent COX-2 expression in macrophages*. J Biol Chem. 2008;283(15):9852-62.

31. Merk D, Zettl M, et al. *Pirinixic acids: flexible fatty acid mimetics with various biological activities*. Future Med Chem. 2015;7(12):1597-616.

32. Ferré P. *The Biology of Peroxisome Proliferator-Activated Receptors*. Diabetes. 2004;53(suppl 1):S43-S50.

33. Mukherjee R, Jow L, et al. *Identification, characterization, and tissue distribution of human peroxisome proliferator-activated receptor (PPAR) isoforms PPARgamma2 versus PPARgamma1 and activation with retinoid X receptor agonists and antagonists*. J Biol Chem. 1997;272(12):8071-6.

34. Zuo Y, Qiang L, et al. *Activation of CCAAT/enhancer-binding protein (C/EBP) alpha expression by C/EBP beta during adipogenesis requires a peroxisome proliferator-activated receptor-gamma-associated repression of HDAC1 at the C/ebp alpha gene promoter*. J Biol Chem. 2006;281(12):7960-7.

35. Tontonoz P, Hu E, et al. *mPPAR gamma 2: tissue-specific regulator of an adipocyte enhancer*. Genes Dev. 1994;8(10):1224-34.

36. Wu Z, Rosen ED, et al. *Cross-regulation of C/EBP alpha and PPAR gamma controls the transcriptional pathway of adipogenesis and insulin sensitivity*. Mol Cell. 1999;3(2):151-8.

37. World Health Organization (WHO). *Global report on diabetes*. Geneva, Switzerland; 2016.

38. American Diabetes Association. *Diagnosis and Classification of Diabetes Mellitus*. Diabetes Care. 2012;35(Suppl 1):S64-71.

39. International Diabetes Federation (IDF). *IDF Diabetes Atlas.* Brussels, Belgium; 2015.

40. Iglay K, Hannachi H, et al. *Prevalence and co-prevalence of comorbidities among patients with type 2 diabetes mellitus*. Curr Med Res Opin. 2016;32(7):1243-52.

41. Steppan CM, Bailey ST, et al. *The hormone resistin links obesity to diabetes*. Nature. 2001;409(6818):307-12.

42. Hardie DG, Ross FA, et al. *AMPK: a nutrient and energy sensor that maintains energy homeostasis*. Nat Rev Mol Cell Biol. 2012;13(4):251-62.

43. Zheng W, Qiu L, et al. *Selective targeting of PPARgamma by the natural product chelerythrine with a unique binding mode and improved antidiabetic potency*. Sci Rep. 2015;5:12222.

44. International Diabetes Federation (IDF). *IDF Consensus Worldwide Definition of the Metabolic Syndrome*. Brussels, Belgium; 2006.

45. Tupper T, Gopalakrishnan G. *Prevention of diabetes development in those with the metabolic syndrome*. Med Clin North Am. 2007;91(6):1091-105, viii-ix.

46. Tenenbaum A, Fisman EZ. *Fibrates are an essential part of modern anti-dyslipidemic arsenal: spotlight on atherogenic dyslipidemia and residual risk reduction*. Cardiovasc Diabetol. 2012;11:125.

47. Willson TM, Brown PJ, et al. *The PPARs: from orphan receptors to drug discovery*. J Med Chem. 2000;43(4):527-50.

48. Staels B, Dallongeville J, et al. *Mechanism of action of fibrates on lipid and lipoprotein metabolism*. Circulation. 1998;98(19):2088-93.

49. Ye JM, Doyle PJ, et al. *Peroxisome proliferator-activated receptor (PPAR)-alpha activation lowers muscle lipids and improves insulin sensitivity in high fat-fed rats: comparison with PPAR-gamma activation*. Diabetes. 2001;50(2):411-7.

50. Fu J, Gaetani S, et al. *Oleylethanolamide regulates feeding and body weight through activation of the nuclear receptor PPAR-[alpha]*. Nature. 2003;425(6953):90-3.

51. Guerre-Millo M, Gervois P, et al. *Peroxisome proliferator-activated receptor alpha activators improve insulin sensitivity and reduce adiposity*. J Biol Chem. 2000;275(22):16638-42.

52. Muscari A, Puddu GM, et al. *Lipid-lowering drugs: are adverse effects predictable and reversible?* Cardiology. 2002;97(3):115-21.

53. Grygiel-Gorniak B. *Peroxisome proliferator-activated receptors and their ligands: nutritional and clinical implications--a review*. Nutr J. 2014;13:17.

54. *European Medicines Agency recommends suspension of Avandia, Avandamet and Avaglim* [press release]. London, United Kingdom: European Medicines Agency, 23.09 2010.

55. Moldes-Anaya A, Saether T, et al. *Two Isomeric C16 Oxo-Fatty Acids from the Diatom Chaetoceros karianus Show Dual Agonist Activity towards Human Peroxisome Proliferator-Activated Receptors (PPARs) alpha/gamma*. Mar Drugs. 2017;15(6).

56. Masters JR. *Human cancer cell lines: fact and fantasy*. Nat Rev Mol Cell Biol. 2000;1(3):233-6.

57. Freshney RI. *Basic Principles of Cell Culture*. In: Vunjak-Novakovic G, Freshney RI, editors. Culture of Cells for Tissue Engineering. Hoboken, NJ, USA: John Wiley & Sons, Inc.; 2006. p. 3-23.

58. Gluzman Y. *SV40-transformed simian cells support the replication of early SV40 mutants*. Cell. 1981;23(1):175-82.

59. Nakabayashi H, Taketa K, et al. *Growth of human hepatoma cells lines with differentiated functions in chemically defined medium*. Cancer Res. 1982;42(9):3858-63.

60. Wabitsch M, Brenner RE, et al. *Characterization of a human preadipocyte cell strain with high capacity for adipose differentiation*. Int J Obes Relat Metab Disord. 2001;25(1):8-15.

61. Fischer-Posovszky P, Newell FS, et al. *Human SGBS cells - a unique tool for studies of human fat cell biology*. Obes Facts. 2008;1(4):184-9.

62. Ruiz-Ojeda FJ, Rupérez AI, et al. *Cell Models and Their Application for Studying Adipogenic Differentiation in Relation to Obesity: A Review*. Int J Mol Sci. 2016;17(7):1040.

63. Mehlem A, Hagberg CE, et al. *Imaging of neutral lipids by oil red O for analyzing the metabolic status in health and disease*. Nat Protocols. 2013;8(6):1149-54.

64. Ramirez-Zacarias JL, Castro-Munozledo F, et al. *Quantitation of adipose conversion and triglycerides by staining intracytoplasmic lipids with Oil red O*. Histochemistry. 1992;97(6):493-7.

65. *Types of Transfection* [Internet]. Thermo Fisher Scientific Inc.; 2017 [cited 17 February 2017]. Available from: https://www.thermofisher.com/no/en/home/references/gibco-cell-culture-basics/transfection-basics/types-of-transfection.html.

66. Chesnoy S, Huang L. *Structure and function of lipid-DNA complexes for gene delivery*. Annu Rev Biophys Biomol Struct. 2000;29:27-47.

67. *Bioluminescent Reporter Gene Assays* [Internet]. Promega Corporation; 2015 [cited 26 January 2017]. Available from: https://no.promega.com/resources/product-guides-and-selectors/protocols-and-applications-guide/bioluminescent-reporters/

68. *Dual-Luciferase® Reporter Assay System* [Internet]. Promega Corporation; [cited February 17 2017]. Available from: https://no.promega.com/-/media/files/resources/protocols/technical-manuals/0/dual-luciferase-reporter-assay-system-protocol.pdf.

69. *Dual-Luciferase® Reporter Assay and Dual-Luciferase® Reporter 1000 Assay Systems Quick Protocol* [Internet]. Promega Corporation; 2009 [cited September 15 2017]. Available from: https://no.promega.com/-/media/files/resources/protcards/dual-luciferase-reporter-assay-and-dual-luciferase-reporter-1000-assay-systems-quick-protocol.pdf.

70. Lodish H, Berk A, et al. *DNA Cloning with Plasmid Vectors*. In: Molecular Cell Biology. 4th ed. New York, USA: W. H. Freeman; 2000.

71. Casali N. *Escherichia coli Host Strains*. In: Casali N, Preston A, editors. E coli Plasmid Vectors: Methods and Applications. Totowa, NJ, USA: Humana Press; 2003. p. 27-48.

72. Hanahan D, Jessee J, et al. *Plasmid transformation of Escherichia coli and other bacteria*. Methods Enzymol. 1991;204:63-113.

73. *PCR clean-up Gel extraction: User manual: NucleoSpin® Gel and PCR Clean-up* [Internet]. Macherey-Nagel GmbH & Co. KG; 2017 [cited April 19 2017]. Available from: http://www.mn-net.com/Portals/8/attachments/Redakteure_Bio/Protocols/DNA%20clean-up/UM_PCRcleanup_Gelex_NSGelPCR.pdf.

74. *Plasmid DNA purification: User manual: NucleoSpin® Plasmid, NucleoSpin® Plasmid (NoLid), NucleoSpin® Plasmid QuickPure* [Internet]. Düren, Germany: Macherey-Nagel GmbH & Co. KG; 2015 [cited April 19 2017]. Available from: http://www.mn-net.com/Portals/8/attachments/Redakteure_Bio/Protocols/Plasmid%20DNA%20Purification/UM_pDNA_NS.pdf.

75. *Plasmid DNA purification: User manual: NucleoBond® Xtra Midi, NucleoBond® Xtra Maxi, NucleoBond® Xtra Midi Plus, NucleoBond® Xtra Maxi Plus* [Internet]. Düren, Germany: Macherey-Nagel GmbH & Co.,; 2016 [cited April 19 2017]. Available from: http://www.mn-net.com/Portals/8/attachments/Redakteure_Bio/Protocols/Plasmid%20DNA%20Purification/UM_pDNA_NuBoXtra.pdf.

76. *Quick-Start Protocol RNeasy® Mini Kit, Part 1* [Internet]. QIAGEN; 2011 [cited April 19 2017]. Available from: https://www.qiagen.com/ch/resources/download.aspx?id=0e32fbb1-c307-4603-ac81-a5e98490ed23&lang=en.

77. *Quick-Start Protocol RNeasy® Mini Kit, Part 2* [Internet]. QIAGEN; 2011 [cited April 19 2017]. Available from: https://www.qiagen.com/ch/resources/download.aspx?id=f9b2e5ef-9456-431a-85ed-2a2b9fbd503d&lang=en.

78. *High-Capacity cDNA Reverse Transcription Kits* [Internet]. Carlsbad, CA, USA: Thermo Fisher Scientific Inc.; 2016 [cited November 17 2017]. Available from: https://assets.thermofisher.com/TFS-Assets/LSG/manuals/4375222_HighCap_cDNA_ReverseTranscripKits_PI.pdf.

79. Arya M, Shergill IS, et al. *Basic principles of real-time quantitative PCR*. Expert Rev Mol Diagn. 2005;5(2):209-19.

80. Schmittgen TD, Livak KJ. *Analyzing real-time PCR data by the comparative CT method*. Nat Protocols. 2008;3(6):1101-8.

81. *KAPA SYBR® FAST qPCR Master Mix (2X) Kit* [Technical Data Sheet]. KAPA Biosystems; 2017 [cited October 23 2017]. Available from: http://www.sigmaaldrich.com/content/dam/sigma-aldrich/docs/Roche/Datasheet/1/sfukbdat.pdf.

82. *Cytotoxicity Detection Kit (LDH)* [Internet]. Mannheim, Germany: Roche Diagnostics GmbH; 2011 [cited April 5 2017]. Available from: http://www.sigmaaldrich.com/content/dam/sigma-aldrich/docs/Roche/Bulletin/1/11644793001bul.pdf.

83. *Product Information: In Vitro Toxicology Assay Kit, XTT based* St. Louis, MO, USA: Sigma-Aldrich Inc.; [cited November 17 2017]. Available from: http://www.sigmaaldrich.com/content/dam/sigma-aldrich/docs/Sigma/Bulletin/tox2bul.pdf.

84. Berridge MV, Herst PM, et al. *Tetrazolium dyes as tools in cell biology: new insights into their cellular reduction*. Biotechnol Annu Rev. 2005;11:127-52.

85. Napal L, Marrero PF, et al. *An intronic peroxisome proliferator-activated receptor-binding sequence mediates fatty acid induction of the human carnitine palmitoyltransferase 1A*. J Mol Biol. 2005;354(4):751-9.

86. Dalen KT, Schoonjans K, et al. *Adipose tissue expression of the lipid droplet-associating proteins S3-12 and perilipin is controlled by peroxisome proliferator-activated receptor-gamma*. Diabetes. 2004;53(5):1243-52.

87. Danaei G, Finucane MM, et al. *National, regional, and global trends in fasting plasma glucose and diabetes prevalence since 1980: systematic analysis of health examination surveys and epidemiological studies with 370 country-years and 2.7 million participants*. Lancet. 2011;378(9785):31-40.

88. Proschak E, Heitel P, et al. *Opportunities and Challenges for Fatty Acid Mimetics in Drug Discovery*. J Med Chem. 2017;60(13):5235-66.

89. Nolan T, Hands RE, et al. *Quantification of mRNA using real-time RT-PCR*. Nat Protocols. 2006;1(3):1559-82.

90. Fleige S, Pfaffl MW. *RNA integrity and the effect on the real-time qRT-PCR performance*. Mol Aspects Med. 2006;27(2-3):126-39.

91. Bustin SA. *Absolute quantification of mRNA using real-time reverse transcription polymerase chain reaction assays*. J Mol Endocrinol. 2000;25(2):169-93.

92. Kozera B, Rapacz M. *Reference genes in real-time PCR*. J Appl Genet. 2013;54(4):391-406.

93. Vandesompele J, De Preter K, et al. *Accurate normalization of real-time quantitative RT-PCR data by geometric averaging of multiple internal control genes*. Genome Biol. 2002;3(7):Research0034.

94. Ballatore C, Huryn DM, et al. *Carboxylic Acid (Bio)Isosteres in Drug Design*. ChemMedChem. 2013;8(3):385-95.

95. Skrede S, Sorensen HN, et al. *Thia fatty acids, metabolism and metabolic effects*. Biochim Biophys Acta. 1997;1344(2):115-31.

96. Olsavsky KM, Page JL, et al. *Gene expression profiling and differentiation assessment in primary human hepatocyte cultures, established hepatoma cell lines, and human liver tissues*. Toxicol Appl Pharmacol. 2007;222(1):42-56.

97. Clarke SD. *Polyunsaturated fatty acid regulation of gene transcription: a mechanism to improve energy balance and insulin resistance*. Br J Nutr. 2000;83 Suppl 1:S59-66.

98. Gottlicher M, Demoz A, et al. *Structural and metabolic requirements for activators of the peroxisome proliferator-activated receptor*. Biochem Pharmacol. 1993;46(12):2177-84.

99. Limor R, Sharon O, et al. *Lipoxygenase-derived metabolites are regulators of peroxisome proliferator-activated receptor gamma-2 expression in human vascular smooth muscle cells*. Am J Hypertens. 2008;21(2):219-23.

100. Nagy L, Tontonoz P, et al. *Oxidized LDL regulates macrophage gene expression through ligand activation of PPARgamma*. Cell. 1998;93(2):229-40.

101. Brown PJ, Stuart LW, et al. *Identification of a subtype selective human PPARalpha agonist through parallel-array synthesis*. Bioorg Med Chem Lett. 2001;11(9):1225-7.

102. Honkakoski P, Negishi M. *Regulation of cytochrome P450 (CYP) genes by nuclear receptors*. Biochem J. 2000;347(Pt 2):321-37.

103. Tansey JT, Sztalryd C, et al. *Perilipin ablation results in a lean mouse with aberrant adipocyte lipolysis, enhanced leptin production, and resistance to diet-induced obesity*. Proc Natl Acad Sci U S A. 2001;98(11):6494-9.

104. Brasaemle DL, Barber T, et al. *Adipose differentiation-related protein is an ubiquitously expressed lipid storage droplet-associated protein*. J Lipid Res. 1997;38(11):2249-63.

105. Lee JY, Hashizaki H, et al. *Activation of peroxisome proliferator-activated receptor-alpha enhances fatty acid oxidation in human adipocytes*. Biochem Biophys Res Commun. 2011;407(4):818-22.

106. Hiuge A, Tenenbaum A, et al. *Effects of peroxisome proliferator-activated receptor ligands, bezafibrate and fenofibrate, on adiponectin level*. Arterioscler Thromb Vasc Biol. 2007;27(3):635-41.

107. Tsuchida A, Yamauchi T, et al. *Peroxisome proliferator-activated receptor (PPAR)alpha activation increases adiponectin receptors and reduces obesity-related inflammation in adipose tissue: comparison of activation of PPARalpha, PPARgamma, and their combination*. Diabetes. 2005;54(12):3358-70.

108. Goto T, Lee JY, et al. *Activation of peroxisome proliferator-activated receptor-alpha stimulates both differentiation and fatty acid oxidation in adipocytes*. J Lipid Res. 2011;52(5):873-84.

109. Jeong S, Yoon M. *Fenofibrate inhibits adipocyte hypertrophy and insulin resistance by activating adipose PPARalpha in high fat diet-induced obese mice*. Exp Mol Med. 2009;41(6):397-405.

110. Dalen KT, Ulven SM, et al. *PPARalpha activators and fasting induce the expression of adipose differentiation-related protein in liver*. J Lipid Res. 2006;47(5):931-43.

111. Maeda N, Takahashi M, et al. *PPARgamma ligands increase expression and plasma concentrations of adiponectin, an adipose-derived protein*. Diabetes. 2001;50(9):2094-9.

112. Massaro M, Scoditti E, et al. *Therapeutic potential of the dual peroxisome proliferator activated receptor (PPAR)alpha/gamma agonist aleglitazar in attenuating TNF-alpha-mediated inflammation and insulin resistance in human adipocytes*. Pharmacol Res. 2016;107:125-36.

113. Belfort R, Berria R, et al. *Fenofibrate reduces systemic inflammation markers independent of its effects on lipid and glucose metabolism in patients with the metabolic syndrome*. J Clin Endocrinol Metab. 2010;95(2):829-36.

114. Hotamisligil GS, Arner P, et al. *Increased adipose tissue expression of tumor necrosis factor-alpha in human obesity and insulin resistance*. J Clin Invest. 1995;95(5):2409-15.

115. Hotta K, Funahashi T, et al. *Plasma concentrations of a novel, adipose-specific protein, adiponectin, in type 2 diabetic patients*. Arterioscler Thromb Vasc Biol. 2000;20(6):1595-9.

116. Arita Y, Kihara S, et al. *Paradoxical decrease of an adipose-specific protein, adiponectin, in obesity*. Biochem Biophys Res Commun. 1999;257(1):79-83.

117. Ouchi N, Kihara S, et al. *Adiponectin, an adipocyte-derived plasma protein, inhibits endothelial NF-kappaB signaling through a cAMP-dependent pathway*. Circulation. 2000;102(11):1296-301.

118. Yamauchi T, Kamon J, et al. *Adiponectin stimulates glucose utilization and fatty-acid oxidation by activating AMP-activated protein kinase*. Nat Med. 2002;8(11):1288-95.

119. Young PW, Cawthorne MA, et al. *Repeat treatment of obese mice with BRL 49653, a new potent insulin sensitizer, enhances insulin action in white adipocytes. Association with increased insulin binding and cell-surface GLUT4 as measured by photoaffinity labeling*. Diabetes. 1995;44(9):1087-92.

120. Armoni M, Kritz N, et al. *Peroxisome proliferator-activated receptor-gamma represses GLUT4 promoter activity in primary adipocytes, and rosiglitazone alleviates this effect*. J Biol Chem. 2003;278(33):30614-23.

121. Misra P, Reddy JK. *Peroxisome proliferator-activated receptor-alpha activation and excess energy burning in hepatocarcinogenesis*. Biochimie. 2014;98:63-74.

122. Polyzos SA, Mantzoros CS. *Adiponectin as a target for the treatment of nonalcoholic steatohepatitis with thiazolidinediones: A systematic review*. Metabolism. 2016;65(9):1297-306.

123. Liss KH, Finck BN. *PPARs and nonalcoholic fatty liver disease*. Biochimie. 2017;136:65-74.

124. Carmona MC, Louche K, et al. *Fenofibrate prevents Rosiglitazone-induced body weight gain in ob/ob mice*. Int J Obes (Lond). 2005;29(7):864-71.

125. Chipscreen Biosciences Ltd. *Study of Chiglitazar Compare With Placebo in Type 2 Diabetes Patients (CMAP)* [Internet]. U.S. National Library of Medicine; 2014 [updated July 25 2017] [cited November 8 2017]. Available from: https://clinicaltrials.gov/ct2/show/NCT0212171.

126. Choi JH, Banks AS, et al. *Antidiabetic actions of a non-agonist PPARgamma ligand blocking Cdk5-mediated phosphorylation*. Nature. 2011;477(7365):477-81.

127. Singh AB, Kan CF, et al. *SREBP2 Activation Induces Hepatic Long-chain Acyl-CoA Synthetase 1 (ACSL1) Expression in Vivo and in Vitro through a Sterol Regulatory Element (SRE) Motif of the ACSL1 C-promoter*. J Biol Chem. 2016;291(10):5373-84.

128. Dube E, Gravel A, et al. *Modulation of fatty acid transport and metabolism by maternal obesity in the human full-term placenta*. Biol Reprod. 2012;87(1):14, 1-1.

129. Murholm M, Isidor MS, et al. *Retinoic acid has different effects on UCP1 expression in mouse and human adipocytes*. BMC Cell Biol. 2013;14:41.

Appendices

Appendix I: Reagents, equipment and software

Reagents, kits and equipment	Manufacturer	Cat. No.
2-Mercaptoethanol	Sigma-Aldrich	7522
3,3′,5-Triiodo-L-thyronine sodium salt	Sigma-Aldrich	T6397
3-Isobutyl-1-methylxanthine	Sigma-Aldrich	I5879
Apo-transferrin, human	Sigma-Aldrich	T4382
Biotin	Sigma-Aldrich	B4639
Bromophenol Blue	Bio-Rad Laboratories	1610404
Cell culture flasks	Corning Inc., Falcon™	
- 75 cm^2		353135
- 150 cm^2		355000
Cell culture plates	Corning Inc., Falcon™	
- 6 wells		353043
- 12 wells		353046
- 24 wells		353047
- 96 wells		353075
Cell Scraper 16 cm	Sarstedt	83.1832
Countess™ Cell Counting Chamber Slides	Invitrogen™	C10228
Cytotoxicity Detection Kit (LDH)	Roche Diagnostics	11644793001
D-pantothenate	Sigma-Aldrich	P5155
Dexamethasone water-soluble	Sigma-Aldrich	D2915
DNA Ladder (1kb Plus)	Invitrogen™	10787018
Dual-Luciferase® Reporter Assay System	Promega	E1960
Dulbecco's modified Eagle's medium, high glucose	Sigma-Aldrich	D6546
Dulbecco's modified Eagle's medium/Nutrient Mix F12 Ham	Sigma-Aldrich	D6421
Fetal Bovine Serum	Sigma-Aldrich	F7524
High-Capacity cDNA Reverse Transcription Kit	Applied Biosystems™	4368814
Hydrocortisone-Water soluble	Sigma-Aldrich	H0396
In Vitro Toxicology Assay Kit, XTT based	Sigma-Aldrich	TOX2-1KT
Insulin, human	Sigma-Aldrich	I2643
ITS Liquid Media Supplement (100×)	Sigma-Aldrich	I3146
KAPA SYBR® FAST qPCR Master Mix (2X) Universal	Kapa Biosystems	KK4601
KpnI	New England Biolabs	R0142S
L-Glutamine	Sigma-Aldrich	G7513
Lipofectamine® 2000 Reagent	Invitrogen	11668-019
MetaPhor™ Agarose	Lonza	50181
Micro tube 1.5 mL SafeSeal	Sarstedt	72.706.400
NEBuffer 2	New England Biolabs	B7002S
NucleoSpin® Gel and PCR Clean-up kit	Macherey-Nagel	740609
Nucleospin® Plasmid kit	Macherey-Nagel	740588
Nucleobond ® Xtra Maxi Plus kit	Macherey-Nagel	740416
Nunc™ F96 MicroWell™ White Polystyrene Plate	Thermo Fischer Scientific	136101
Oil Red O	Sigma-Aldrich	O0625
Penicillin/Streptomycin solution	Sigma-Aldrich	P4458

Reagents, kits and equipment	Manufacturer	Cat. No.
PfuUltra II Fusion HS DNA Polymerase	Agilent	600670
Purified BSA (100×)	New England Biolabs	B9001S
qPCR 96-well plate non-skirted, low profile, frosted	Eurogentec	RT-PL96-OP
qPCR optical seals	Eurogentec	RT-OPSL-100
RNase Away	Molecular BioProducts	7005-11
RNeasy Mini Kit	Qiagen	74104
Rosiglitazone	LKT Laboratories	R5773
SacII	New England Biolabs	R0157S
Serological pipettes	Corning Inc., Falcon™	
- 5 mL		357543
- 10 mL		357551
- 25 mL		357535
Sterican® cannulas 21G (0.8×40 mm)	B. Braun Medical	612-0142
SYBR™ safe DNA Gel Stain	Invitrogen	S33102
T4 DNA ligase	New England Biolabs	M0202S/L
Triton X-100	Sigma-Aldrich	T8787
Tryphan Blue Stain 0.4 %	Invitrogen	T10282
Trypsin-EDTA Solution	Sigma-Aldrich	T3924
WY-14643	Sigma-Aldrich	C7081

Instruments	Manufacturer
CFX96 Touch™ Real-Time PCR Detection System	Bio-Rad Laboratories
Countess™ Automated Cell Counter	Invitrogen™
Heraeus Multifuge 3+ Centrifuge	Thermo Fischer Scientific
Heraeus Pico21 Centrifuge	Thermo Fischer Scientific
Forma™ Steri-Cycle™ CO_2 Incubator	Thermo Fischer Scientific
Nanodrop® ND-1000 Spectrophotometer	NanoDrop Technologies
Olympus CKX41 inverted microscope	Olympus®
PowerPac™ Basic Power Supply	Bio-Rad Laboratories
Spectrafuge™ Mini	Labnet International Inc.
Synergy 2 Multi-Mode Reader	BioTek® Instruments
Synergy H1 Hybrid Multi-Mode Microplate Reader	BioTek® Instruments
Sub-Cell® GT Horizontal Electrophoresis System	Bio-Rad Laboratories
Thermomixer® comfort	Eppendorf®
Veriti™ 96 Well Thermal Cycler	Applied Biosystems™
ColorView IIIu light microscope CCD camera	Olympus®

Software	Manufacturer
Bio-Rad CFX Manager 3.1	Bio-Rad Laboratories
cell* v.3.4 (Build 2677)	Olympus Soft Imaging Solutions GmbH
EndNote X8.0.1 (Build 10444)	EndNote
Gen5™ 1.11 (Build 1.11.5)	BioTek® Instruments Inc.
Gen5™ 3.02	BioTek® Instruments Inc.
GraphPad Prism 6	GraphPad Software Inc.
IBM® SPSS® Statistics v.24	IBM Corporation
Microsoft Office Plus 2010	Microsoft Corporation
NanoDrop 1000 Operating Software (ND-1000) v.3.8.1	NanoDrop Technologies
Serial Cloner v.2.5	Serial Basics

Appendix II: Buffer and reagents recipes

PBS

For 1 liter of 1×PBS, prepare 8.00 g NaCl (MW = 58.440 g/mol), 0.20 g KCl (MW = 74.551 g/mol), 1.44 g Na_2HPO_4 (MW = 141.960 g/mol), and 0.24 g KH_2PO_4 (MW = 136.086 g/mol) in 500 mL dH_2O.

Adjust the pH to 7.4 with HCl, and adjust volume to 1000 mL. Dispense the solution into aliquots as desired and sterilize by autoclaving (20 min, 121°C, liquid cycle). Store at room temperature.

1×TE buffer

For 1 liter of 1×TE buffer, prepare 0.6120 g Tris base (MW = 157.60 g/mol) and 0.1866 g EDTA•H_2O (MW = 372.24 g/mol) in 450 mL dH_2O.

Adjust pH to 8 with NaOH or HCl. Adjust volume to 500 mL with dH_2O. Sterilize by autoclaving (20 min, 121°C, liquid cycle) and store at room temperature. Dilute the 1xTE buffer 1:10 in dH_2O to make 1:10 TE buffer.

Loading dye

For 10 mL loading dye, prepare 0.2 g Bromophenol Blue (Bio-Rad Laboratories #1610404) and 6 mL glycerol (50 %) in 4 mL TE-buffer.

High salt solution

For 50 mL HSS, prepare 4.4 g NaCl (1.5 M) and 5.4 NaAc (0.8 M, pH 5.5) in 50 mL ddH_2O. Sterile filter before use.

Appendix III: SGBS cell culturing media

F0 medium

Reagents	Volume
DMEM/Nutrient Mix F12	500 mL
Vitamin mix*	5 mL
L-Glutamine (Sigma-Aldrich, #G7513)	10 mL
Penicillin (50 U/mL)-Streptomycin (50 µg/mL) (Sigma-Aldrich, #P4458)	5 mL

*Vitamin mix stock composed of 0.04 g biotin (Sigma-Aldrich #B4639) and 0.02 g D-pantothenate (Sigma-Aldrich #P5155) in 50 mL ddH_2O.

FBS-containing medium

Reagents	Volume
F0 medium	500 mL
FBS (Sigma-Aldrich, #F7524, lot. 012M3397) (not heat inactivated)	50 mL

3FC medium

Reagents	Volume	Final conc.
0F medium	10 mL	
Human apo-transferrin (Sigma-Aldrich, #T4382) (1 mg/ml stock)	100 µL	0.01 mg/mL
Human insulin (Sigma-Aldrich, #I6635) (100 µM stock)	2 µL	20 nM
Cortisol (Sigma-Aldrich, #H0396) (100 µM stock)	10 µL	100 µM
T3 (Sigma-Aldrich, #T6397) (200 nM stock)	10 µL	0.2 nM

Quickdiff medium

Reagents	Volume	Final conc.
3FC medium	10 mL	
Dexamethasone (25 µM stock)	10 µL	25 nM
IBMX (22.5 mM stock)	222 µL	500 µM
Treatment agents, either		
Rosiglitazone (LKT Laboratories, #R5773) (10 mM stock),	2 µL	2 µM
ADAM1 (100 mM stock) + 24 µM BSA,	2.5 µL	25 µM
or DMSO (100 % stock) + 24 µM BSA	100 µL	0.1 %

Appendix IV: DNA plasmids

Plasmid	Description
pCDNA3.1	Mammalian expression vector with CMV promoter
pCDNA3.1-hPPARα-FLAG	FLAG-tagged human PPARα expression plasmid with constitutive CMV promoter
pCDNA3.1-hPPARγ2-FLAG	FLAG-tagged human PPARγ expression plasmid with constitutive CMV promoter
pCDNA3.1-hRXRa	Human RXRα expression plasmid with constitutive CMV promoter
pGL3-5xUAS-SV40	Gal4 responsive firefly luciferase reporter
pGL3-hCPT1A-Int	Firefly luciferase reporter plasmid with human CPT1A promoter
pGL3-hCPT1A-Int PPREmut	Firefly luciferase reporter plasmid with human CPT1A promoter with mutation of PPRE with non-functional recognition elements
pGL3-hPLIN1-3'del	Firefly luciferase reporter plasmid with human PLIN1 promoter.
pGL3-hPLIN1-3'del PPRE3mut	Firefly luciferase reporter plasmid. Human PLIN1 promoter with mutation of PPRE with non-functional recognition elements.
pRL-CMV	Mammalian renilla luciferase co-reporter control plasmid with constitutive CMV promoter
pSG5-GAL4	Mammalian cloning vector for Gal4-tethering construct
pSG5-GAL4-DBD-hLXRα-LBD	Human LXRα-LBD Gal4-tethering expression plasmid with SV40 promoter
pSG5-GAL4-DBD-hLXRβ-LBD	Human LXRβ-LBD Gal4-tethering expression plasmid with SV40 promoter
pSG5-GAL4-DBD-hPPARα-LBD	Human PPARα-LBD Gal4-tethering expression plasmid with SV40 promoter
pSG5-GAL4-DBD-hPPARγ-LBD	Human PPARγ-LBD Gal4-tethering expression plasmid with SV40 promoter
pSG5-GAL4-DBD-hPPARδ-LBD	Human PPARδ-LBD Gal4-tethering expression plasmid with SV40 promoter
pSG5-GAL4-DBD-hRXRα-LBD	Human RXRα-LBD Gal4-tethering expression plasmid with SV40 promoter

Appendix V: Human qPCR primer sequences

Target gene (GenBank acc. no.)	Primer sequence 5' → 3'		Amplicon (bp)	Ref
ACOX1	F	CTTCAACCCGGAGCTGCTTA	78	
(NM_004035.6)	R	ATGTTCTCGATCTCTCGGCG		
ADIPOQ	F	AAGGAGATCCAGGTCTTATTGGT	108	
(NM_001177800)	R	GTTCTCCTTTCCTGCCTTGGA		
ANGPTL4	F	TCCACCGACCTCCCGTTAG	117	
(NM_139314.2)	R	GGCCACCTTGTGGAAGAGTT		
ACSL1	F	CTTCTGGTACGCCACGAGAC	115	(127)
(NM_001286708.1)	R	GTCGCTGTCAAGTAGTGCG		
ACSL3	F	TGCGACAGCTTTGTTTTCCG	70	
(NM_004457.3)	R	CACCACACAACAGGAGACGA		
CD36	F	CCTGGCTGTGTTTGGAGGTAT	83	
(NM_000072.3)	R	CTTCGAGGACAACTTGCTTTT		
CPT1A	F	CAGGAGACAGAGTTCCCTGG	109	
(NM_001876.3)	R	TCTAACGTCACGAAGAACGCT		
FABP1	F	CGGAAGAGCTCATCCAGAAG	193	(128)
(NM_001443)	R	TTGTCACCTTCCAACTGAACC		
FABP4	F	ATGGGGGTGTCCTGGTACAT	117	
(NM_001442.2)	R	TCGTGGAAGTGACGCCTTTC		
LEP	F	AGCTGTGCCCATCCAAAAAGT	99	
(NM_000230.2)	R	GAGGAGACTGACTGCGTGT		
NR1H3 (LXRA)	F	TGCATGCCTACGTCTCCATC	111	
(NM_005693.3)	R	ACACTTGCTCTGAGTGGACG		
PLIN1	F	GACAAGGAAGAGTCAGCCCC	107	
(NM_002666)	R	GAGAGGGTGTTGGTCAGAGC		
PPARA	F	TCGGCGAGGATAGTTCTGGA	98	
(NM_001001928.2)	R	TGAAAGCGTGTCCGTGATGA		
PPARG	F	ACAGATCCAGTGGTTGCAGA	71	
(NM_015869.4)	R	TCCACTTTGATTGCACTTTGGT		
RNA18S1	F	GCTTAATTTGACTCAACACGGGA	69	
(NR_003286.2)	R	AGCTATCAATCTGTCAATCCTGTC		
SCD1	F	ACACCCAGCTGTCAAAGAGA	97	
(NM_005063.4)	R	GCCAGGTTTGTAGTACCTCCTC		
SREBF1 a and c	F	CCGCTCCTCCATCAATGACA	124	
(NM_001005291.2)	R	GCTGTGTTGCAGAAAGCGAA		
TBP	F	TTGTACCGCAGCTGCAAAAT	96	
(NM_003194.4)	R	TATATTCGGCGTTTCGGGCA		
UCP1	F	CCAACTGTGCAATGAAAGTGT	81	(129)
(NM_021833.4)	R	CAAGTCGCAAGAAGGAAGGTA		

Bp, base pairs; Ref, reference

Appendix VI: Cloned pSG5-GAL4-hRXRα-LBD plasmid sequence chromatogram

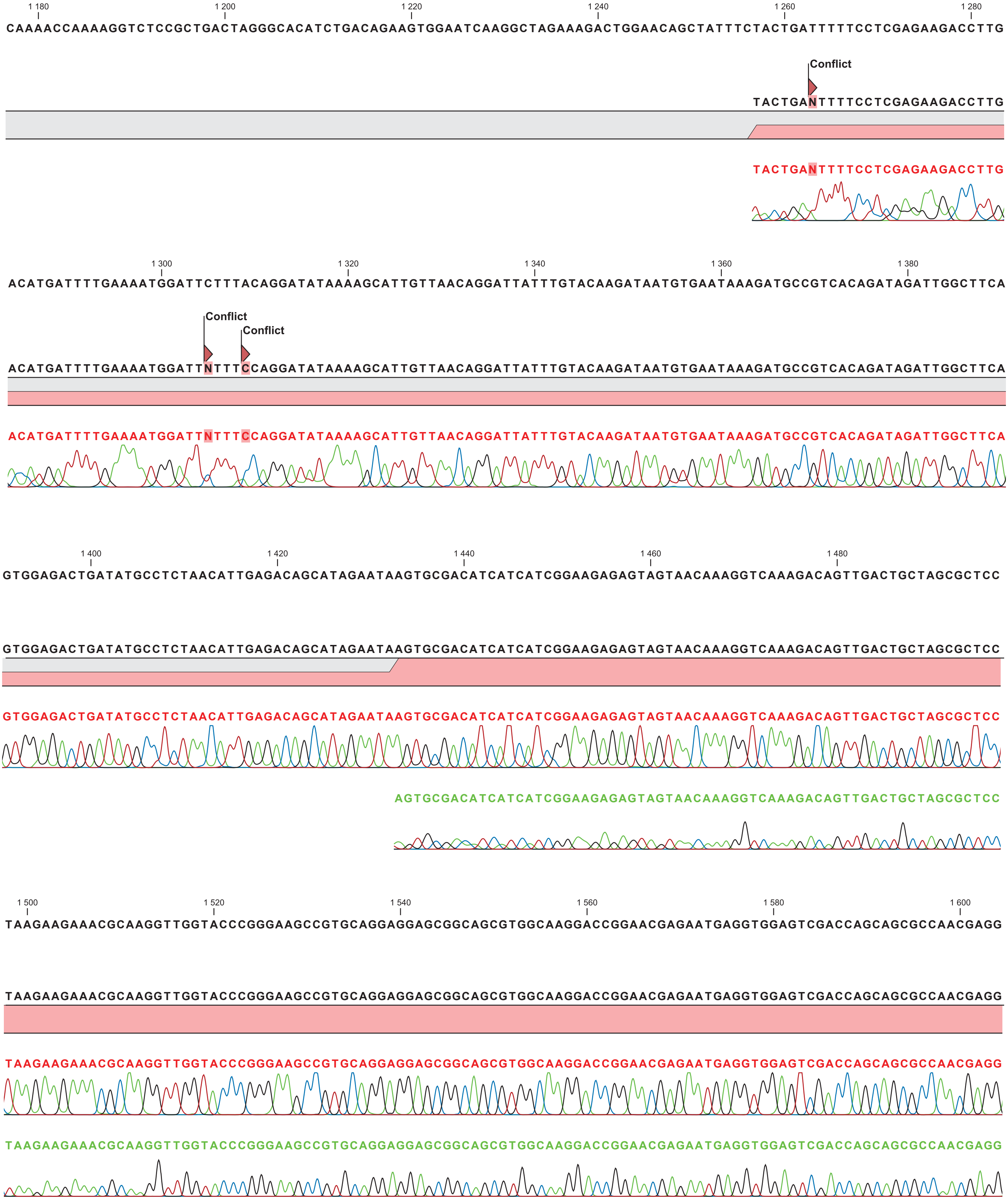

1 620 1 640 1 660 1 680 1 700

ACATGCCGGTGGAGAGGATCCTGGAGGCTGAGCTGGCCGTGGAGCCCAAGACCGAGACCTACGTGGAGGCAAACATGGGGCTGAACCCCAGCTCGCCGAACGACCCT

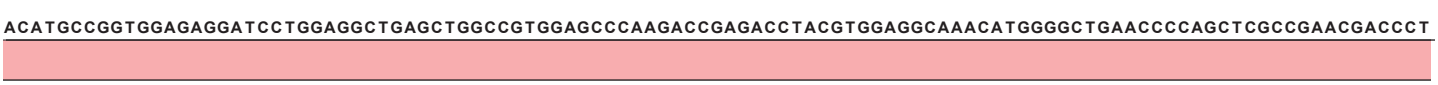

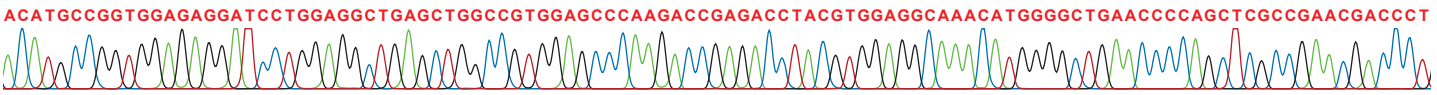

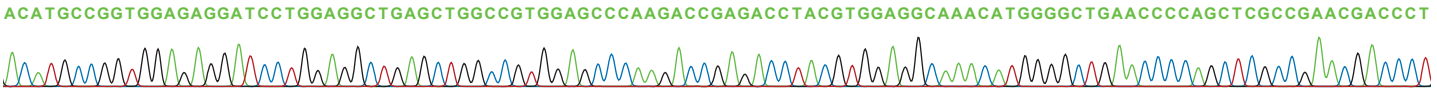

1 720 1 740 1 760 1 780 1 800

GTCACCAACATTTGCCAAGCAGCCGACAAACAGCTTTTCACCCTGGTGGAGTGGGCCAAGCGGATCCCACACTTCTCAGAGCTGCCCCTGGACGACCAGGTCATCCT

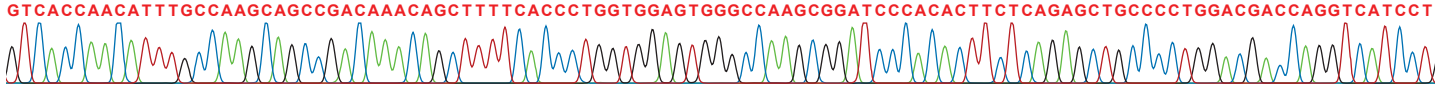

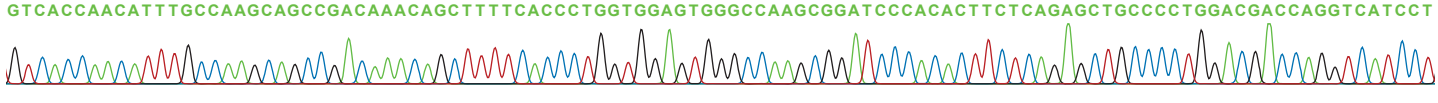

1 820 1 840 1 860 1 880 1 900 1 920

GCTGCGGGCAGGCTGGAATGAGCTGCTCATCGCCTCCTTCTCCCACCGCTCCATCGCCGTGAAGGACGGGATCCTCCTGGCCACCGGGCTGCACGTCCACCGGAACA

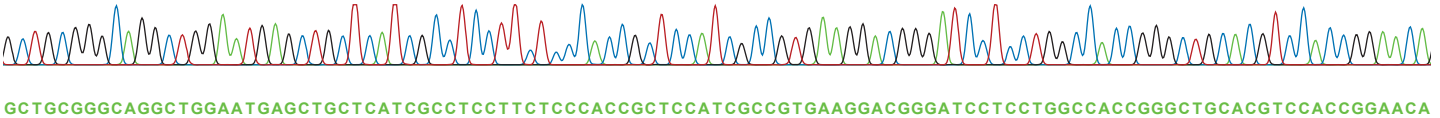

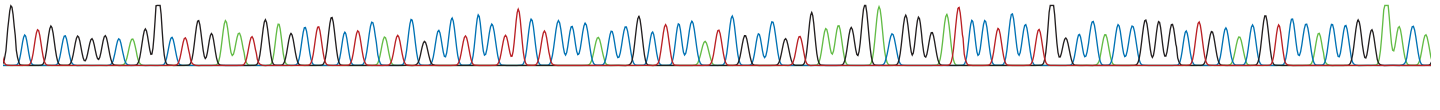

1 940 1 960 1 980 2 000 2 020

GCGCCCACAGCGCAGGGGTGGGCGCCATCTTTGACAGGGTGCTGACGGAGCTTGTGTCCAAGATGCGGGACATGCAGATGGACAAGACGGAGCTGGGCTGCCTGCGC

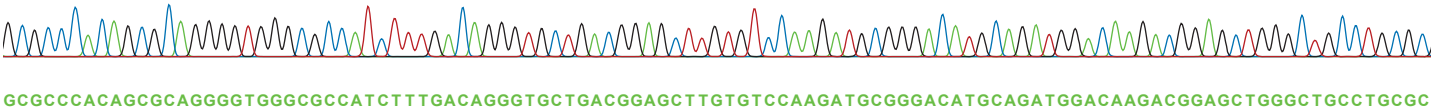

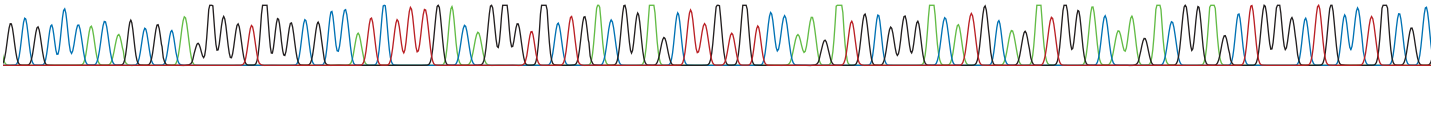

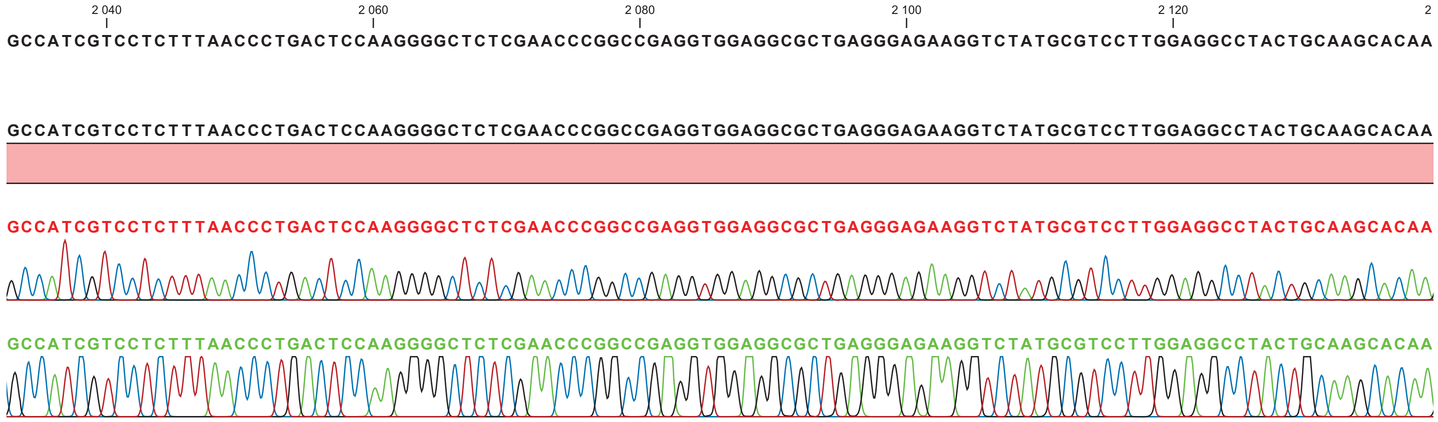
2 040
2 060
2 080
2 100
2 120
2
GCCATCGTCCTCTTTAACCCTGACTCCAAGGGGCTCTCGAACCCGGCCGAGGTGGAGGCGCTGAGGGAGAAGGTCTATGCGTCCTTGGAGGCCTACTGCAAGCACAA
GCCATCGTCCTCTTTAACCCTGACTCCAAGGGGCTCTCGAACCCGGCCGAGGTGGAGGCGCTGAGGGAGAAGGTCTATGCGTCCTTGGAGGCCTACTGCAAGCACAA
GCCATCGTCCTCTTTAACCCTGACTCCAAGGGGCTCTCGAACCCGGCCGAGGTGGAGGCGCTGAGGGAGAAGGTCTATGCGTCCTTGGAGGCCTACTGCAAGCACAA
GCCATCGTCCTCTTTAACCCTGACTCCAAGGGGCTCTCGAACCCGGCCGAGGTGGAGGCGCTGAGGGAGAAGGTCTATGCGTCCTTGGAGGCCTACTGCAAGCACAA

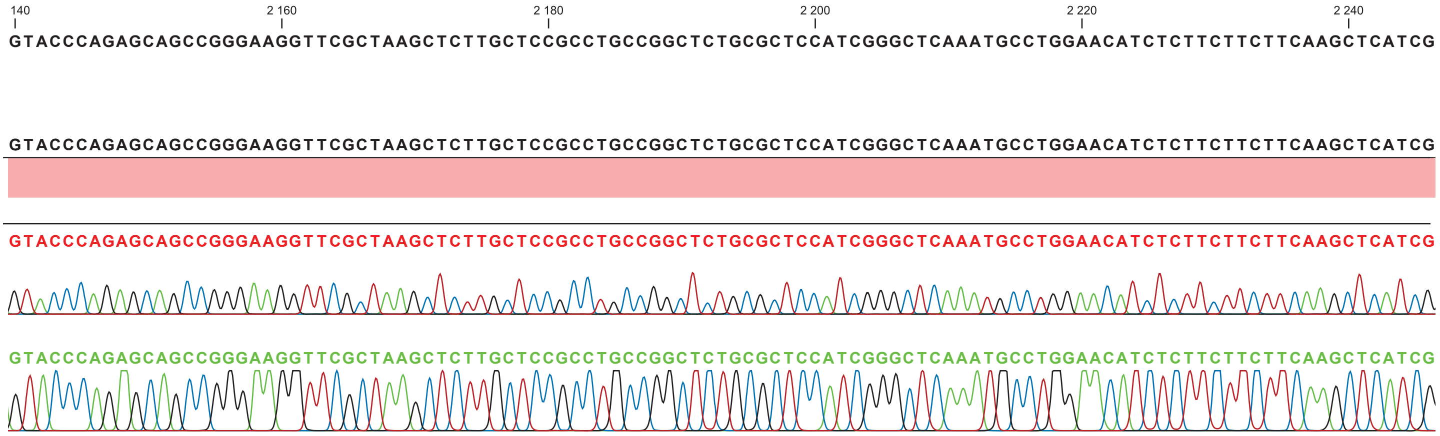
140
2 160
2 180
2 200
2 220
2 240
GTACCCAGAGCAGCCGGGAAGGTTCGCTAAGCTCTTGCTCCGCCTGCCGGCTCTGCGCTCCATCGGGCTCAAATGCCTGGAACATCTCTTCTTCTTCAAGCTCATCG
GTACCCAGAGCAGCCGGGAAGGTTCGCTAAGCTCTTGCTCCGCCTGCCGGCTCTGCGCTCCATCGGGCTCAAATGCCTGGAACATCTCTTCTTCTTCAAGCTCATCG
GTACCCAGAGCAGCCGGGAAGGTTCGCTAAGCTCTTGCTCCGCCTGCCGGCTCTGCGCTCCATCGGGCTCAAATGCCTGGAACATCTCTTCTTCTTCAAGCTCATCG
GTACCCAGAGCAGCCGGGAAGGTTCGCTAAGCTCTTGCTCCGCCTGCCGGCTCTGCGCTCCATCGGGCTCAAATGCCTGGAACATCTCTTCTTCTTCAAGCTCATCG


2 260
2 280
2 300
2 320
2 340
GGGACACACCCATTGACACCTTCCTTATGGAGATGCTGGAGGCGCCGCACCAAATGACTTAATAACCGCGGATCCAGATCTTATTAAAGCAGAACTTGTTTATTGCA
GGGACACACCCATTGACACCTTCCTTATGGAGATGCTGGAGGCGCCGCACCAAATGACTTAATAACCGCGGATCCAGATCTTATTAAAGCAGAACTTGTTTATTGCA
GGGACACACCCATTGACACCTTCCTTATGGAGATGCTGGAGGCGCCGCACCAAATGACTTAATAACCGCGGATCCAGATCTTATTAAAGCAGAACTTGTTTATTGCA
GGGACACACCCATTGACACCTTCCTTATGGAGATGCTGGAGGCGCCGCACCAAATGACTTAATAACCGCGGATCCAGATCTTATTAAAGCAGAACTTGTTTATTGCA

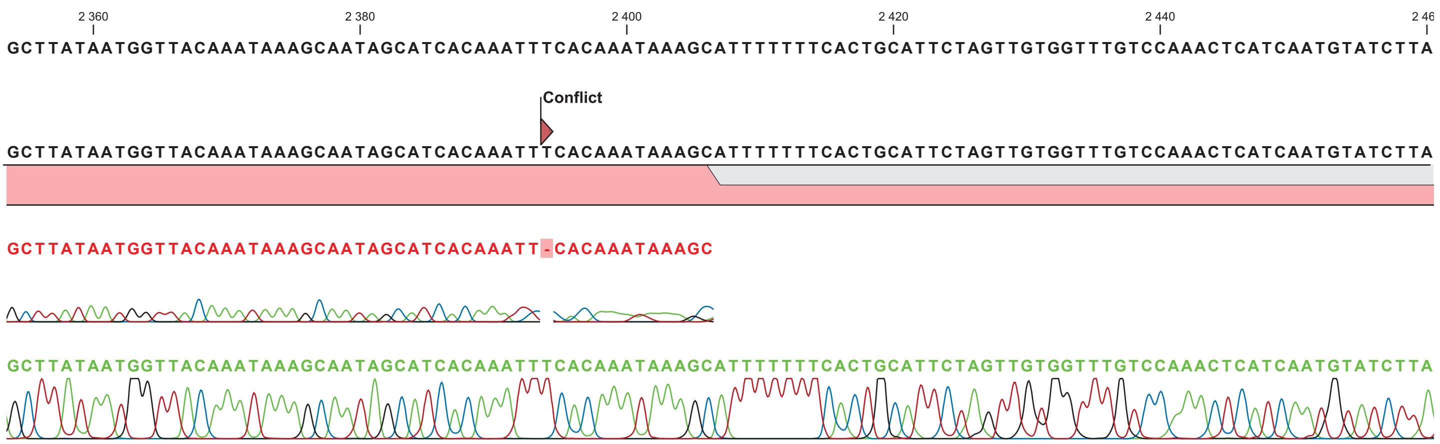
2 360
2 380
2 400
2 420
2 440
2 46
GCTTATAATGGTTACAAATAAAGCAATAGCATCACAAATTTCACAAATAAAGCATTTTTTTCACTGCATTCTAGTTGTGGTTTGTCCAAACTCATCAATGTATCTTA
Conflict
GCTTATAATGGTTACAAATAAAGCAATAGCATCACAAATTTCACAAATAAAGCATTTTTTTCACTGCATTCTAGTTGTGGTTTGTCCAAACTCATCAATGTATCTTA
GCTTATAATGGTTACAAATAAAGCAATAGCATCACAAATT-CACAAATAAAGC
GCTTATAATGGTTACAAATAAAGCAATAGCATCACAAATTTCACAAATAAAGCATTTTTTTCACTGCATTCTAGTTGTGGTTTGTCCAAACTCATCAATGTATCTTA